Photoelectrochemical studies of dye-sensitized solar cells using organic dyes

Tannia Marinado

Doctoral Thesis

Stockholm 2009

School of Chemical Science and Engineering
Kungliga Tekniska Högskolan, Stockholm 2009

Akademisk avhandling som med tillstånd av Kungliga Tekniska Högskolan i Stockholm
framlägges till offentlig granskning för avläggande av doktorsexamen i kemi
fredagen den 30 oktober 2009, kl 10.00 i sal F3, Lindstedtsvägen 26, KTH.
Opponent: Dr. Ryuzi Katoh,
National Institute of Advanced Industrial Science and Technology (AIST), Tsukuba, Japan

Printed in Sweden
Universitetsservice US-AB, Stockholm 2009

TRITA-CHE Report 2009:50
ISSN1654-1081
ISBN 978-91-7415-461-0

Abstract

Tannia Marinado **2009**
Doctoral thesis
"Photoelectrochemical studies of dye-sensitized solar cells using organic dyes"
Physical Chemistry, Chemical Science and Engineering,
KTH, Royal Institute of Technology, SE-100 44 Stockholm, Sweden.

The dye-sensitized solar cell (DSC) is a promising efficient low-cost molecular photovoltaic device. One of the key components in DSCs is the dye, as it is responsible for the capture of sunlight.

State-of-the-art DSC devices, based on ruthenium dyes, show record efficiencies of 10-12 %. During the last decade, metal-free organic dyes have been extensively explored as sensitizers for DSC application. The use of organic dyes is particularly attractive as it enables easy structural modifications, due to fairly short synthetic routes and reduced material cost. Novel dye should in addition to the light-harvesting properties also be compatible with the DSC components.

In this thesis, a series of new organic dyes are investigated, both when integrated in the DSC device and as individual components. The evaluation methods consisted of different electrochemical and photoelectrochemical techniques. Whereas the light-harvesting properties of the dyes were fairly easily improved, the behavior of the dye integrated in the DSC showed less predictable photovoltaic results.

The dye series studied in *Papers II* and *IV* revealed that their dye energetics limited vital electron-transfer processes, the dye regeneration *(Paper II)* and injection quantum yield *(Paper IV)*. Further, in *Papers III-VI,* it was observed that different dye structures seemed to alter the interfacial electron recombination with the electrolyte. In addition to the dye structure sterics, some organic dyes appear to enhance the interfacial recombination, possibly due to specific dye-redox acceptor interaction (*Paper V*).

The impact of dye sterical modifications versus the use of coadsorbent was explored in *Paper VI*. The dye layer properties in the presence and absence of various coadsorbents were further investigated in *Paper VII*.

The core of this thesis is the identification of the processes and properties limiting the performance of the DSC device, aiming at an overall understanding of the compatibility between the DSC components and novel organic dyes.

Keywords: additive, charge recombination, coadsorbent, conduction band shift, dye-sensitized, electron lifetime, electron-transfer, organic dye, photoelectrochemical, photovoltaic, sensitizer, semiconductor, solar cell, solar cell efficiency, titanium dioxide

Abbreviations

DSC	Dye-sensitized solar cell
HOMO	Highest occupied molecular orbital
LUMO	Lowest unoccupied molecular orbital
WE	Working electrode
CE	Counter electrode
FTO	Flourine-doped tin oxide
SC	Semiconductor
CB	Conduction band
VB	Valence band
$E_{F,n}$	Quasi-Fermi energy level of electrons
$E_{F,n}/q$	Quasi-Fermi potential of electrons
n_{CB}	Electron concentration in the conduction band
N_{CB}	Effective density of states in the conduction band
E_{CB}	Conduction band energy
$E\ (D/D^+)$	Ground state redox energy of dye
$E_{pot}(D/D^+)$	Ground state redox *potential* of dye
$E\ (D^*/D^+)$	Excited state redox energy of dye
$E_{pot}(D^*/D^+)$	Excited state redox *potential* of dye
$E\ (I^-/I_3^-)$	Redox energy of iodide/triiodide
$E_{pot}\ (I^-/I_3^-)$	Redox *potential* of iodide/triiodide
V_{oc}	Open-circuit voltage
J_{sc}	Short-circuit current
η	Efficiency
FF	Fill factor
h	Planck constant
IPCE	Incident Photon to Current-conversion Efficiency
APCE	Absorbed Photon to Current-conversion Efficiency
LHE	Light harvesting efficiency
Φ_{inj}	Injection efficiency
η_{reg}	Regeneration efficiency
η_{cc}	Collection efficiency
Q_{oc}	Extracted charge at open-circuit voltage
EtOH	Ethanol
DCM	Dichloromethane
MeCN	Acetonitrile
Tol	Toluene
THF	Tetrahydrofuran
DPA	Dodecylphosphonic acid
CDCA	Chenodeoxycholic acid
DINHOP	Dineohexyl phosphinic acid
TPA	Triphenylaminen

Note that different abbreviations are used in articles and in the thesis.
The dye **D5** (*Paper I*) is abbreviated **L2** throughout the thesis.
The rhodanine dyes **L0**, **L1** and **L2** (*Paper IV*) are abbreviated **L0A3**, **L1A3** and **L2A3** throughout the thesis.

List of Publications

I. A novel organic chromophore for dye-sensitized nanostructured solar cells
Daniel. P Hagberg, Tomas Edvinsson, Tannia Marinado, Gerrit Boschloo, Anders Hagfeldt and Licheng Sun
Chem. Comm. **2006**, 2245-2247.

II. Influence of π-conjugation units in organic dyes for dye-sensitized solar cells
Peng Qin, Xichuan Jang, Ruikui Chen and Licheng Sun
[a]Tannia Marinao, Tomas Edvinsson, Gerrit Boschloo and Anders Hagfeldt
J. Phys. Chem. C, **2007**, 111, 1853–1860.

III. Tuning the HOMO and LUMO energy levels of organic chromophores for dye-densitized Solar cells
Daniel P. Hagberg, Tannia Marinado, Karl Martin Karlsson, Kazuteru Nonomura, Peng Qin, Gerrit Boschloo, Tore Brinck, Anders Hagfeldt and Licheng Sun
J. Org. Chem. **2007**, 72, 9550-9556.

IV. Rhodanine dyes for dye-sensitized solar cells: spectroscopy, energy levels and photovoltaic performance
Tannia Marinado, Daniel P. Hagberg, Maria Hedlund, Tomas Edvinsson, Erik M. J. Johansson, Gerrit Boschloo, Håkan Rensmo, Tore Brinck, Licheng Sun and Anders Hagfeldt
Phys. Chem. Chem. Phys. **2009**, 11, 133-141.

V. How the nature of triphenylamine-polyene dyes in dye-sensitized solar cells affects the open circuit voltage and the electron lifetimes
Tannia Marinado, Kazuteru Nonomura, Jarl Nissfolk, Martin. K. Karlsson, Daniel P. Hagberg, Licheng Sun, Shogo Mori and Anders Hagfeldt
Accepted *Langmuir* **2009**

VI. Structural modification of organic dyes for efficient coadsorbent-free dye-sensitized solar cells
Xiao Jiang, Tannia Marinado, Erik Gabrielsson, Daniel P. Hagberg, Licheng Sun and Anders Hagfeldt
Submitted to *J. Phys. Chem. C* **2009**

VII. Surface molecular quantification and photoelectrochemical characterization of mixed organic dye and coadsorbent layers on TiO_2 for dye-sensitized solar cells
Tannia Marinado, Maria Hahlin, Xiao Jiang, Maria Quintana, Erik M. J. Joahansson, Erik Gabrielsson, Daniel P. Hagberg, Gerrit Boschloo, Shaik M. Zakeeruddin, Michael Grätzel, Hans Siegbahn, Licheng Sun, Anders Hagfeldt and Håkan Rensmo
Manuscript

[a] Shared first author

Publications related to but not included in the thesis

VIII. **Molecular engineering of organic chromophores for dye-sensitized solar cell applications**
Daniel P. Hagberg, Jun-Ho Yum, Hyojoong Lee, Filippo De Angelis, Tannia Marinado, Karl Martin Karlsson, Robin Humphry-Baker, Licheng Sun, Anders Hagfeldt, Michael Grätzel and Mohammad K. Nazeeruddin
J. Am. Chem. Soc. **2008**, 130, 6259-6266.

IX. **A comparative studie of a polyene-diphenylaniline dye and $Ru(dcbpy)_2(NCS)_2$ in electrolyte-based and solid-state dye-sensitized solar cells**
Gerrit Boschloo, Tannia Marinado, Kazuteru Nonomura, Thomas Edvinsson, Alexander G. Agrios, Daniel P. Hagberg, Licheng Sun, Maria Quintana, Chedarambet S. Karthikeyan, Mukundan Thelakkat and Anders Hagfeldt
Thin Solid Films, **2008**, 7214-7217.

X. **A Light-resistant organic sensitizer for solar-cell applications**
Jun-Ho Yum, Daniel P. Hagberg, Soo-Jin Moon, Karl Martin Karlsson, Tannia Marinado, Licheng Sun, Anders Hagfeldt, Mohammad K. Nazeeruddin and Michael Grätzel
Angew. Chem. Int. Ed. **2009**, 48, 1576-1580.
Angew. Chem. **2009**, 121, 1604-1608.

XI. **Organic chromophore-sensitized ZnO solar cells: Electrolyte-dependent dye desorption and band-edge shifts**
Maria Quintana, Tannia Marinado, Kazuteru Nonomura, Gerrit Boschloo and Anders Hagfeldt
J. Photochem. Photobiol, A: Chemistry, **2009** (202) 2-3, 159-163.

XII. **Effect of anchoring group on electron injection and recombination dynamics in organic dye-sensitized solar cells**
Joanna Wiberg, Tannia Marinado, Daniel P. Hagberg, Licheng Sun, Anders Hagfeldt and Bo Albinsson
J. Phys. Chem. C, **2009**, 113, 3881-3886.

XIII. **The effect of UV-irradiation (under short-circuit condition) on dye-sensitized solar cells sensitized with a Ru-complex dye functionalized with a (diphenylamino)styryl-thiophene group**
Kazuteru Nonomura, Yunhua Xu, Tannia Marinado, Daniel Hagberg, Rong Zhang, Gerrit Boschloo, Licheng Sun and Anders Hagfeldt
Photochem. Photoenergy , **2009,** doi:10.1155/2009/471828.

XIV. **Highly efficient organic sensitizers for solid-state dye-sensitized solar cells**
Son-Jin Moon, Jun-Ho Yum, Robin Humphry-Baker, Karl Martin Karlsson, Daniel P. Hagberg, Tannia Marinado, Anders Hagfeldt, Licheng Sun, Michael Grätzel and Mohammad K. Nazeeruddin
J. Phys. Chem. C, **2009**, 113, 16816-16820.

XV. **Symmetric and unsymmetric donor functionalization. Comparing structural and spectral benefits of chromophores for dye-sensitized solar cells**
Daniel. P. Hagberg, Xiao Jiang, Erik Gabrielsson, Mats Linder, Tannia Marinado, Tore Brinck, Anders Hagfeldt and Licheng Sun
J. Mater. Chem. **2009** DOI: 10.1039/b911397p

Participation in conferences and research visits

i. **16th International conference on photochemical conversion and storage of solar energy**, Uppsala, Sweden. July 22-26, **2005**.

ii. **Research visit**. State Key Laboratory of Fine Chemicals, Dalian University of Technology (DUT), Dalian, China. September 1-21, **2006**.

iii. **The second international conference in semiconductor photochemistry**, Gordon University, Aberdeen, Scottland. July 23-25, **2007.**

iv. **2nd International conference on the industrialisation of dye solar cells**, DSC-IC 07, St-Gallen, Switzerland. September 11-13, **2007.**

v. **17th International conference on photochemical conversion and storage of solar energy**, Sidney, Australia. July 24-25, **2008**.

vi. **Research visit**. Division of Chemistry and Materials, Shinshu University, Ueda, Japan, April 7-20, **2009**.

vii. **3rd International conference on the industrialisation of dye solar cells**, **DSC-IC 09**, Nara, Japan, April 22-24, **2009**.

viii. **Hybrid and organic photovoltaics conference**, Benidorm, Spain. May 10-13, **2009**.

Till min familj

1. Introduction

1.1. Using solar energy - Solar cells

At present the world is in great need of technologies providing renewable energy. The challenge is how to meet the increasing global energy consumption without sacrificing our future environment. More solar energy strikes the earth in one hour than all the energy consumed on the earth in a year.[1] Solar energy provides clean abundant energy and is therefore an excellent candidate for a future environmentally friendly energy source. Solar cells are devices that are able to convert solar energy into electrical energy. The aim of solar cell research is to increase the solar energy conversion efficiency at low cost to provide a cost-effective sustainable energy source.

There are various types of solar cells and some of them will be mentioned here. Crystalline silicon solar cells are the most widely used solar cells and dominate the market at present. Stable devices and the possibility to use knowledge and technologies from the microelectronics industry have given crystalline solar cells a leading role among other types of solar cells. To meet the demand of reducing material and purification costs thin film solar cells have been developed. Thin film solar cells are based on thin layers of various semiconductor materials such as amorphous silicon, cadmium telluride (CdTe), copper indium gallium diselenide (CIGS). Even though the thin film solar cell requires less material, the complex production processes of the different combinations of rare materials are expensive and may limit a future large-scale production.

An alternative solar cell technology is the dye-sensitized solar cell (DSC),[b] which is the subject of the present thesis. DSCs consist of a dye-sensitized semiconductor material, often titanium dioxide (TiO_2), where dye molecules attached onto the semiconductor act as light absorbers. This is in contrast to the solar cells mentioned above where the light is absorbed by the semiconductor material itself.

In 1972 Honda and Fujishima reported that water splitting was possible by illumination of TiO_2.[2] The large bandgap of TiO_2 yielded quite low conversion efficiencies due to the ability to absorb photons only in the ultraviolet region. Gerischer and Memming further showed that the enhanced light harvesting could be attained by sensitizing flat semiconductor electrodes.[3,4] In 1976 Tsubomura et al. presented a working dye-sensitized porous zinc oxide photocell using a platinum counter electrode and a iodide/triidodie redox couple.[5] In 1985, Desilvestro et al. used a rough TiO_2 electrode sensitized with a ruthenium complex yielding enhanced photo conversion efficiency.[6] The breakthrough for DSCs occurred in 1991,[7] when Grätzel and O'Regan managed to build a, 7.1 %, photovoltaic device based on a dye-sensitized 10 μm thick porous TiO_2 electrode. DSC research has since then expanded and today there is a quite large research community trying to understand and improve the photovoltaic efficiency of the DSC.

The record efficiency of a DSC (single cell) has been reported to be 7 % in 1991, 10.4 % in 1993, 11.1 % in 2006 and 12 % have been presented in conferences this year.[7-10] In recent years significant investigation has been performed on a module (multi cell) scale by institutes and companies, such as Sharp, Panasonic and Sony.[10-12] In 2007 a

[b] The Dye-sensitized solar cell is also called "The Grätzel cell" after Professor Michael Grätzel, at the Swiss Federal Institute of Technology at Lausanne, Switzerland, responsible for the breakthrough of DSCs.

DSCs manufacturing facility, G24 innovations, started up with a capacity of 25 MW located in Cardiff, Wales. The DSC technology may be considered among the most advanced solar cell techniques on the verge of commercialization. DSC is an appropriate candidate in the view of materials and production cost and device performance trade off. In the near future, the venture of DSCs as a competitive technology will thus be revealed.

1.2. The dye-sensitized solar cell (DSC)

The dye-sensitized solar cell, DSC, consist of a photo active working electrode and a counter electrode contacted by a liquid redox electrolyte, see Figure 1.2.1. The main components in a DSC are,

- Working electrode (WE): porous nanostructured TiO_2 attached to a conducting substrate, often fluorine-doped tin oxide (FTO).
- Counter electrode (CE): platinized conducting substrate.
- Light-absorbing layer: adsorbed sensitizing dye.
- Redox system (charge conducting medium): liquid electrolyte containing the redox couple iodide/triiiodide (I^-/I_3^-).

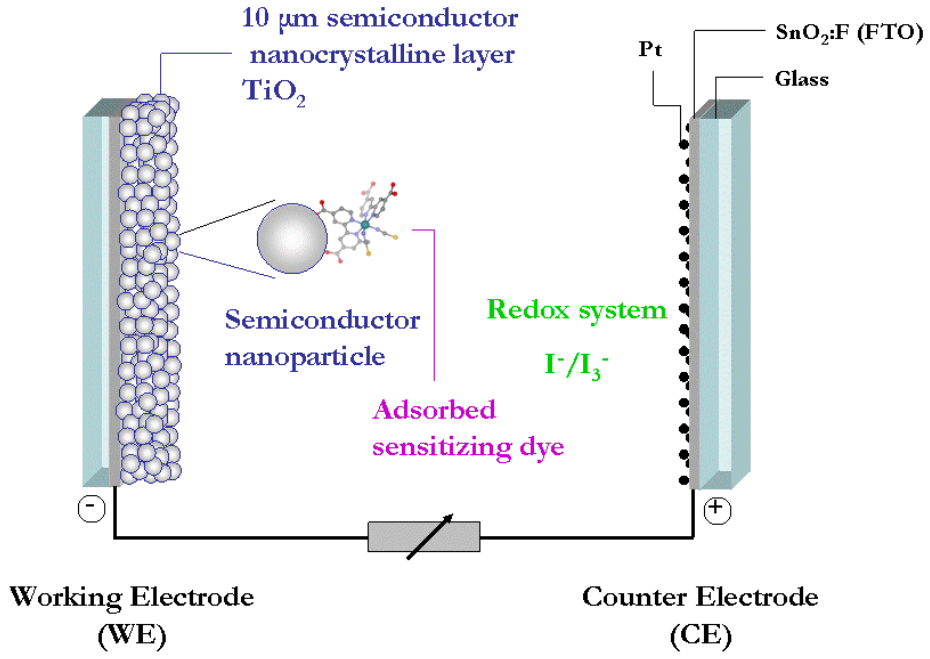

Figure 1.2.1 Schematic illustration of the DSC.

1.2.1. The working principle of DSCs

The aim of any solar cell device is to convert solar light energy into electrical energy. The working principle of DSCs involves some key processes, *light absorption*, *charge separation* and *charge collection*; it is illustrated in Figure 1.2.2.

Under sunlight illumination the dyes will absorb photons (light) and become photoexcited, step [1]. The adsorbed dye molecules will inject electrons into the TiO_2

working electrode and thus become oxidized, step [2]. Charge separation is attained across the semiconductor interface where an electron is located in the TiO_2 and a hole is located in the oxidized dye molecule. The electrons will then percolate through the porous network of TiO_2 and eventually reach the back contact of the working electrode where charge collection and charge extraction occurs, step [3]. The extracted charge can subsequently perform electrical work in the external circuit and eventually return to the counter electrode, where reduction of the redox mediator takes place, step [4]. The liquid redox electrolyte will complete the circuit by reducing the oxidized dye, step [5].

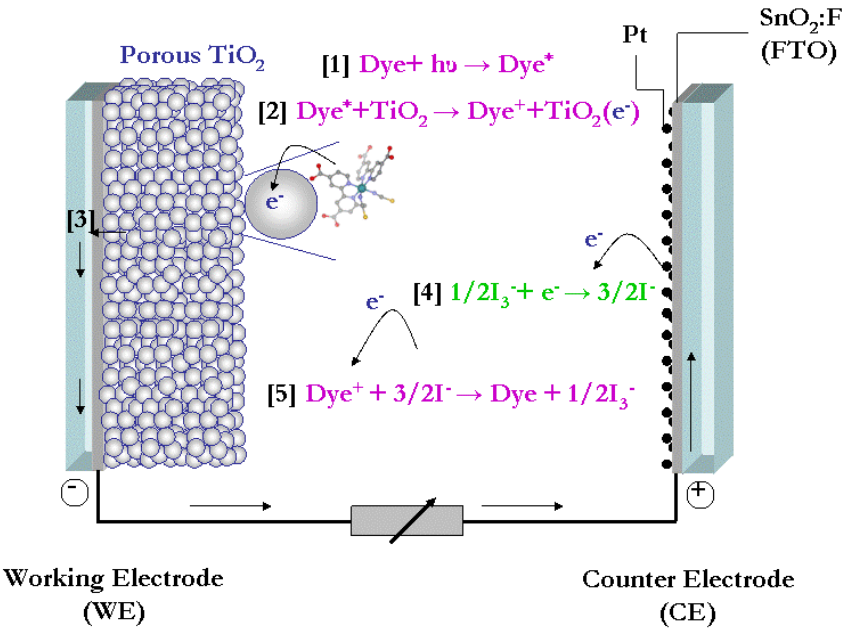

Figure 1.2.2 Schematic illustration of the electron flow in an operating DSC. [1] Dye excitation, [2] electron injection from photoexcited dye into TiO_2, [3] charge collection at working electrode, [4] reduction of triiodide at counter electrode and [5] regeneration (reduction) of the oxidized dye.

1.3. The components of the DSCs

1.3.1. The working electrode

The working electrode in a DSC consists of a nanostructured semiconductor material, attached to a transparent conducting substrate. The most extensively utilized semiconductor material is TiO_2 (anatase bandgap 3.2 eV), although other semiconductor materials such as ZnO,[13-15] SnO_2[16] and NiO[17,18] can also be used. TiO_2 is an inexpensive, non-toxic abundant material widely used in paint, sunscreens and food.

The electrode consists of interconnected nanoparticles, in the size of 15-30 nm. They form a transparent porous (~ 50 % porosity) electrode, with a typical thickness of 1-15 μm. The deposition methods predominantly used for the film preparation are screen printing and doctor blading.[c] Both techniques involve the deposition of viscous colloidal TiO_2 paste[19] onto a substrate prior to the sintering process. Sintering is usually

[c] Doctor blading: a smooth glass rod spreads a viscous colloid on a glass surface (FTO) to a specific thickness with help of a tape frame, the solvent is thus evaporated and the tape is removed.

performed at temperatures of 450-500 ºC. The high temperature results in electrical interconnection between the nanoparticles and ultimately forms the nanostructured porous electrode. The dye sensitization is performed by immersing the electrode into a dye solution for a given time. If compared to a flat electrode, the porous nature of the working electrode provides a significantly enhanced surface area. This allows a high concentration of the absorbed sensitizing dye and thus an efficient light harvesting.

1.3.2. The redox mediator

At present the most successful redox mediator used in DSCs consists of a liquid electrolyte containing the redox couple iodide/triiodide. The charge transport between the electrodes occurs by diffusion of iodide/triiodide, completing the circuit of the solar cell device. The redox potential of the redox couple will dictate the electrochemical potential at the platinized counter electrode. The reactions consist of the reduction of the oxidized dye by iodide producing triiodide at the working electrode and reduction of triiodide producing iodide at the counter electrode.

The redox electrolyte consists of iodides, iodine and often additional additives. Different iodides provide the presence of different-sized cations such as lithium (Li^+), tetrabutylammonium (TBA^+) and different imidazolium (Im^+) counterions. Some examples of extensively used additives are 4-tertbutylpyridine (4-TBP) and guanidiniumthiocyanate (GuSCN). The different additives will affect the energetics of the semiconductor/dye/electrolyte interface. The effect of 4-TBP will be discussed in section 3.8. The success of the iodide/triiodide redox couple originates in a suitable redox potential in the context of DSC that provides efficient dye regeneration. Electrons in TiO_2 shows modest electron recombination with the redox couple in comparison to many alternative charge mediators. The cause of the slow electron recombination reaction is debated. The reasons may be the nature of the negative oxidized species (I_3^-) and the two electron-transfer reaction of the redox reaction involving several intermediate steps.[20,21]

At present a non-volatile redox mediator is desired to avoid leakage and instability problems inherent to the liquid system. Ionic liquids are a promising electrolyte alternative providing advantages such as non volatility, high thermal and chemical stability and excellent ionic conductivity. However, DSCs based on highly viscous ionic liquids often result in mass transport limitations restraining the photovoltaic performance in particular at high light intensities.[22]

A solid state hole conductor is an alternative charge transport material where the charge transport occurs via a hole hopping mechanism. The solid state hole-conducting material spiro-MeOTAD has resulted in device efficiencies of 5.1 %.[23,24] Problems concerning solid state hole conductors discussed at present are enhanced charge recombination, pore filling problems and limited charge mobilities.[25,26] Up to date, a superior redox couple is yet to be found. An alternative redox couple could provide a more positive redox potential and thus a higher open circuit voltage for the solar cell. To find a superior redox couple is one of the main challenges for future DSC research.

1.3.3. The sensitizing dye[d]

The sensitizing dye is responsible for the capture of sunlight in DSCs. Due to the central role of the sensitizing dye in DSCs much effort is invested in the synthesis and investigation of novel dyes. The dyes used in DSCs can be divided into two categories: metal based complexes and metal-free organic dyes. The photovoltaic performances of ruthenium based complexes are still unsurpassed (11-12 %). Some of the superior ruthenium dyes up to date are **N3**,[8] **N719**,[27] **Black dye**,[28,29] **K19**[30] and **K77**.[31] **N3** is the pioneer dye reported in 1993 by Nazeeruddin et al. and is depicted together with two other dyes also reported by the same group, see Figure 1.3.1. The latter are hydrophobic alternatives that have shown improved light-harvesting efficiencies and long time stabilities.[30,31]

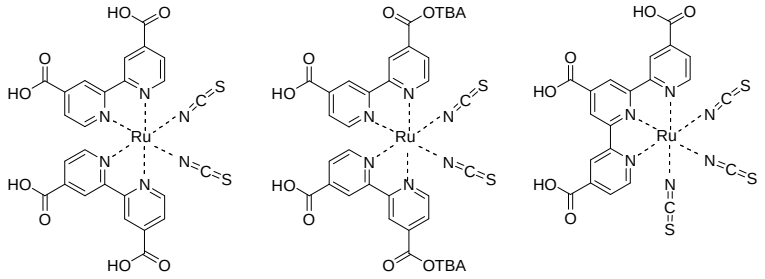

Figure 1.3.1 The molecular structure of (left) **N3**,[8] (middle) **N719**[27] and (right) **Black dye**.[28]

From the year of 2000 the interest in organic dyes has steadily increased yielding record efficiencies from 4 % to 9 % for DSCs based on fully organic dyes.[32-42] The recent advance in molecular design of organic dyes has been thoroughly reviewed elsewhere.[43] The main advantages of organic dyes are the short established synthetic routes enabling fairly easy dye structural modifications. In addition, organic dyes usually show significantly higher extinction coefficients compared to metal-based complexes. As a consequence organic dyes have quite narrow absorption bands in comparison to metal-based dyes. The high extinction coefficients of organic dyes reduce the amount of dye required for efficient light harvesting and make organic dyes suitable for thin TiO_2 films required for solid-state DSCs.

The structure of three well investigated organic dye families, triphenylamine (TPA), coumarin and indoline, are shown in Figure 1.3.2.

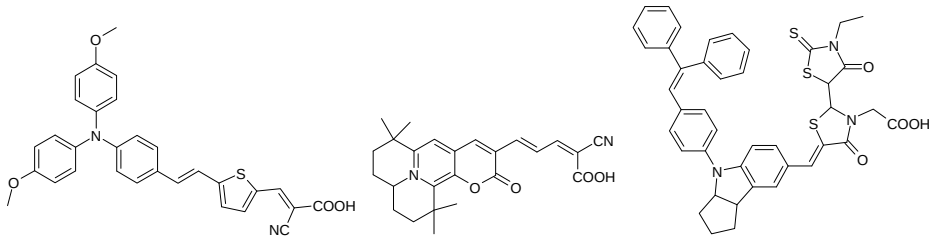

Figure 1.3.2 The molecular structure of (left) TPA based **D9**,[39] (middle) coumarin based **NKX-2311**[33] and (right) indoline based **D149**.[35,36]

[d] Semiconductor sensitization: extension of the photosensitivity towards longer wavelengths where the semiconductor itself is not sensitive to light excitation. Memming, R. *Semiconductor Electrochemistry*, Wiley-VCH Verlag GmbH, Weinheim, **2001.**

In this thesis several novel organic dyes were studied as sensitizers in DSCs. The development of new organic dyes for DSC application started with the triphenylamine (TPA) donor unit of the dye **L2** described in *Paper I*. The structure of the dye is a hybrid of, at the time, already existing similar organic dyes. The **L2** dye revealed the great potential of TPA-based dyes for DSCs. TPA-based dyes are now, three years later, dominating the research of organic dyes for DSCs application.[43]

1.4. Requirements for a working DSC

1.4.1. The two electrode DSC

For a solar cell to be able to generate electric power, it must convert light energy into electrical energy. The solar cell must generate a current flow (a flow of electrons) that can be transferred to energy in an external circuit. To obtain a current flow there needs to be a potential difference between the two electrodes in the solar cell device providing a driving force for electrons to perform electrical work by flowing from one electrode to the other.

The electrochemical potential of the solar cell is determined by the voltage difference between the quasi-Fermi potential of electrons ($E_{F,n}/q$) at the working electrode and the redox potential $E_{pot}(I^-/I_3^-)$ at the counter electrode. The redox potential of the redox couple is considered to be unchanged whereas the Fermi level of electrons in TiO_2 will be different at dark compared to light conditions. At dark conditions, in equilibrium, there is no potential difference between the two electrodes. Under light illumination the concentration of electrons in the TiO_2 increases due to electron injection from the dye. The electrochemical potential of the electrons in TiO_2 is raised towards more negative potentials yielding the solar cell its overall potential difference and a driving force for the electrons to perform electrical work in the system. The Fermi potential of electrons is illustrated in Figure 1.4.1 for both dark and light conditions.

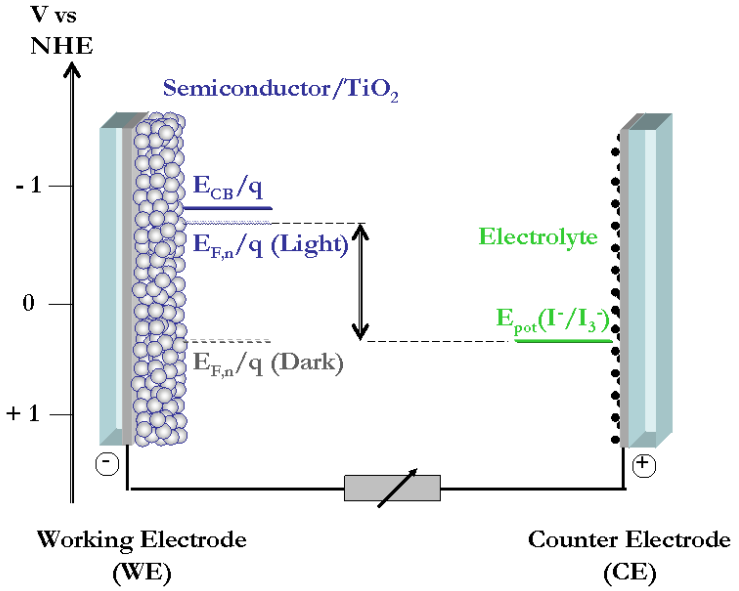

Figure 1.4.1 Illustration of the potential difference between the working and the counter electrodes in the solar cell. The quasi-Fermi level of electrons will vary with the electron concentration and hence be different at light and dark condition.

1.4.2. Energy levels in DSCs - an overview

The working principle of the DSCs relies on various interfacial electron-transfer reactions providing a pathway for the electrons in the solar cell.The existence of energetic driving force is one of the primary requirements for electron-transfer reactions to be viable.

Two important processes involving the dye are electron-transfer from the excited dye into the conduction band of the TiO_2 referred to as the *electron injection* (red arrow) and reduction of the oxidized dye by the redox mediator, the *dye regeneration* (black arrow), see Figure 1.4.2. For efficient electron injection the donating excited state of the dye, $E_{pot}(D^+/D^*)$, needs to be at more negative potentials compared to the accepting conduction band edge, E_{CB}/q of the semiconductor TiO_2. For efficient dye regeneration the redox potential of the redox mediator, $E_{pot}(I^-/I_3^-)$, needs to be at less positive potentials than the redox potential of the dye ground state, $E_{pot}(D/D^+)$.

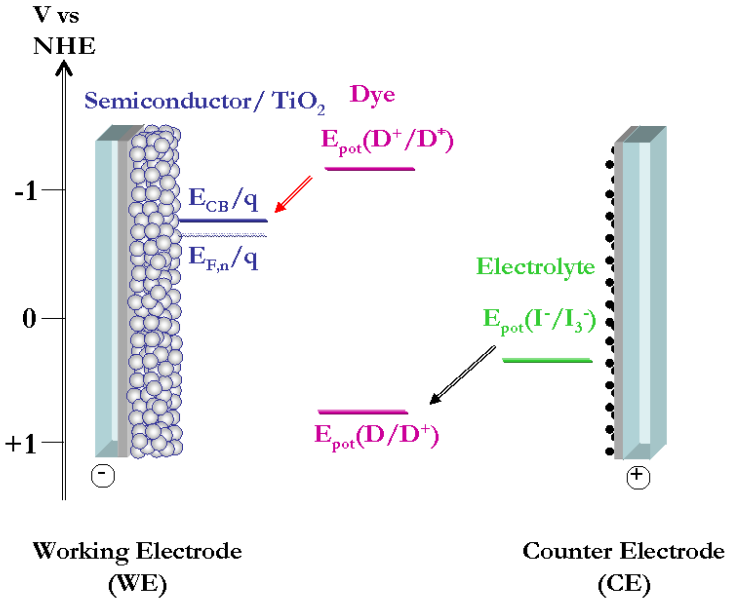

Figure 1.4.2 Illustration of suitable position of the potential for each component in DSCs. Red arrow indicates electron injection and black arrow indicates dye regeneration.

There are several interfacial electron-transfer processes in the solar cell with favorable energetics, for a well working DSCs only some of them will occur. This implies that there must be a second parameter determining the pathways of the reactions in an operating system. The second parameter is kinetics, how fast the electron-transfer occurs for the desired process in comparison to competing loss processes.

1.4.3. A matter of kinetic competition

For an electron-transfer reaction to be viable over other competing reactions it must be favored both by appropriate energetics and kinetics.

After photoexcitation of the dye an electron will be located in the dye excited state. The excited electron can either relax back to the dye ground state by radiative/non-radiative processes or be injected into the TiO_2 as illustrated by Figure 1.4.3 (a). For high electron injection efficiency the time for electron injection (τ_{inj}) should be significantly shorter than the time for de-excitation of the excited dye (τ_{exc}). The injection efficiency (Φ_{inj}) can be expressed as Equation 1.4.1. After successful electron injection the dye is oxidized and can be reduced either by electrons in TiO_2 or by the redox donor in the electrolyte as illustrated in Figure 1.4.3 b. The time for dye regeneration (τ_{reg}) should be shorter than the time to recombine (τ_{rec}) to the oxidized dye. The regeneration efficiency (η_{reg}) can be expressed as Equation 1.4.2. After electrons are injected into the TiO_2, the electrons should preferentially be transported to the back contact, where they can be extracted to perform electrical work. During the transport through the porous TiO_2 network the electrons can recombine to either the oxidized dye or to triiodide as shown in Figure 1.4.3 (c).

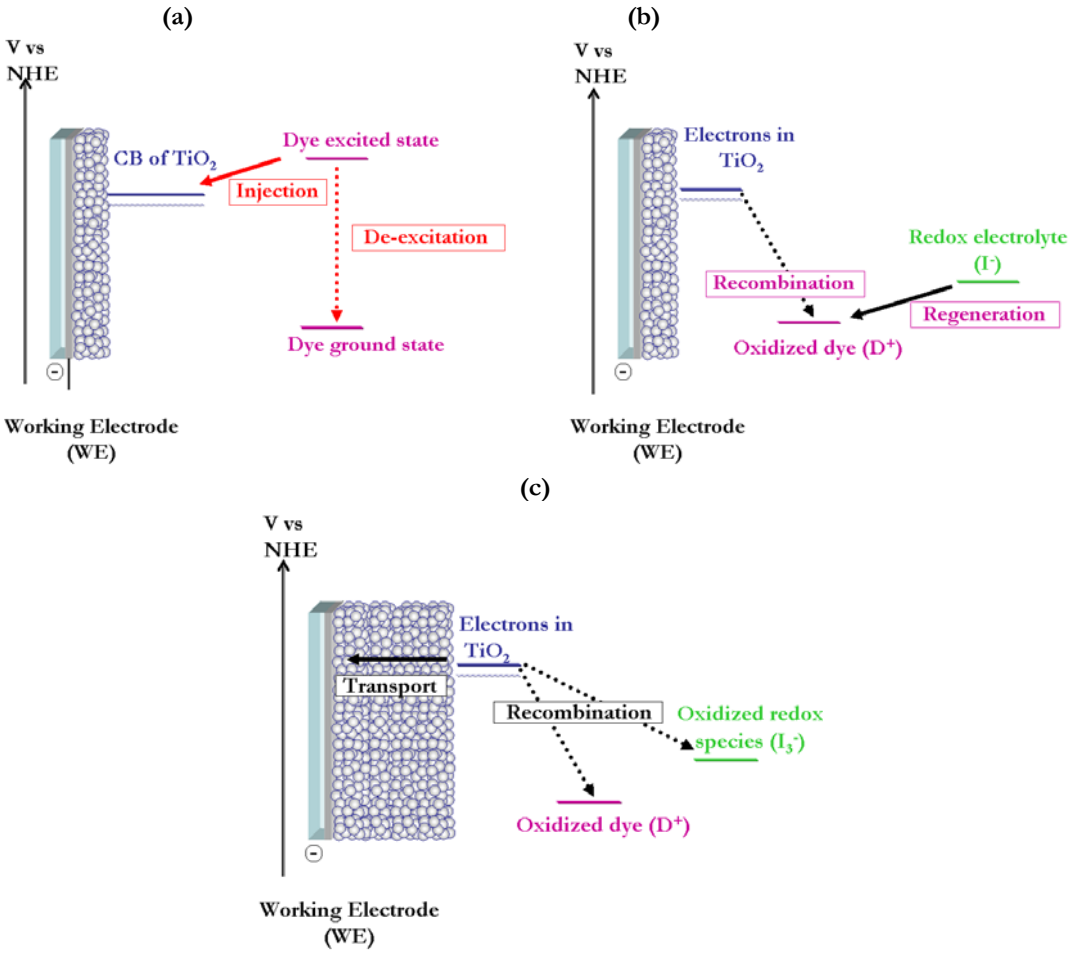

Figure 1.4.3 Illustrations of the competing processes for (a) the electron in the dye excited state, electron injection (solid arrow) into the TiO_2 or de-excitation (dotted arrow) back to the dye ground state, (b) the reduction of the oxidized dye; the dye should preferentially be reduced by iodide (solid arrow), i.e. dye regeneration and not by electrons in the TiO_2 (dotted arrow), (c) the electron situated in the TiO_2, successful electron transport reaching the back contact (solid arrow) or recombination with either the oxidized dye and/or the oxidized species in the electrolyte (dotted arrows).

These recombination reactions are referred to as losses in the system impeding the electrons from performing electrical work in the external circuit. The charge collection efficiency depends on the two competing processes, the electron transport and the electron recombination. Experimentally, the processes yield different time constants and are referred to as electron transport times (τ_{tr}) and electron lifetimes (τ_e). The charge collection efficiency (η_{cc}) can be expressed as Equation 1.4.3.

$$\Phi_{inj} = 1 - \frac{\tau_{inj}}{\tau_{exc}} \tag{1.4.1}$$

$$\eta_{reg} = 1 - \frac{\tau_{reg}}{\tau_{rec}} \tag{1.4.2}$$

$$\eta_{cc} = 1 - \frac{\tau_{tr}}{\tau_e} \tag{1.4.3}$$

The time constant of a reaction can also be given as rate constant k (s^{-1}) that is equal to the inverted time constant.

The kinetics of an electron-transfer reaction can be described by Marcus theory.[4,44] Marcus theory describes how factors such as reorganization energy (λ), driving force (ΔG) and electronic coupling (V_{DA}) affects the rate of an electron-transfer reaction. To apply this equation on the different electron-transfer processes occurring in the solar cell is non-trivial, see sections 3.5-3.7.[45]

$$k_{ET} \propto (V_{DA})^2 \exp\left(-\frac{(\Delta G^{\circ} + \lambda)^2}{4\lambda k_B T} \right) \tag{1.4.4}$$

1.4.4. Interfacial electron-transfer kinetics - an overview

The kinetics of the different processes will determine how efficiently the electrons are collected to perform electrical work. For a conventional DSC, based on a ruthenium dye, typical time constants for the different interfacial electron-transfer processes are presented in Figure 1.4.4. The electron injection has been reported to occur in less than 100 femotoseconds (fs) to 100 picoseconds (ps) depending on the experimental conditions.[46] The electron injection is significantly faster than the de-excitation of the dye that occurs in ~20 nanoseconds (ns).[46,47] The recombination of electrons in the TiO_2 with the oxidized dye or the redox electrolyte occurs in micro-milliseconds (μs-ms) and competes with the regeneration of the dye that occurs in ~ μs.[48-50] The regeneration times should be several orders faster than the recombination for an efficient solar cell. The interfacial electron-transfer kinetics varies with the nature of the components. In the view of new organic dyes, the kinetics of different processes in the solar cell is an open question.

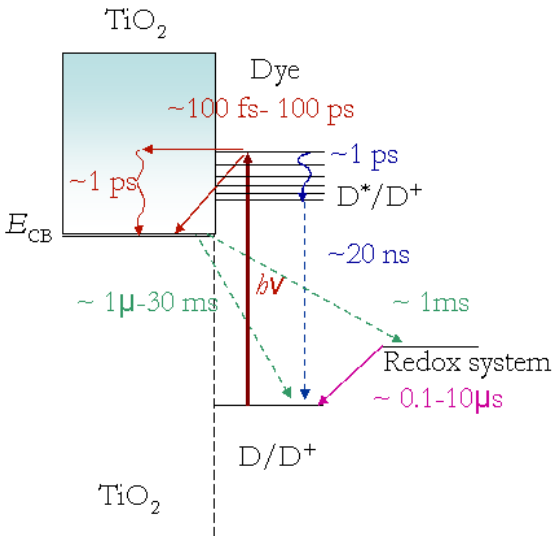

Figure 1.4.4 Illustration of the interfacial electron-transfer kinetics in DSCs based on conventional ruthenium-based dyes.

In conclusion; the important processes in the solar cell are *electron injection*, *electron transport* and *dye regeneration*. For these reactions to operate efficiently some prerequisites should be fulfilled. The processes must be energetically favorable and should have appropriate kinetics. The difference in electron-transfer kinetics is decisive for the operation of DSCs.

1.5. The semiconductor interface

1.5.1. Bulk versus nanoparticles - charge separation

The working electrode consists of nanocrystalline semiconductor TiO_2 forming the porous electrode. As compared to the bulk material, the nanocrystalline TiO_2 possesses different properties upon contact with a liquid redox electrolyte. When a bulk semiconductor comes in contact with a redox electrolyte electron-transfer occur across the interface to reach electrochemical equilibrium. As a consequence of the interfacial electron-transfer, a region on each side of the interface where the charge distribution differs from the bulk material is formed; this is known as the space-charge layer, see Figure 1.5.1. The potential difference between the interface and the bulk is referred to as band bending.

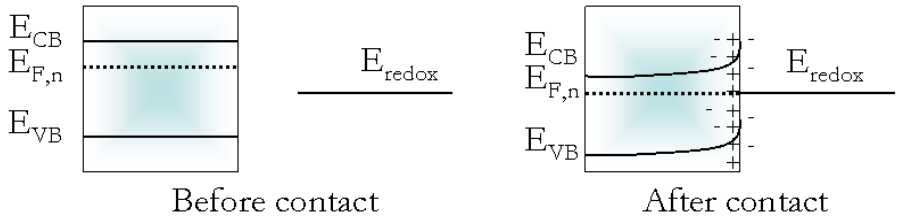

Figure 1.5.1 Illustration of a bulk n-type semiconductor (SC) before and after being contacted with a redox system with slightly lower redox potential. Upon contact, electrons will be transferred from the SC to the redox system leaving a positive space charge layer at the SC interface, band bending occurs.

The most important difference between bulk and nanostructured TiO_2 is that the approximately 20 nm anatase nanoparticles are expected to have too small charge (donor) density to form a space charge layer.[4,51] Upon light excitation of a semiconductor, bulk versus nanoparticle, an electron and a hole will be generated.

In a bulk semiconductor, further charge separation is attained due to a charge flow in the existing electrical field formed by the space charge layer; see Figure 1.5.2 (a).

In the nanoparticle, such an electrical field does not exist. However, the charge separation can still be attained with appropriate kinetics of the redox reactions of interest. In the case of photocatalysis, the desired process is for external species to undergo reduction and oxidation with the electron and hole, respectively, before the electron hole recombination occurs, see Figure 1.5.2 (b).

In a dye-sensitized TiO_2 nanoparticle, the charge separation occurs across the interface. Upon dye excitation and consequently electron injection, an electron is generated in the TiO_2, whereas the hole stays in the dye molecule (oxidized dye), see Figure 1.5.2 (c), the dye acts as a molecular diode. In the DSC, the charge separation is attained due to favorable kinetics of the electron-transfer processes across the interface. In DSC, several nanoparticles are fused together to form the porous working electrode. The electrons in the TiO_2 can either recombine across the interface with oxidized species (dye, electrolyte) or they can move to the next nanoparticle, see Figure 1.5.2 (d). Due to the absence of a space charge layer in nanostructured TiO_2 and the screening by the quite concentrated redox electrolyte, the electrons are suggested to move through the porous network by diffusion.[51,52]

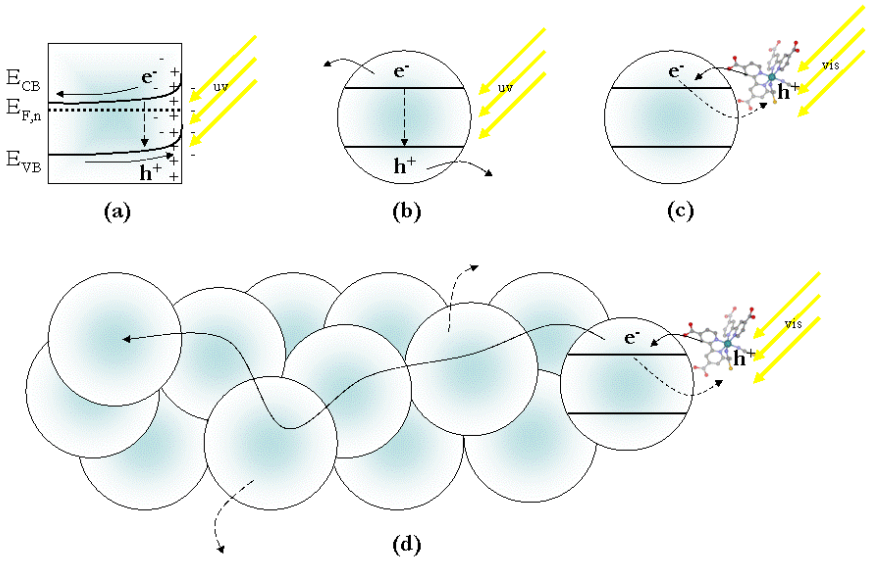

Figure 1.5.2 Illustration of how charge separation is attained in an n-type semiconductor (SC) under illumination. (a) In bulk (dimensions>>nm) SC, the charges move due to an electrical field, (b) In a SC nanoparticle (NP) (radius~ nm), the charge separation depends on the surface reaction kinetics (solid arrows) versus internal hole-electron recombination kinetics (dotted arrow). (c) In a dye-sensitized SC NP, the charge separation occurs at the interface upon electron injection in turn generating electrons in the NP and an oxidized dye. (d) In a dye-sensitized SC NP network, the generated electron can move to an adjacent NPs and further through the porous NP network. During the electron transport (solid curved arrow) it is possible for the electrons to recombine at the NP interface (dotted arrows).

1.5.2. Electron transport in TiO_2

The electron diffusion in the porous TiO_2 electrode has been measured to be several orders of magnitude lower than in bulk TiO_2.[52] Experiments show that the charge transport in mesoporous TiO_2 becomes faster with increased incident light intensity.[53] These observations have lead to suggestions of the existence of additional energy levels below the conduction band, these additional energy levels are referred to as trap states.[54,55] The origin of these trap states is still debated. Possible sources might be grain boundaries, unsaturated bonds, structure defects normally absent in the bulk material.[55] The electron transport has been suggested to occur by a trapping/detrapping-limited diffusion mechanism.[54,56]

The electrons move faster when the electron concentration in the TiO_2 is increased, i.e. by increasing the light intensity or applying a potential. How fast the electrons move will affect the transport through the porous network as well as the rate of the interfacial recombination. These two processes are referred to as electron transport times and electron lifetimes (see section 1.4.3).

1.5.3. Surface charge and TiO_2 energetics

The energy bands of TiO_2 will shift upon changes of the equilibrium of adsorbed charges.[4] For bulk TiO_2 immersed in aqueous electrolyte the flatband potential shifts with 59 mV per pH unit, due to adsorption and desorption of H^+ and OH^- groups on the surface.[4] The flatband potential is the applied potential needed obtain flat bands in a semiconductor.

In the solar cell ions can adsorb at the TiO_2 surface and thereby affect the surface charge and the TiO_2 energetics. The surface charge will differ due to the nature of the dye and/or the surrounding redox electrolyte. The electrolyte conventionally used in DSCs is non-aqueous and consists of the iodide/triiodide redox couple and a variety of ions and additives, as mentioned in section 1.3.2. Changing the nature of the electrolyte can change the position of the conduction band edge of the TiO_2.[57,58]

This property is used in the solar cell to tune the open-circuit voltage[59,60] as well as tuning the compatibility between the dye excited states and the conduction band of TiO_2, for efficient electron injection (*Paper IV*).[61] The conduction band position will be different depending on the density and the nature (positive or negative) of the adsorbed ions forming the interfacial Helmholtz layer. The position of the conduction band edge will be at more negative potentials vs. NHE in the presence of negative adsorbed ions and more positive in the presence of positive adsorbed ions.

If applying a negative potential on TiO_2, the current generation will occur at potentials in agreement with the conduction band edge position of the TiO_2. In the presence of the small adsorptive lithium cation (Li^+) the surface will be charged positively compared to in the presence of the less adsorptive cation tetrabutylammonium (TBA^+).[57] The positively charged surface in the case of Li^+ will lead to a positive conduction band edge shift compared to the case of TBA^+, as illustrated in Figure 1.5.3. Different TiO_2 conduction band edge positions will result in generation of dark current at different potential onsets, as shown in Figure 1.5.4.

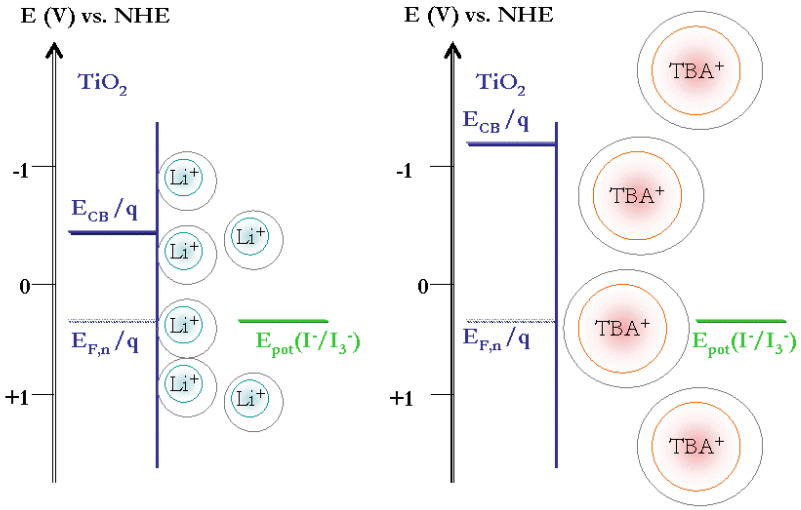

Figure 1.5.3 The different conduction band edge positions of TiO_2 in the presence of two different-sized cations, the adsorptive lithium (Li^+) and the less adsorptive tetrabutylammonium (TBA^+). The figure illustrates short-circuit conditions.

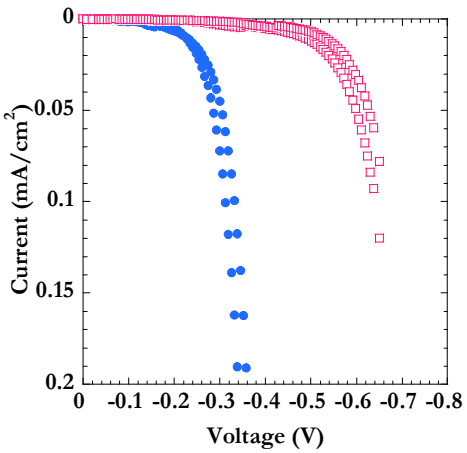

Figure 1.5.4 Dark current-voltage characteristics of a cell based on 0.7 M LiI, 0.05 M I_2 (filled spheres) and 0.7 M TBAI, 0.05 M I_2 (empty squares), respectively, in acetonitrile. The onset of the (dark) current generation is more positive for the case a small adsorptive cation as Li^+.

1.5.4. TiO_2 and the quasi-Fermi level of electrons

The charge separation achieved in dye-sensitized solar cell occurs at the interface and provides an enhanced electron concentration in the TiO_2. The majority of the charge carriers in DSCs are electrons and will therefore govern the nature of the semiconductor, the semiconductor is said to be n-doped (n as in negative). Taking into account the effective density of states in the TiO_2 conduction band and the probability of occupation of these states, the Fermi level for electrons is given by:[62]

$$E_{F,n} = E_{CB} + kT \ln\left(\frac{n_{CB}}{N_C}\right) \qquad (1.5.1)$$

E_{CB} is the conduction band energy, n_{CB} is the electron concentration in the conduction band, N_c is the effective density of conduction band states.[63] The voltage of the solar cell can therefore be expressed as:

$$V_{cell} = \frac{E_{F,n}}{q} - \frac{E_{\mathrm{Re}\,dox}}{q} \qquad (1.5.2)$$

The balance between the E_{CB} and the $E_{F,n}$ will determine the maximum attainable open-circuit voltage. The E_{CB} will be determined by the interfacial charge. The position of the $E_{F,n}$ will depend on both the position of E_{CB} and the total concentration of electrons in the TiO_2.

1.6. The aim of the thesis

The aim of the thesis was to develop and study the performance of a new generation of organic dyes for DSC application within the Centre of Molecular Devices (CMD) at The Royal Institute of Technology, KTH. In collaboration with organic chemists, new organic molecules were designed and studied as sensitizers in the solar cell. The crucial role of the sensitizing dye is to harvest as much visible light as possible. The task consisted of structural modification of the dyes to enable enhanced absorbance in the visible region. The improved absorption properties were attained fairly easily by different structural modifications.

On the other hand, the behavior of the novel dyes integrated in the DSC showed less predictive photovoltaic results. The challenge consisted of finding the limiting position of the dye energetics without sacrificing the operation of the vital electron-transfer processes related to the dye. The core of this thesis is the identification of the processes and properties limiting the performance of the DSC device. The overall aim of this thesis is to formulate improved guidelines for further development of organic dyes for DSCs.

2. Experimental

2.1. Characterization methods of complete devices

The relevant techniques used for dye and solar cell characterization are described in the present section. Techniques used to characterize the complete solar cell device are very important since the properties of all components are dependent on the complex interplay arising in a complete device. The techniques used provide appropriate illumination intensities close to real operation conditions of a solar cell. Additional techniques are used for characterization of the dyes in solution and when adsorbed on TiO_2 films. The combination of results obtained for the complete devices as well as for the individual components is utilized to indentify and understand the role of novel organic dyes in DSCs.

2.1.1. Synthesis of organic dye

The synthesis and NMR characterization of the dyes used in this thesis, is not included in the discussion here, and has been published in the different papers and also recently in the PhD thesis of Hagberg.[64]

2.1.2. Current-voltage characteristics

The solar cell efficiency is determined by its current-voltage (JV) characteristics under standard illumination conditions. A standard solar spectrum of air mass 1.5 (AM 1.5) with an intensity of 1000 W/m^2 also referred to as 1 sun, is used for solar cell characterization. The AM 1.5 spectrum corresponds to sunlight that has path through the atmosphere 1.5 times longer than when the sun is directly overhead.[62] The sunlight will be attenuated differently by the earth atmosphere dependent on the incident radiation angle. In the lab, the illumination conditions are provided by a calibrated lamp source.

The current-voltage characteristics are monitored under illumination by varying an external load from zero load (short-circuit condition) to infinite load (open-circuit condition). The photovoltaic performance can be illustrated by a JV-curve, see Figure 2.1.1.

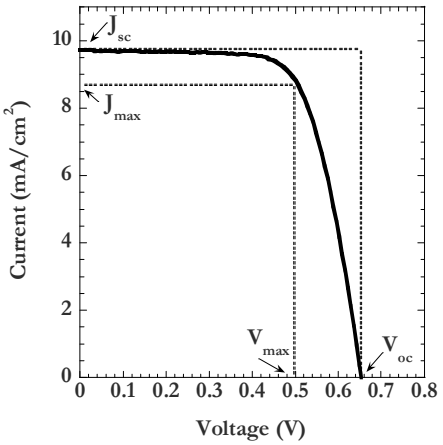

Figure 2.1.1 Current-voltage characteristics of a DSC illustrating short-circuit current (J_{sc}), open-circuit voltage (V_{oc}), current at maximum power point (J_{max}) and voltage at maximum power point (V_{max}).

The maximum power generated is when the product of the current and voltage is maximum, since the electrical power is given by current (J) times voltage (V), i.e P=JV. The degree of the squared shape of the JV-curve is given by the fill-factor (FF), Equation 2.1.

$$FF = \frac{J_{power-\max} \cdot V_{power-\max}}{J_{sc} \cdot V_{oc}} \tag{2.1}$$

The solar cell efficiency is the ratio between the power generated and power of the incident light, see Equation 2.2.

$$\eta = \frac{P_{out}}{P_{in}} = \frac{J_{sc} \cdot V_{oc} \cdot FF}{P_{in}} \tag{2.2}$$

The current-voltage characteristics can also be monitored at dark conditions. The difference between light and dark measurement is that in light, the recombination current (also called dark current) is counter balanced by the photocurrent, reaching at open circuit conditions when both currents are equal and no net current is longer extracted. At voltages higher than open circuit conditions ($V>V_{oc}$) the net current is dominated by the dark current and is going in the opposite direction.

The dark current-voltage characteristics give information exclusively about the recombination to the redox electrolyte.
Light and dark current-voltage characteristics are illustrated in Figure 2.1.2.

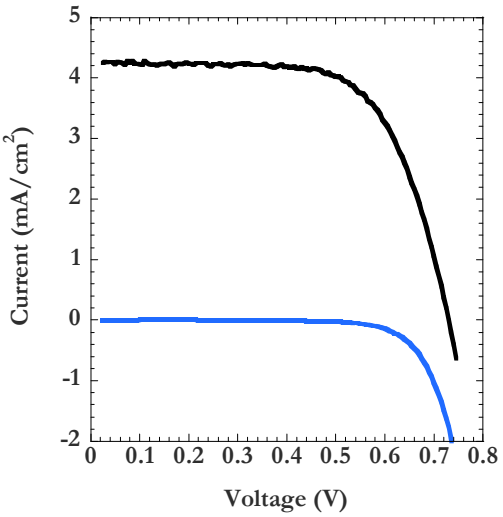

Figure 2.1.2 Light and dark current-voltage characteristics of a DSC.

2.1.3. Incident photon to current conversion efficiency

Incident photon to current-conversion efficiency (IPCE), reveals how efficiently light of a specific wavelength is converted to current, see Equation 2.3.

$$IPCE = \frac{\frac{h \cdot c}{\lambda} \cdot \frac{J_{sc}(mAcm^{-2})}{q}}{P_{in}(mWcm^{-2})} = \frac{1240 \cdot J_{sc}(mAcm^{-2})}{\lambda(nm) \cdot P_{in}(mWcm^{-2})} \tag{2.3}$$

Where h is Planck constant, c is the speed of light, λ is the wavelength of the incident light, P_{in} is the intensity of the incident light and q is the elementary charge.

The APCE (Absorbed photon to current conversion efficiency) reveals how efficient the numbers of absorbed photons are converted into current; the IPCE and APCE are related trough the LHE (Light harvesting efficiency), transmittance (T) and absorbance (A) according to:

$$\begin{aligned} APCE(\%) &= \frac{IPCE(\%)}{LHE(\%)} \cdot 100 \\ LHE &= 1 - T \\ T &= 1 - 10^{-A} \end{aligned} \tag{2.4}$$

If the amount of dye present on the surface is enough to yield close to 100% LHE, the IPCE and the APCE will be equal. The factors determining the IPCE can be expressed as follows:

$$IPCE(\%) = LHE \cdot \Phi_{inj} \cdot \eta_{reg} \cdot \eta_{cc} \tag{2.5}$$

Where Φ_{inj}, η_{reg}, η_{cc} are the quantum yield of charge injection, dye regeneration and charge collection efficiency, respectively (see Equations 1.4.1-1.4.3).

2.1.4. Charge extraction

To obtain the relation between charge (Q) and open-circuit voltage (V_{oc}), charge extraction measurements are performed. This is a very important relation since it provides information about how the Fermi level of electrons depends on the electron concentration in the TiO_2 (see Equations 1.5.1-1.5.2). Any alteration of this relation indicates that the energetics of the TiO_2 has changed.

Practically it is performed by measuring the open-circuit voltage at a certain light intensity, the light is then turned off and the cell is set to short-circuit conditions; the current is thus integrated over time to obtain the amount of accumulated charge in the film.[65]

2.1.5. Electron lifetimes at open circuit

The electron lifetime measurement provides information about the electron recombination process in the solar cell. At open circuit the voltage will be determined by the balance between electron injection and electron recombination since no charge is extracted at open circuit. By monitoring how the photovoltage responds upon a change in light intensity it is possible to obtain information about the electron recombination. By only inducing a small light change a linear response can be obtained.

Practically this is performed by illuminating the solar cell under open-circuit conditions by a small (< 10%) light intensity illumination under bias light. The small modulation induces a small photovoltage response that normally follows a single exponential decay, see Equation 2.6.[60,66]

The photovoltage decay yields a time constant that is the average time for the electrons to recombine, this time constant is referred to as the electron lifetime. The measurement is performed at several light intensities yielding a range of electron lifetimes at different light intensities.

$$V_{oc} = V_{oc,0} + \Delta V \exp(-t/\tau_e) \tag{2.6}$$

2.1.6. Electron transport times at short circuit

The electron transport measurements provide information of how fast the electrons are transported in the porous TiO_2 film. At short circuit conditions the majority of the injected electron will be extracted at the back contact, a charge collection efficiency, η_{cc} (see section 1.4.3), of unity is expected for a well working DSCs. Deviation from this generalized behavior is encountered for alternative material components such as novel dyes and redox mediators. By monitoring how the photocurrent responds upon a change in light intensity it is possible to obtain information about the electron transport.

The solar cell is illuminated under open-circuit conditions by a small light intensity illumination under bias light. The small modulation induces a small photocurrent response[60,66] that normally follows a single exponential decay, see Equation 2.7. The photocurrent decay yields a time constant that is the average time for the electrons to move in the porous system. This time constant is referred to as the electron transport time. The measurement is done at several light intensities yielding a range of electron transport times at different light intensities.

$$J_{sc} = J_{sc,0} + \Delta J \exp(-t/\tau_{tr}) \tag{2.7}$$

2.1.7. Measured parameters used in this thesis

As mentioned in section 1.5.2 the transport times and electron lifetimes will vary with light intensity, i.e. with the electron density in TiO_2. Therefore it is important to compare these times under relevant and comparable conditions. How to measure and compare these parameters is not straightforward and are being extensively discussed at the moment.

The charge collection efficiency, η_{cc}, (Equation 1.4.3) is of interest and can be estimated for short circuit conditions by combining electron transport times, extracted

charge at short-circuit, electron lifetimes and charge extraction at open circuit measurements (*Paper IV*, Supporting information). A deviation from charge collection efficiency of unity may lead to reduced short-circuit currents/IPCE.

In the present thesis, the influence of different novel dyes was investigated. The presence of the dye at the surface may alter the charge-voltage relation, transport times and electron lifetimes, respectively. It was noticed that the influence of the dye on the charge voltage relations and transport time was negligible whereas the electron lifetimes appeared to have pronounced dye dependence. The electron lifetimes between different samples must be compared under comparable charge densities in the working electrode. By measuring the extracted charge as function of open-circuit voltage for different sample, it is possible to combine these with the electron lifetimes as function of open-circuit voltage. If no alteration of the charge-voltage relation was found, the electron lifetime was normally plotted directly against the open-circuit voltage.

2.2. General characterization methods

2.2.1. Electrochemistry

Electrochemistry provides information about the dye ground state oxidation potentials in solution and when adsorbed onto TiO_2. Cyclic voltammetry (CV) and Differential pulse voltammetry (DPV) was performed with 0.1 M tetrabutylammonium hexafluorophosphate ($TBAPF_6$) in acetonitrile as supporting electrolyte. A platinum working electrode, platinum counter electrode and a Ag/Ag^+ reference electrode were normally used. The system was internally calibrated with ferrocene/ferrocenium (Fc/Fc^+). The cyclic voltammograms of the **L0** (*Paper III* and *V*) and **D21L6**[41] are depicted in Figure 2.2.

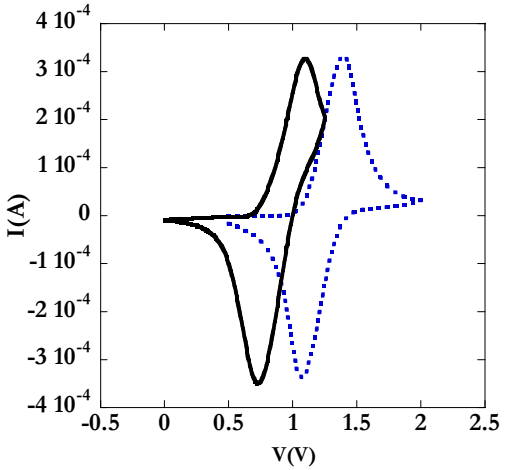

Figure 2.2.1 Comparison of the cyclic voltammograms of dye sensitized FTO/TiO_2 with **L0**, used in *Papers III* and *V* (dotted line) and **D21L6**[41] (solid line). Supporting electrolyte: 0.1 M $TBAPF_6$ in 3-MPN, scan rate: 5 mV/s, electrode area: 0.25 mm^2 and thickness: 1 μm.

2.2.2. Optical characterization

Absorption spectroscopy was used to identify the absorption properties of the dyes in solution and when adsorbed onto TiO_2. The UV-vis absorption spectra were measured on a Lambda 750 spectrophotometer by using a 1x1 cm quartz cuvette. Emission measurements on the dyes in solution were performed on a Cary Eclipse fluorescence spectrophotometer.

2.2.3. Vibrational spectroscopy

The vibrational modes of the anchoring group of the dye were studied by means of IR spectroscopy. Measurements were performed both on the dye powder and on the dye when adsorbed onto TiO_2. A Bio-Rad FTS375C IR spectrometer with Near-IR accessory was used to obtain IR spectra of the sensitizer in KBr (1:100) solid pellets. The ATR data were obtained using a Perkin Elmer Spectrum FTIR 2000 spectrometer, with a Speac Golden gate accessory crystal.

2.2.4. Photoinduced absorption (PIA)

Photoinduced absorption (PIA) spectroscopy is used to study dye-sensitized TiO_2 films under intensities comparable to sunlight.[67] In PIA measurements the transient absorption spectrum of the oxidized dye can be followed in the absence and presence of redox electrolyte giving qualitative information on the dye regeneration. Any restrictions concerning the dye regeneration will appear as spectral evidence of the surviving oxidized dye in the presence of the redox electrolyte. The PIA spectra are shown in Figure 2.2.1 for the linker series (**L0**-**L4**) when adsorbed on TiO_2 films on microscopic glass in air.

PIA experiments were performed using white probe light provided by a tungsten-halogen lamp and superimposed on-off modulated light (450 nm or 530 nm) for excitation. The transmitted probe light was focused onto a monochromator and detected by an UV-enhanced silicon photodiode connected to a current amplifier and lock-in amplifier. PIA measurements were performed slightly above room temperature (25-28 ºC), the samples used were dye-sensitized TiO_2 films on microscope glass in air or with a drop of electrolyte and a cover glass.

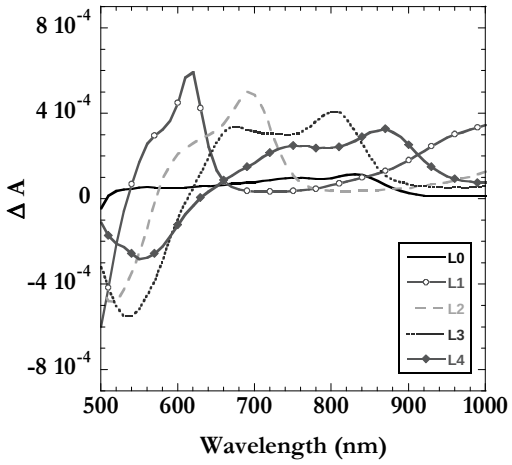

Figure 2.2.2 Photoinduced absorption spectra of TiO_2 films sensitized with **L0**, **L1**, **L2**, **L3** and **L4** in the presence of inactive redox electrolyte. Excitation wavelength used was 450 nm, and a light on-off modulation of 10 Hz.

3. The role of dyes in DSCs - novel organic dyes

In this section, general strategies to enhance the dye spectral response by structural modifications are described. The spectral properties of the dye in solution and adsorbed onto TiO_2 as well as the importance of the anchoring group will be briefly presented. Thereafter the three main electron-transfer processes occurring in the solar cell will be discussed in relation to the dye. The final section will deal with "dye aggregate" related issues and the role of coadsorbents in DSCs. The work of this thesis is presented and discussed within the subsections.

3.1. Strategies to enhance the dye spectral response

The ability of absorbing as much visible light as possible is one of the most important properties of novel dyes for DSC application. The spectral response of the dyes can be tuned by modification of the dye structures. To get electronically excited, the dye is only able to absorb photons with energy matching the excitation energy of the dyes. Since the photon flux (see Figure 3.1.1) of solar radiation varies with the wavelength the dye needs to have a broad absorption spectrum and have a high molar extinction coefficient to harvest as many photons as possible.

Enhanced spectral response of the dye component can be attained by structural modifications of the individual dye or by using a combination of dyes that complement each other in their spectral properties.[68] The former approach was followed in this thesis.

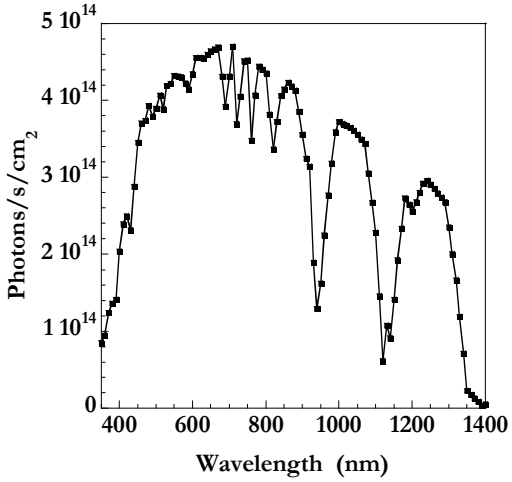

Figure 3.1.1 How the photon flux (ph $s^{-1}cm^{-2}$) varies as a function of wavelength at AM1.5 in the visible and NIR region.

The expansion of the spectral response is achieved by reducing the dye excitation energy by structural modifications. For organic dyes the major electronic transition is mainly of HOMO-LUMO character, thus it is desirable to reduce the HOMO-LUMO gap.[e] For the efficiency of the solar cell, a too small HOMO-LUMO gap will limit the output efficiency due to the trade-off between photovoltage and photocurrent (see section 2.2.2). There is thus a balance between the dye spectral response and the

[e] Results obtained from quantum chemical calculations indicate that the dye excitation in the visible region is mainly of HOMO-LUMO character (*Papers I* and *III*).

attainable photovoltage, as well as the required driving forces for the electron-transfer reactions involving the dye.

The design of organic dye molecules used in this thesis follows a three-unit approach where donor-linker-acceptor units are combined into a larger conjugated system. For the linker dyes the triphenylamine (TPA) is considered to be the donor, the cyanoacrylic acid the acceptor and the conjugated system referred to as the linker (see Figure 3.1.2).

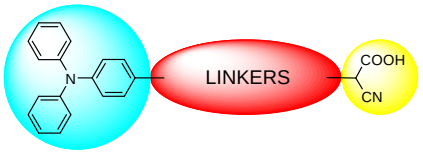

Figure 3.1.2 The donor-linker-acceptor combination used for many dyes in this thesis. The triphenylamine (TPA) acts donor, different conjugated units acts linkers and cyanoacetic acid acts acceptor.

One approach for enhancing the spectral response is to extend the linker conjugation by increasing the number of double bonds and thiophene units, as observed in Figure 3.1.3 (*Paper III*).

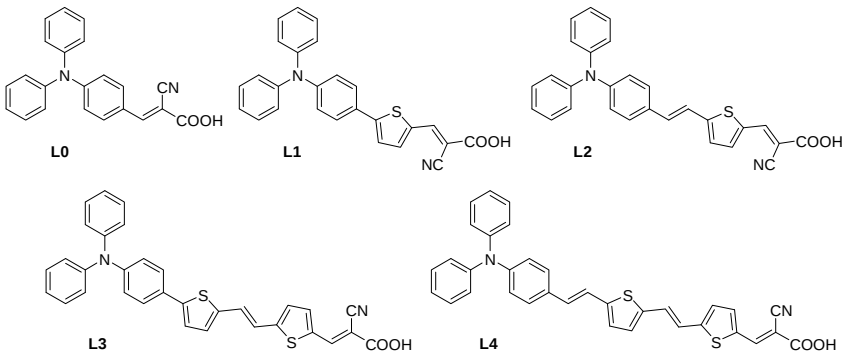

Figure 3.1.3 Molecular structure of the linker dyes (**L0**-**L4**) based on the acceptor group cyanoacrylic acid. The linker conjugation is extended to enhance the absorbance in the visible region (*Paper III*).

By introducing functional groups destabilizing the ground state and stabilizing the excited state the HOMO-LUMO gap can be reduced. Electron-donating groups can be introduced on the donor unit and electron withdrawing groups can be introduced on the acceptor unit. Some examples of dye structures (**D29**, **D37**, **D35**) with varying electron donating units are depicted in Figure 3.9.1 (*See Paper VI*).[39,69]

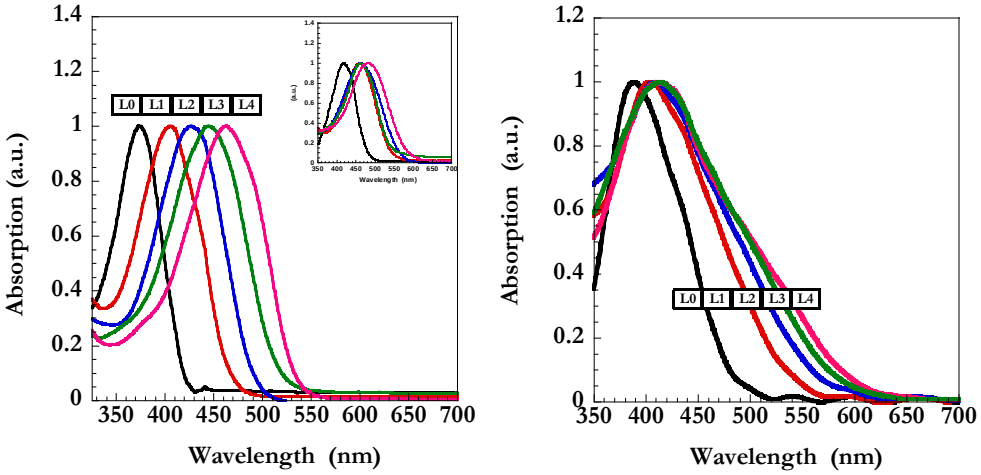

Figure 3.1.4 Normalized absorption spectra of the linker dyes in (left) acetonitrile solution upon addition of TBAOH, inset: linker dyes in plain acetonitrile solution and (right) adsorbed onto TiO_2 (*Paper III*).

In Figure 3.1.4 the absorption spectra of some linker dyes in solution and adsorbed onto TiO_2 are presented (*Paper III*). In solution a clear red shift of the absorption maximum is observed with increasing linker conjugation whereas on TiO_2 the absorption spectra were broadened and the absorption onset was shifted toward longer wavelengths upon increased linker conjugation of the dye. The enhanced absorption properties for the more conjugated dyes should consequently enhance the photocurrent response when used in the DSC. In Figure 3.1.5 the IPCE spectra of the linker dyes are depicted. It is observed that the IPCE onset is shifted to longer wavelengths for the more conjugated dyes in agreement with the corresponding absorption spectra.

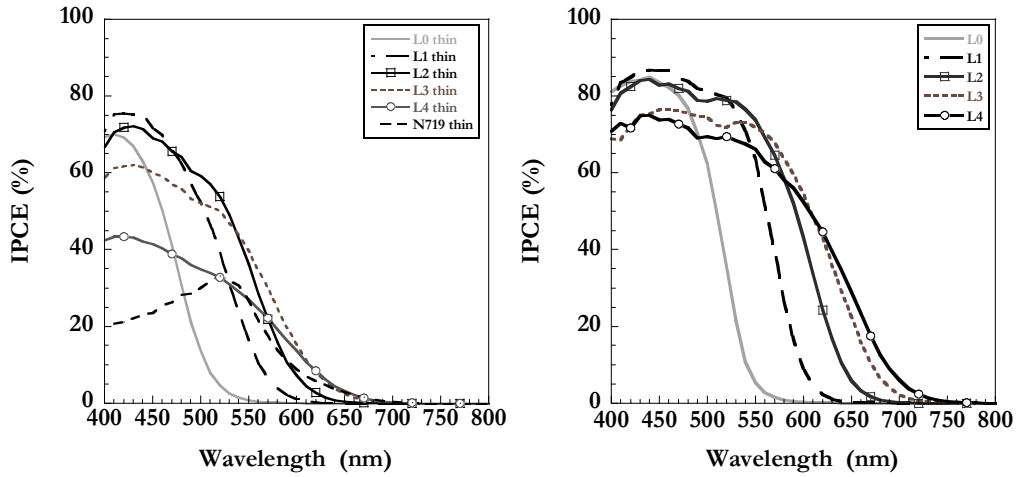

Figure 3.1.5 Spectra of monochromatic incident photon to current conversion efficiency (IPCE) for DSCs (left) 3 µm (*Paper III*) and (right) 10 µm thick working electrodes based on the linker series **L0**-**L4**, respectively. Electrolyte: 0.6 M TBAI, 0.1 M LiI, 0.5 M 4-TBP and 0.05 M I_2 in acetonitrile.

The extension of the linker conjugation of the cyanoacrylic acid dyes as described in *Paper III* resulted in an increased efficiency up to the **L2** linker dye. An equivalent linker approach was therefore tested for a dye series with an alternative acceptor group,

rhodanine-3-acetic acid, in *Paper IV*.[f] The molecular structures of these dyes are depicted in Figure 3.1.6.

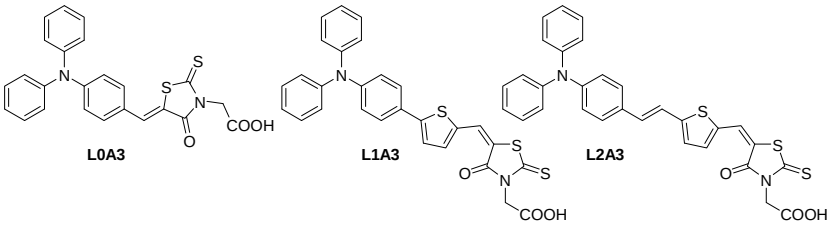

Figure 3.1.6 Molecular structure of linker dyes, **L0A3**, **L1A3** and **L2A3** based on the acceptor group rhodanine-3-acetic acid studied in *Paper IV*.

The rhodanine-3-acetic acid acceptor group induces a bathochromic (red) shift in absorption spectra compared to the linker dyes based on cyanoacrylic acid. Figure 3.1.7 depicts how the absorption spectra vary between the dye linker series when adsorbed onto TiO_2 based on cyanoacrylic acid (**L0**, **L1**, **L3**) and rhodanine-acetic acid (**L0A3**, **L1A3**, **L2A3**), respectively.

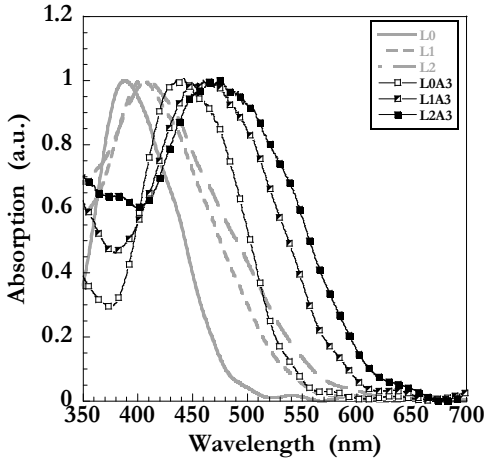

Figure 3.1.7 Normalized absorption spectra of the linker dyes adsorbed onto TiO_2, **L0**, **L1** and **L2** are based on the acceptor group cyanoacrylic acid and **L0A3**, **L1A3** and **L2A3** are based on the acceptor group rhodanine-3-acetic acid.

3.1.1. Dye structural modification

Examples of structural modifications made for the series of dyes used in this thesis are summarized as follows (Appendix C, see Chart 1). The dye modification was accomplished by strategically modifying each unit with established groups known to induce a red shift in the absorption spectra.

Starting from the successful dye structure of **L2**,[g] *Paper I*, further dye modifications were made. In *Paper II* the *linker* unit was varied with two thiophene units versus one thiophene and one phenyl unit, where the dye with two thiophenes units showed a more pronounced red shift in absorption. In *Paper III* an expansion of the pi-conjugation was performed. The aim was to obtain a systematic variation of the dye

[f] Note that different abbreviations are used for the linker series based on the rhodanine acceptor group (*Paper IV*). In this thesis the rhodanine series will be referred to as **L0A3**, **L1A3** and **L2A3**.
[g] Note that the linker dye **D5** (*Paper I*) is abbreviated as **L2** in this thesis in accordance with *Papers III* and *V*.

energy levels and to establish the optimal dye HOMO-LUMO bandgap for the performance in the solar cell. In *Paper IV* an additional red shift was obtained by using an alternative *acceptor* group to the cyanoacrylic acid, the rhodanine-3-acetic acid, in combination with extension of the linker conjugation. The introduction of electron-donating *donor* substituents, such as alkoxy and dimethylamine groups, successfully resulted in enhanced absorption properties, see *Paper VI*.

Enhanced spectral properties were attained fairly easily by dye structure modifications. In contrast, there is no simple correlation between the dye spectral properties and the DSC photovoltaic performance. How the dye properties influence the interplay of the dye/semiconductor/electrolyte components in the DSC will be discussed in the following sections.

3.2. Spectral properties of dyes in solution and on TiO_2

3.2.1. Spectral shifts in solution and on TiO_2

For organic dyes used in DSCs it is desired that the dye shows a pronounced intramolecular charge separation upon excitation (see section 3.4.2). The donor-acceptor dye design is intended to provide this property and has been supported by calculations (*Papers I* and *III*). As a consequence of the redistribution of ground state and excited state orbitals the dyes are expected to show solvatochromic behavior.[h]

The absorption and emission spectra of **L2** in three solvents are depicted in Figure 3.2.1. These solvents were chosen to keep **L2** neutral (protonated) and avoid influence of deprotonation induced spectral shifts (see below). The emission spectra showed a clear red shift with increasing solvent polarity,[i] Tol, THF, DCM, see Figure 3.2.1. The stoke shifts[j] increase in the same order, 118 nm, 188 nm and 216 nm. It may be noted that the trend in absorbance does not show a clear red shift with increasing solvent polarity, whereas how the Stokes shift increases as function of increased polarity is more apparent. This behavior supports the existence of an intramolecular charge separation upon excitation

[h] *Solvatochromism* is used to describe spectral shifts in the absorption and fluorescence (emission) spectra as function of change in the polarity of the surrounding medium (fluorescence bases solvatochromism may also be called *solvatofluorochromism*).

[i] Solvent properties can be given by many parameters, empirical solvent parameter E_T^N, relative permittivity (ε_r) and dipole moment (μ). The E_T^N is based on the solvatochromism of a reference molecule. For solvents DCM, THF and Tol: E_T^N: 0.309, 0.207, 0.099,; ε_r: 8.93, 7.58, 2.38,; μ 10^{30}/Cm: 13, 3.8, 1, respectively.

[j] The *Stokes shift* is referred to as the gap between the maximum of the absorption band and the corresponding fluorescence band.

Reichardt, C. *Solvents and Solvent Effects in Organic Chemistry,* Third Edition. WILEY-VCH Verlag GmbH & Co. KGaA, Weinheim. **2003**

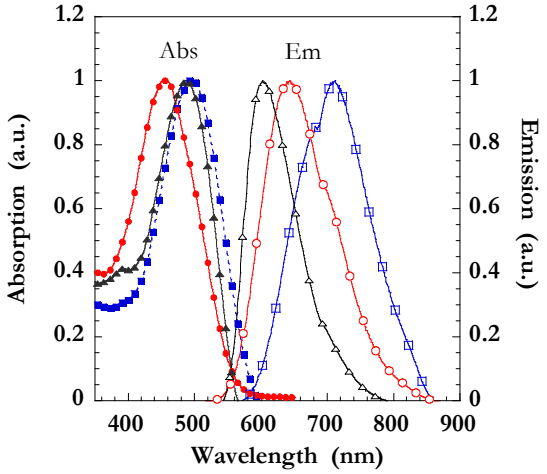

Figure 3.2.1 Normalized absorption and emission spectra of the **L2** dye in organic solvent with increasing polarity from Tol (triangles), THF (circles) and DCM (squares). Observed stokes shifts, 118 nm, 188 nm and 216 nm, respectively.

In addition to the solvatochromic behavior the dyes appear to also undergo deprotonation/protonation of the carboxylic group in different solvents which will affect the spectral shifts. This is shown in Figure 3.2.2 for **L2** in EtOH and DCM with the addition of a weak acid and base, respectively. It appears that the **L2** dye is mainly deprotonated in EtOH and protonated in DCM. The absorption spectra of the dyes adsorbed onto TiO_2 show a blue shift compared to most solvents. Figure 3.2.3 depicts the absorption spectra of the **L2** dye in MeCN, in the presence of weak acid and base, and when adsorbed onto TiO_2. It is noticeable that the absorption maximum of the deprotonated **L2** dye is in well agreement with spectra of the adsorbed dye onto TiO_2. On the other hand, the absorption onset of the protonated spectra was in agreement with the spectra of the adsorbed dye onto TiO_2.

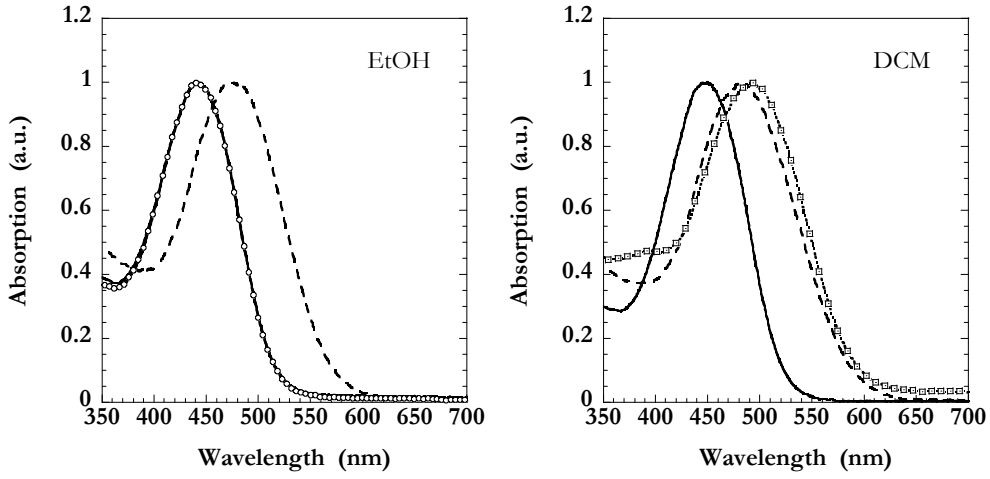

Figure 3.2.2 Normalized absorption spectra of the **L2** dye in (left) EtOH and (right) DCM. No additions (circles/squares) added acetic acid (dotted line) and added base, TBAOH, (solid) line, mol ratios ~1 to 10 of [dye:acid] and [dye:base], respectively.

It was also observed, that the absorption maximums red shifts with higher dye concentrations in MeCN, as seen in Figure 3.2.3. The concentration effect was most pronounced in acetonitrile. Concentration-dependent spectral shifts have previously been observed by Kitamura et al. for coumarin dyes in EtOH.[37] It was discussed that the dyes could interact in a dimer conformation where the cyanoacrylic acid moieties interact via hydrogen bonds. The absorption spectra red-shifted over time and blue-shifted by ultrasonication of the dye solution (see Appendix B, Figures 1(right) and 2) supporting the presence of a significant dye-dye interaction in solution.

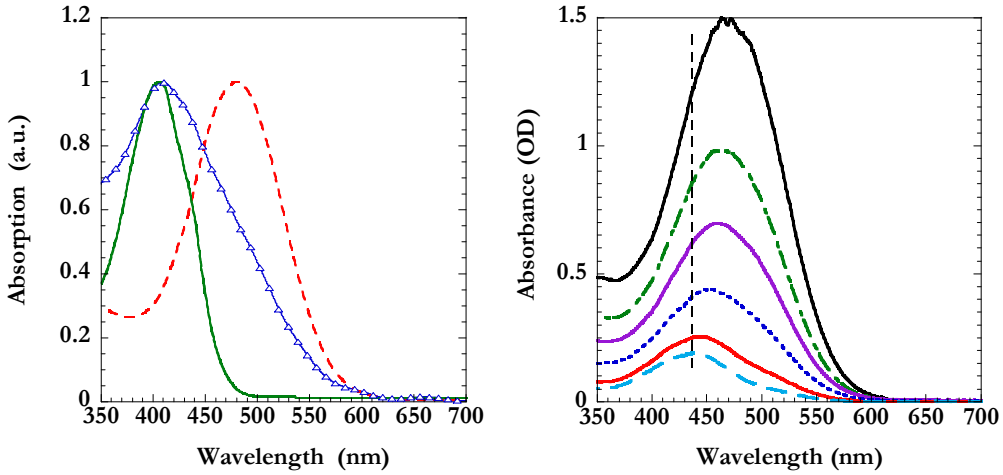

Figure 3.2.3 Absorption spectra of **L2** dye (left) for three different conditions adsorbed onto TiO_2, (triangles) in MeCN with addition of acetic acid (dotted line) and TBAOH (solid line), mol ratios ~1 to 10 of [dye:acid] and [dye:base], respectively, (right) in MeCN at different concentrations.

The variety of spectral shifts observed under various conditions is of importance for the assessment of the $E_{0\text{-}0}$, usually estimated from the intercept between the absorption and the emission spectra, see section 3.4.1. The $E_{0\text{-}0}$ transition estimated in different solvents and on TiO_2 films, yields a variation of ~0.3 eV (see Appendix B, Table 2). An alternative estimation can be made by using 10 % of the absorption on the low energy side from the spectrum of the dye-sensitized TiO_2. In this thesis the solution values were normally used which resulted in slightly varying results. This rough estimation of $E_{0\text{-}0}$, can still be used as a relative comparison of the dye potentials when examined under identical conditions. The estimated energy levels of **L0**, **L1**, **L2** and **L0A3**, **L1A3**, **L2A3** linker dyes using both solution and TiO_2 are presented in Appendix B, Table 3.

The discussion about spectral shifts is of major importance, given that dye aggregates are also known to cause spectral shifts.[68] Spectral shifts in solution and/or on TiO_2 films has been attributed to J-like aggregates, H-like aggregates, interaction between the anchoring group and TiO_2[70-72] and also by the protonation effect of the carboxylic group (*Papers I* and *III*).

3.2.2. The influence of the solvent dye bath

To further investigate how the dye sensitization is influenced by the different solvents, **L2** was investigated in EtOH, MeCN and DCM. Figure 3.2.4 depicts the absorption spectra of **L2** in the different solvents and adsorbed onto TiO_2 for sensitization performed in same set of solvent dye baths, EtOH, MeCN and DCM. The absorption spectra of dye-sensitized TiO_2 are fairly similar for the different conditions, even though a slight red shift is observed going from DCM, MeCN to EtOH. The absorbance, i.e. the dye load, also varied between the different dye bath solvents. From absorbance measurements the dye loads were observed to increase in the order of EtOH<MeCN<DCM (Figures 3.2.4 (right)-3.2.5 (left)). The IPCE trend showed highest currents for MeCN and similar results for EtOH and DCM (Figure 3.2.5).

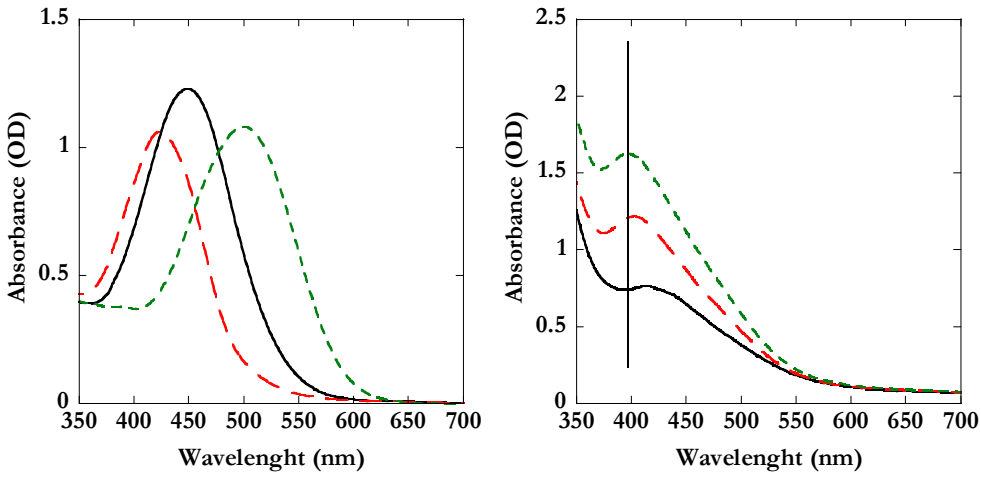

Figure 3.2.4 (left) Absorption spectra of **L2** dye solutions in EtOH (——), MeCN (— —) and in DCM (**- - -**). (right) Absorption spectra of **L2** adsorbed onto 1 µm thick TiO_2 film on microscopic glass sensitized in the three former dye solutions.

It is noticeable that the **L2** dye solution in MeCN, yielding DSCs with highest photocurrents also showed an indication of dye-dye interactions in the dye solution. The sensitization in different solvents may result in slightly different dye orientations and dye/dye interactions when adsorbed onto TiO_2. Highest dye load did not yield highest photocurrents, possibly due to unfavorable dye/dye interactions and/or dye orientation on the surface. Photoelectron spectroscopy studies on **L2** and the rhodanine dyes (*Paper IV*) adsorbed onto porous TiO_2 confirms that the dominating dye binding orientation on TiO_2 is with the cyano group close to the surface while the TPA unit is pointing out from surface.[73] Further detailed investigations about dye-dye interaction and dye orientation are currently being performed.

In general, more fundamental studies are needed to gain information of the in situ dye layer formed under different sensitization conditions. In addition, it is of high interest to link fundamental studies to the outcome and performance of complete DSC devices.

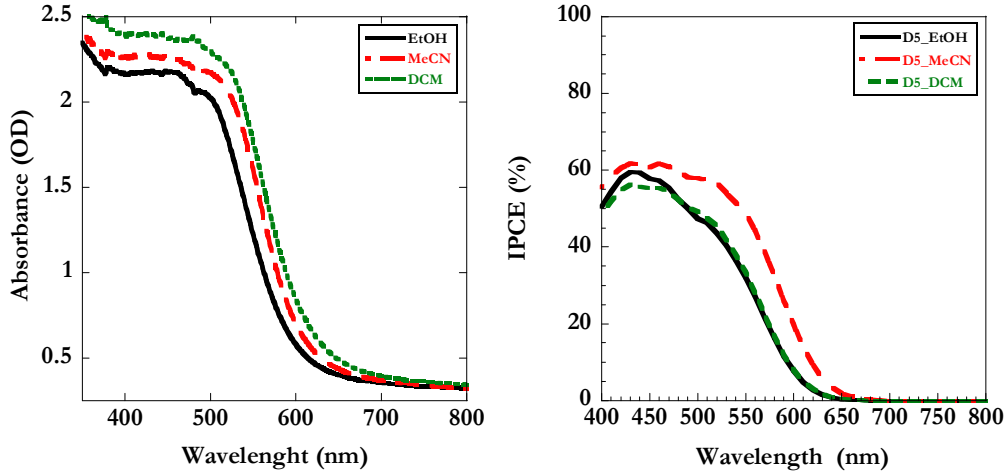

Figure 3.2.5 (left) Absorption spectra of **L2** sensitized in different solvents EtOH (——), MeCN (— —) and in DCM (- - -) adsorbed onto 4 μm thick TiO_2 film on FTO (air was used as blank). (right) Spectra of monochromatic incident photon-to-current conversion efficiency (IPCE) for DSCs based on **L2** sensitized in different solvents EtOH (——), MeCN (— —) and in DCM (- - -). Electrolyte: 0.6 M TBAI, 0.1 M LiI, 0.5 M 4-TBP and 0.05 M I_2 in acetonitrile.

3.3. Dye anchoring group

The dyes are bonded to the TiO_2 surface through an anchoring group. The anchoring group should provide close contact between the dye acceptor unit and the TiO_2 surface for efficient electron injection and in general a strong bond is desired to avoid dye desorption over time. The former requisite is achieved by designing dyes with anchoring groups also acting acceptor group upon dye excitation.

The most used anchoring group for DSCs is the carboxylic acid, in particular for organic dyes.[43] Phosphonic acids,[74,75] alcohol and various others[76] have also been tested with less successful results. The dye anchoring group is thought to bind to the oxide via a reaction involving surface hydroxyl groups. The exact binding mechanism and binding mode to the oxide is debated both in terms of the dye anchoring mode (ester or carboxylate) and the dye coordination on the oxide crystal (unidentate, bidentate, bridging), see Figure 3.3.1.

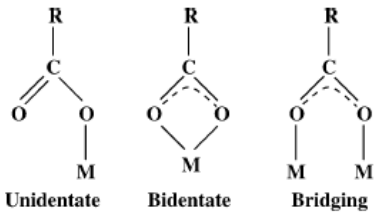

Figure 3.3.1 Different types of binding of the carboxylic acid anchoring group onto a metal oxide.[77]

To determine the binding modes of the anchoring group infrared (IR) spectroscopy is typically used. The binding modes yield information about the carboxylic acid anchoring groups, i.e. are COOH, $(COO\text{-})_{as}$, and$(COO\text{-})_{s}$.[78,79, k] The preferential binding mode of the carboxylic group of ruthenium dyes has been addressed to be bidentate bridging[77,78] and the same have been observed for many organic dyes.[33,80] The presence of the bidentate mode is identified by the absence of the characteristic carbonyl mode and the appearance of modes for the symmetric and asymmetric carboxylate vibrations.

In *Paper II* it is described how two pyrrolidine cyanoacrylic acid dyes, **PT** and **TT** (Figure 3.6.1) with carboxylic acid anchoring groups showed dissimilar photovoltaic results. The two dyes showed different binding modes when adsorbed onto TiO_2. The IR spectra are shown in Figure 3.3.2 for the protonated neat dyes in their powder form, showing a carbonyl (C=O) peak at 1672 and 1658 cm^{-1} for **PT** and **TT**, respectively.[l]The absence of a strong carbonyl mode for the **PT** dye adsorbed onto TiO_2 may indicate the absence of a unidentate ester bond. For the adsorbed **TT** dye on the other hand, the carbonyl mode was still present. The origin of the carbonyl was discussed to be unidentate binding and/or protonated non-bonded dyes. Most of the organic dyes studied in this thesis showed the same behavior as the **PT** dye, supporting the observation by others,[43] that the most common binding of the carboxylate anchoring group appears to have a bidentate nature.

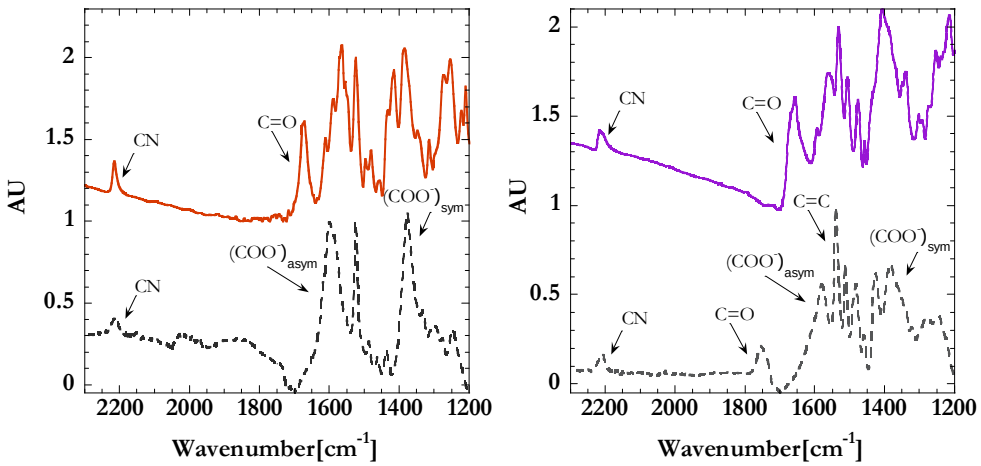

Figure. 3.3.2 IR spectra of (left) **PT** and (right) **TT** dyes both in neat condition (solid line) and adsorbed on TiO_2 (dotted line), (*Paper II*).

[k] The characteristic band for a free carboxylic acid (COOH) lies in the region 1715-1690 cm^{-1}. For the $(COO^{-})_{sym}$ and $(COO\text{-})_{asym}$ modes at 1420-1300 cm^{-1} and 1610-1550 cm^{-1} are expected. Williams D. H.; Flemming, I. *Spectroscopic Methods in Organic Chemistry*. McGraw-Hill. **1995**.

3.4. Exploring the dye-DSC compatibility

Interfacial electron-transfer processes are central for the working principle of the DSC device. The dye has an important role in several of the electron-transfer processes occurring in the solar cell, such as (see Figure 3.4.1):

0. Dye excitation.
1. Electron injection.

2a. Electron recombination with dye cations.

2b. Electron recombination with redox electrolyte.

3. Dye regeneration

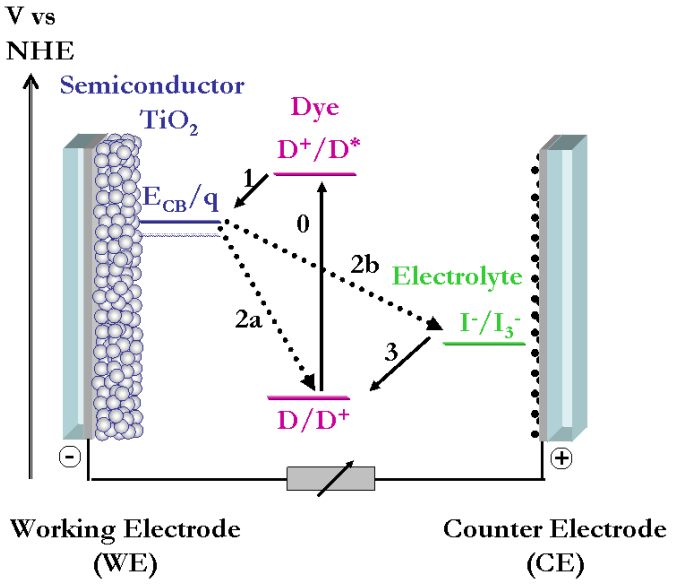

Figure 3.4.1 Illustration of the number electron-transfer processes occurring in the DSC.

There are many theories that describe interfacial electron-transfer reactions; which model to use will depend on the nature of the processes (time regime, components involved).[4,44,45] The DSC is a complex device combining a number of components involved in several interfacial electron-transfer processes. Taking into consideration that among the component is an inhomogeneous TiO_2 surface and that there are wide distributions of dye states and redox states, an ideal behavior is not expected.

Independently of the interfacial electron-transfer model used there are some basic parameters that determine the kinetics of an electron-transfer reaction. More specifically, the probability of an electron-transfer reaction is related to the electronic coupling (orbital overlap) the between donor and acceptor states and the energetic driving force for the electron-transfer reaction, see Equation 1.4.4.

These parameters are not straightforward to determinate/estimate for all the interfacial electron-transfer reactions occurring in the solar cell. Changing the dye structure may affect these two parameters directly or indirectly, resulting in alteration in one or several electron-transfer processes in turn affecting the photovoltaic performance of the DSC.

The characterization of the dye properties as individual components and when integrated in DSCs is discussed in the next sections.

3.4.1. Estimation of dye energetics

The energy levels of the ground and excited states of the dye are of importance for electron-transfer reactions *1*, *2a* and *3*, shown in Figure 3.4.1. Results from *Papers I* and *II* are used to illustrate how the dye energetics are estimated experimentally. As mentioned in section 1.4.2, there are two key requirements for the DSC performance when it comes to the energy levels of the dyes. Firstly, for efficient dye regeneration, the ground state oxidation potential of the dye, $E_{pot}(D/D^+)$, must be located at more positive potentials vs. NHE than the redox potential of the electrolyte, $E_{pot}(I^-/I_3^-)$. Secondly, for efficient electron injection the dye excited state potential, $E_{pot}(D^*/D^+)$, must be located at more negative potentials vs. NHE than the conduction band edge of the TiO_2.

The ground state oxidation potential of the dyes in solution or adsorbed onto TiO_2 is determined by electrochemistry (see section 2.2.1). For internal comparisons between series of dyes the ground state oxidation potential in solution was normally used. The ground state oxidation potentials were measured for **L0** and **L3** both in liquid and adsorbed onto TiO_2; negligible differences in the measured redox potentials were found (see Appendix B, Table 1).

The estimation of the excited state potential[m] of the dye is determined by subtracting the zeroth-zeroth energy ($E_{0\text{-}0}$), see Figure 3.4.2, obtained from the intersection of absorption and emission spectra, to the redox potential of the dye $E_{pot}(D/D^+)$, see Equation 3.4.1[4]

$$E_{pot}\left(D^+/D^*\right) = E_{pot}\left(D^+/D\right) - E_{0-0} \qquad (3.4.1)$$

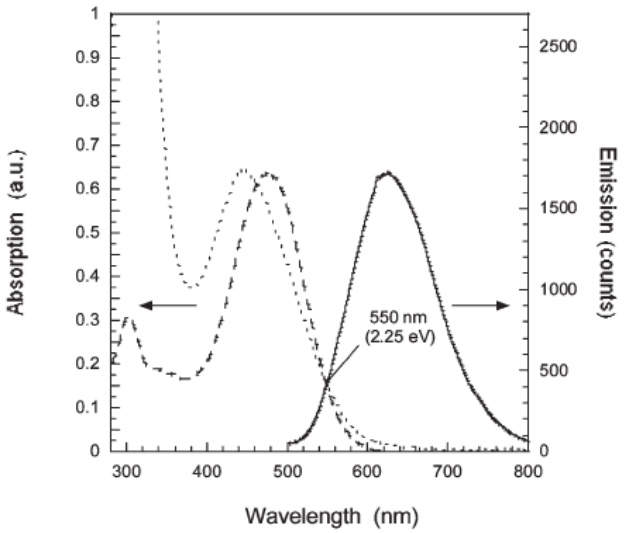

Figure 3.4.2 Absorption spectra of **L2** in MeCN (---), adsorbed onto TiO_2 (····) and emission spectrum (—) of L2 in MeCN. The zeroth-zeroth transition ($E_{0\text{-}0}$) is indicated at the intersection of absorption and emission spectra (*Paper I*).

[m]The estimated excited state refers to the excited state oxidation potential for the oxidation of the thermally equilibrated state. Memming, R. *Semiconductor Electrochemistry*, Wiley-VCH Verlag GmbH, Weinheim, **2001**.

The *Gerischer model* can be used to describe electron-transfer processes at semiconductor surfaces.[4] For illustration of the ground and excited state potentials in reference to the semiconductor energy states a *Gerischer diagram* is depicted for the dye/semiconductor interface. The diagram includes the distribution functions of the oxidized and reduced states in the ground and excited states of the dye (assuming equal concentrations). The redistribution of the solvation shell upon the redox reaction is given by the reorganization energy (λ), see Figure 3.4.3.

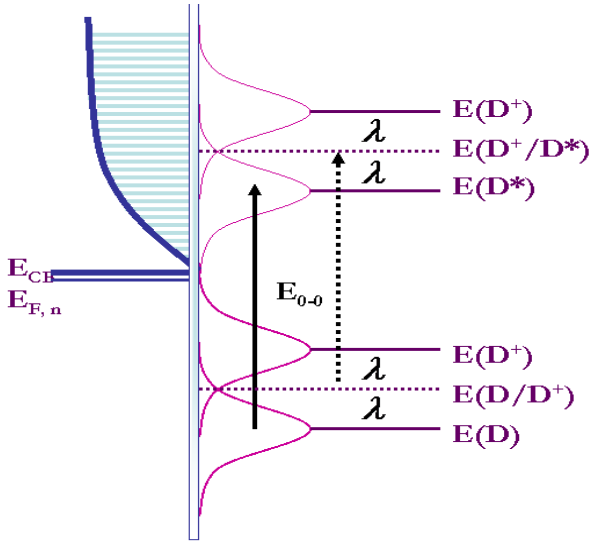

Figure 3.4.3 Gerischer diagram showing energies of a semiconductor and a redox system. Dye energy states, E(D), E(D$^+$) and E(D*) are the positions of the reduced, oxidized and excited dye, respectively. The E(D/D$^+$) and E(D$^+$/D*) are the redox energy levels of the dye ground state and excited state, respectively. The reorganization energy, λ, originating from redistribution of the surrounding solvent molecules upon electron-transfer is also indicated.[4]

The optical excitation energy is given by $E_{0\text{-}0}$ referring to the electron transition between the relaxed dye (D) in the ground state to the relaxed excited dye (D*) as indicated in Figure 3.4.3 (solid arrow). If the electron injection from the dye excited state to the conduction band of the TiO_2 occurs in time scales of fs, the injection is assumed to occur from the unrelaxed excited state.[n] The estimation of the excited state redox potential (see dotted arrow) is therefore a decent approximation. The measured ground and the estimated excited state potentials for the linker series (*Paper III*) are depicted in Figure 3.4.4. For all linker dyes both the ground state and excited state potentials appear to fulfil the requirements in reference to the TiO_2 (E_{CB}~0.5 V vs. NHE) and redox electrolyte potential (0.4 V vs. NHE).[51]

[n] Electronic transitions occur in *ca* fs, molecular vibrations and solvent reorganization can occur in *ca* 1-100 ps. Reichardt, C. *Solvents and Solvent Effects in Organic Chemistry,* Third Edition. WILEY-VCH Verlag GmbH & Co. KGaA, Weinheim. **2003**

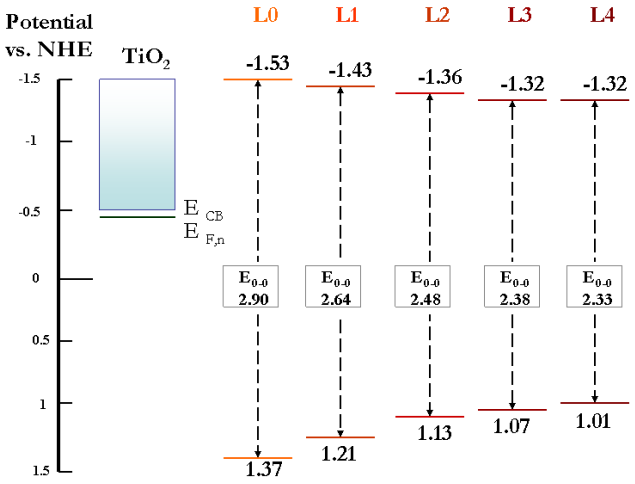

Figure 3.4.4 Potential level diagram for linker dyes (**L0**-**L4**) versus NHE, the $E_{0\text{-}0}$ decreases with increasing linker conjugation of the dyes.

3.4.2. The importance of orbital distribution

The sensitizing dye should show a pronounced intramolecular charge separation upon excitation. Assuming a vectorial orientation of the dye molecule when anchored to the TiO_2 surface, see Figure 3.4.5, the charge transfer upon excitation should occur from the ground state orbitals (HOMO) mainly located on the donating unit and to the excited state orbitals (LUMO) on the acceptor unit close to the TiO_2 surface.

Designing a dye with an anchoring group which also acts as an electron acceptor upon dye excitation provides thus a prerequisite for efficient electron injection. After the electron injection the dye is oxidized. Assuming negligible changes in orbital energies upon oxidation; the ground state orbital (HOMO) will now be the accepting orbital in the regeneration reaction when the oxidized dye is reduced by the redox electrolyte. The HOMO should preferentially be located on the donating part of the molecules far away from the anchoring group and/or the TiO_2 surface to minimize the probability of electrons in the TiO_2 recombining back with the oxidized dye.

In these ways desirable and undesirable electron-transfer reactions can be partially controlled by appropriate dye structure design. It should be noted that the orbitals of interest can be other than HOMO and LUMO. The electronic transition in the visible region for organic molecules usually involves quite defined transitions between two orbitals (usually HOMO and LUMO), whereas metal-based complexes have a series of orbital transitions contributing to the visible band.

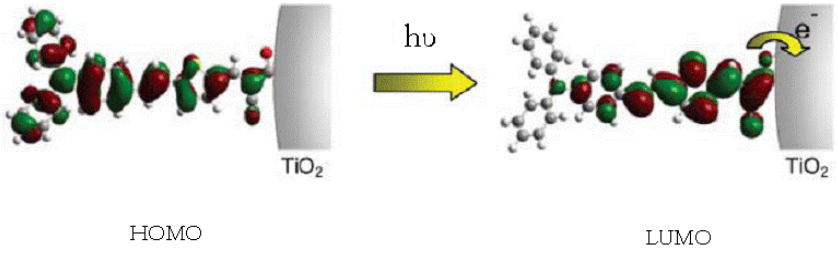

Figure 3.4.5 Frontier molecular orbitals of the HOMO and LUMO of **L2** calculated by TD-DFT on B3LYP/6-31 + G(d) level. Calculations performed by Tomas Edvinsson. Observe that the TiO_2 is only shown for illustration of the interfacial electron injection from the dye excited state (*Paper I*).

3.5. The influence of electron injection on the DSC performance

The electron injection from the dye excited state provides an interfacial charge separation generating electrons in the TiO_2. As mentioned is section 1.4.3, the electron injection efficiency is given by the kinetic competition between injection times and dye excited state lifetimes, see Equation 1.4.1. The injection rate depends on parameters such as energetic driving force, reorganization energy and electronic coupling between the dye excited state and the conduction band states in the TiO_2. The electron injection process has been studied to a great extent due to its fascinating ultrafast electron-transfer kinetics. Injection time constants in the order of subpicoseconds have been reported.[45,81,82] A multi-exponential nature of the electron injection is expected due to the heterogeneous interfacial properties arising from the non-ideal TiO_2-dye interface (varieties of TiO_2 surface states and dye binding modes).[83,84] Due to the ultrafast electron injection kinetics, this process has generally not been considered to be limiting the DSCs photovoltaic performance.[47]

3.5.1. Factors limiting the electron injection

In view of the development of novel materials for DSCs, remaining questions concerning the electron injection have again come to be in focus. Processes functioning efficiently for the standard system might become limiting when using new combinations of material components.

How fast does the injection occur, how fast does it need to occur, what are the limiting factors? These are all central questions still being debated by the DSC community. Durrant and co-workers discussed the influence of kinetic redundancy in terms of the correlation between quantum yields of unity and actual required injection rates.[46,85] In addition, the injection kinetics have been claimed to occur on much slower timescales than subpicoseconds in the presence of redox electrolyte which could be of importance for novel organic dyes with absent longer lived excited states.[46,86,87] Injection studies performed on organic dyes have shown injection times of subpico-pico seconds in inert electrolytes.[61,72,83,87,88] Fast injection does not automatically lead to high IPCEs, in particular for organic dyes which may have aggregate/inactive dyes also being present on the surface.

The timescales of ultrafast injection indicate that the electron-transfer may occur from the thermally relaxed excited state but also from the initial Franck-Condon excited state. The latter is referred to as hot electron injection.[89] Different dyes injecting from different relaxed states will show different injection kinetics and yields even though similar thermally relaxed excited states potentials are estimated.

A well-established observation is that the injection and device efficiency depend on the overlap between dye excited states and accessible TiO_2 conduction band states. Altered injection kinetics have been studied as function of the dye excited state potential[33,83,90] and the TiO_2 energetics,[61] where the latter can be energetically tuned by ions[66] and additives[60,66] in the electrolyte. [46,47,61,91] The dependence of how the electron injection rate varies as function of the donor-acceptor distance (electronic coupling shows exponential dependence on spatial separation) has resulted in more diverse

results, presumably due to a variety of dye structures making it difficult to control the dye orientation on the surface.[92-94]

In *Papers III* and *IV* two series of dyes with different acceptor groups were tested in DSCs, cyanoacrylic acid and rhodanine-3-acetic acid (A3), respectively. Both acceptor groups are shown in Figure 3.5.1 for the smallest dyes **L0** and **L0A3**, respectively.

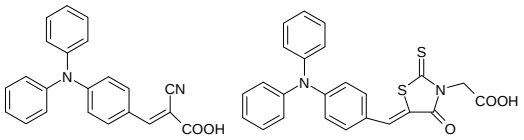

Figure 3.5.1 Molecular structures of two dyes with different acceptor groups (left) **L0**, cyanoacrylic acid (*Paper III*) and (right) **L0A3**, rhodanine-3-acetic acid (*Paper IV*).

As mentioned in section 3.1, a red shift was introduced by the rhodanine acceptor unit, due to a reduced energy difference between the ground and excited states (HOMO-LUMO gap), see Figure 3.5.2. The measured ground state potentials and the estimated excited state potentials are depicted in Figure 3.5.3. The dyes based on the rhodanine-3-acetic acid show about 0.2 V lower excited state potentials compared to the dyes based on the cyanoacrylic acid acceptor group. This implies that the driving force for electron injection is different for these two series of dyes differing in their dye acceptor units.

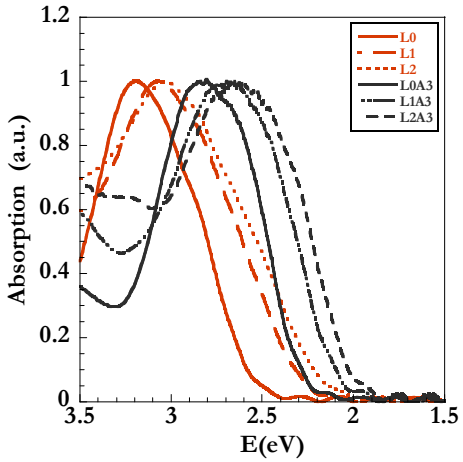

Figure 3.5.2 The absorption spectra as function of energy for the linker series based on cyanoacrylic acid and rhodanine-3-acetic acid when adsorbed on TiO_2.

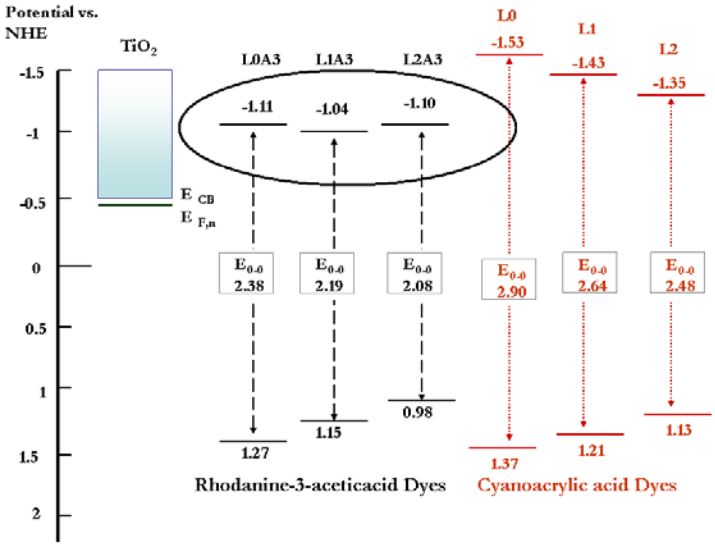

Figure 3.5.3 Potential level diagram showing ground and excited state potentials for cyanoacrylic acid and rhodanine-3-acetic based linker dyes (*Paper III* and *IV*).

The device efficiencies of solar cells based on the rhodanine dyes were significantly decreased by the addition of 4-TBP additive (*Paper IV*). This additive is known to shift the TiO_2 conduction band edge towards negative potentials. If the dye excited state potential initially is fairly close to the conduction band edge of the TiO_2 it is possible that the reduced energetic difference in the presence of 4-TBP significantly limits the injection yield.[46,91]

This problem has been described for other organic dyes showing more positive excited state potentials compared to the state-of-the-art ruthenium complex. Thus, a great sensitivity of the photocurrents in the presence of 4-TBP has been discussed to most likely depend on a reduced injection efficiency.[33,95]

The possible overlap between dye donor states and TiO_2 conduction band states is illustrated in Figure 3.5.4. In addition, the absence of conjugation located on the rhodanine acceptor group may result in different electronic coupling. The altered electronic coupling may limit the electron injection leading to a decrease in IPCE.[94,96,97]

There are various reasons possible for the photovoltaic performance to be influenced by the conduction band edge position of TiO_2. The effect of 4-TBP on the photovoltaic performance will be further discussed in section 3.8.

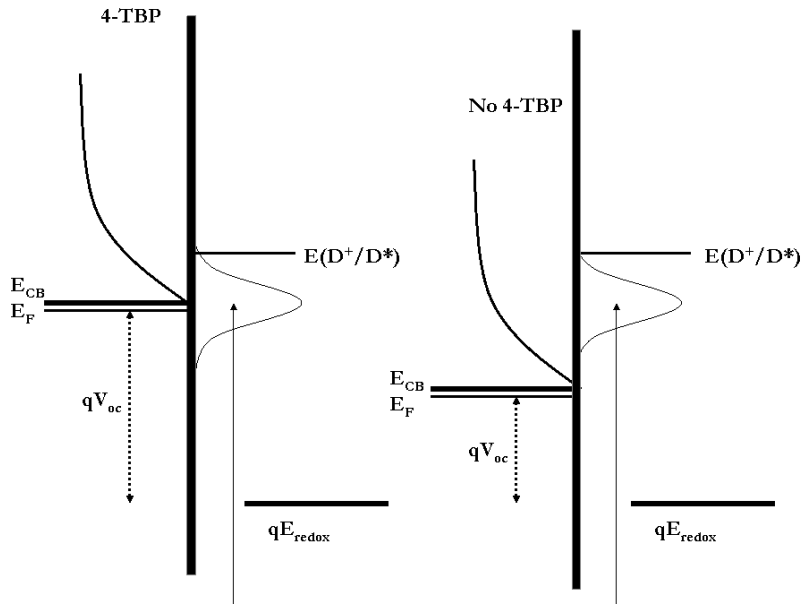

Figure 3.5.4 Energy scheme of the different conduction band edge (E_{CB}) positions in the presence and absence of 4-TBP. This causes a possible variation in overlap between the dye excited states and TiO_2 conduction band states (*Paper IV*).

The injection rates for **L2** and **L2A3** were further characterized by Wiberg et al. measuring similar injection rates (within ~100 fs) for dyes based both on the cyanoacrylic acid and the rhodanine-3-acetic acid acceptor groups.[87] Instead, a significant difference in the ultrafast (subnanoseconds) recombination with the dye cation was observed and was suggested to originate from electron injection into different TiO_2 states. The electron recombination with the oxidized dye is further discussed in section 3.7.1.

3.6. The influence of dye regeneration on the DSC performance

After ultrafast electron injection the dye becomes oxidized. To be able to harvest additional photons the dye needs to be reduced, i.e. regenerated. The regeneration reaction occurs efficiently if there is a satisfactory difference between the dye ground state oxidation potential and the iodide/triiodide redox potential. The iodide/triiodide redox couple has a redox potential of about 0.4 V vs NHE in acetonitrile,[51] the ground state oxidation potential of the champion dye **N3** is 1.1 V vs NHE,[8] resulting in an electrochemical potential difference of ~0.7 V. The regeneration of the oxidized dye by the redox couple has been discussed in terms of "a loss of half a volt".

It is of great interest to utilize a redox couple with a more positive redox potential to be able to gain a higher open-circuit voltage in the solar cell.

3.6.1. Factors limiting the dye regeneration

Studies on dyes with less positive redox potentials than the conventional ruthenium dye have both reported functioning[50,98] and non-functioning/slow[49,99] dye regeneration kinetics due to altered driving force. Meyer and co-workers showed that an osmium complex showed poor photovoltaic efficiency due to sluggish regeneration.[100] A 340 mV less positive dye ground state oxidation potential compared to a Ru-complex analogue resulted in a minimal change in the recombination with the oxidized dye but significantly slower regeneration of the oxidized dye by the redox couple.

In *Paper II*, two organic dyes with similar structures differing in one of the linker units were tested as sensitizers in DSCs. The dyes, referred to as phenyl-thiophene (**PT**) and thiophene-thiophene (**TT**), are presented in Figure 3.6.1.

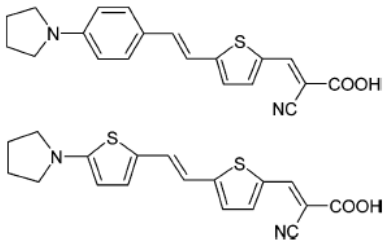

Figure 3.6.1 Molecular structure of the pyrrolidine cyanoacrylic acid dyes studied in *Paper II*, (top) **PT** and (bottom) **TT**.

The **TT** dye showed a bathochromical shift in the absorption spectrum compared to the **PT** dye showing that the thiophene unit red shifts the absorption more effectively than the phenyl unit. Interestingly, the photovoltaic performance of these dyes in DSCs showed very different results, see Table 3.6.1.

Table 3.6.1 Photovoltaic performance of DSCs based on **PT** and **TT** dyes (*Paper II*).

Dye	J_{sc}/mA cm^{-2}	V_{oc}/V	FF	η/%
PT	7.57	0.58	0.59	2.3
TT	0.39	0.26	0.45	<0.05

Photoinduced absorption spectroscopy was used to study the oxidized state of the dyes adsorbed onto TiO_2 films. In Figure 3.6.2 the differential spectra of sensitized TiO_2 films with **PT** and **TT**, respectively, are depicted in the presence and absence of redox electrolyte.

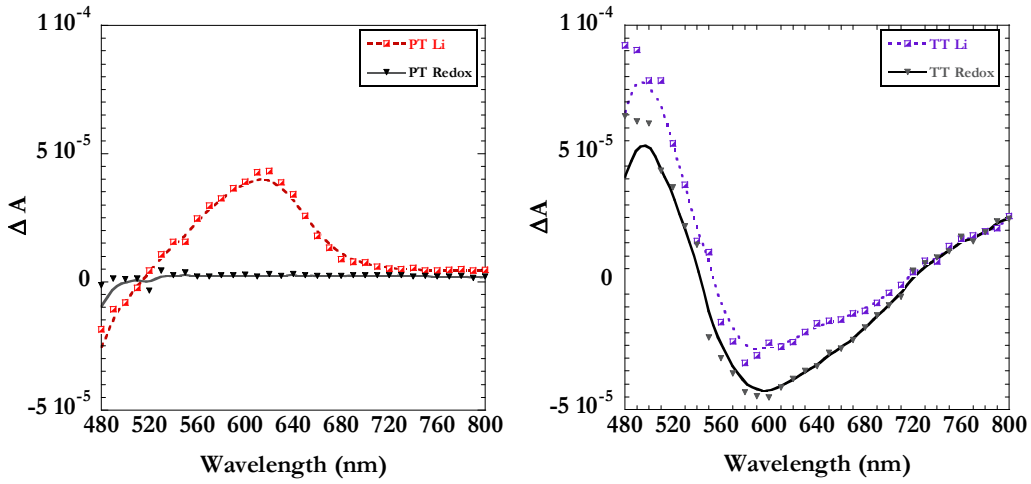

Figure 3.6.2 Photoinduced absorption spectra of TiO_2 films sensitized with (left) **PT** and (right) **TT**, in the presence (solid) and in the absence (dotted) of redox electrolyte (*Paper II*).

In the presence of redox electrolyte the differential spectrum of the oxidized **PT** dye is not longer visible whereas the differential spectrum of the oxidized **TT** dye still remains. This indicates that the **PT** dye is successfully regenerated whereas the **TT** dye is not.

The ground state oxidation potentials of the dyes with respect to the semiconductor and the redox couple are illustrated in Figure 3.6.3. The change of one unit, from a phenyl to a thiophene, in the dye structure reduced the ground state oxidation potential of **TT** by 0.3 V compared to the **PT** dye. A redox potential of 0.4 V vs. NHE for the iodide/triiodide and a ground state potential of 0.5 V vs. NHE for **TT** yields an electrochemical potential difference of ~0.1 V for the dye regeneration reaction to occur. Therefore, the inability of the redox couple to regenerate the oxidized **TT** dye was suggested to originate from the less positive ground state potential of the **TT** dye.

An important aspect elucidated by Boschloo et al. is that the relevant redox potential among the series of intermediate redox potentials of the iodide/triiodide redox couple is located at a much more positive potential than the redox potential for $E_{pot}(I^-/I_3^-)$.[21] The relevant redox potential that should be considered for the regeneration reaction is $E_{pot}(I_2^-/I^-)$, being located at <0.9 V vs NHE. This may possibly explain the sensitivity of the regeneration reaction with respect to driving force, and that "half a volt" in fact is needed. Thus, speculatively, the limit of the iodide/triiodide redox couple might be reached.

In addition to the electrochemical driving force, the complex interplay between dye, redox couple and ions/additives should also be considered for the regeneration process. Some aspects discussed in the literature that may affect the dye regeneration process are: the importance of cations in the electrolyte for electrostatic attraction of iodide to the dye and the requirement of complex formation between oxidized dye and iodide for efficient dye regeneration. [48,49]

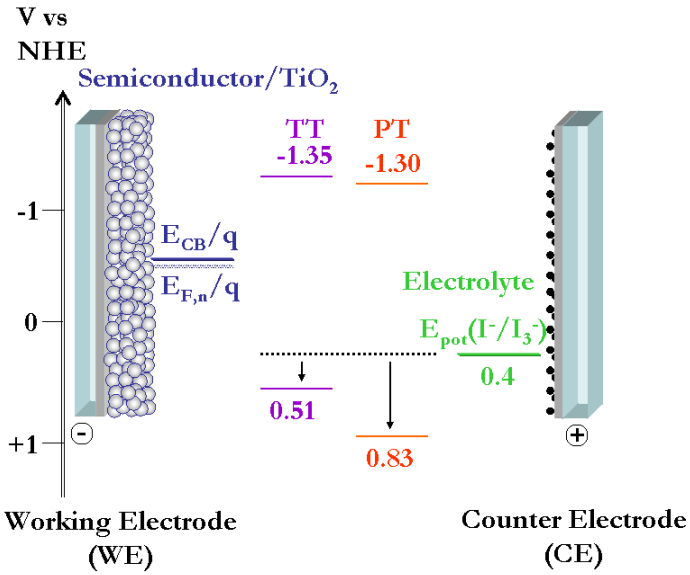

Figure 3.6.3 Potential level diagram for the pyrrolidine cyanoacrylic acid dyes, **TT** and **PT,** with respect to the DSC components.

3.7. The influence of electron recombination on the DSC performance

In principle there is a number of interfaces where the recombination can take place: the TiO_2-electrolyte, TiO_2-dye and FTO-electrolyte interfaces. In the following section the recombination pathways will be discussed in relation to the dye. The recombination of electrons in the TiO_2 with acceptors in the DSC can be divided into two categories; recombination with the oxidized dye (next section) and recombination with oxidized redox species in the electrolyte (section 3.7.2).

3.7.1. Recombination with the oxidized dye

For a DSC based on a conventional ruthenium dye in the presence of excess of iodide (>0.1 M) the recombination with the oxidized dye is not limiting for the device efficiency.[8,49] The recombination with the oxidized dye has nevertheless been extensively studied due to the intriguing rectifying behavior of the electron-transfer across the TiO_2-dye interface.[101-104] For a conventional DSC, the beneficial electronic coupling between the dye excited-state orbitals (LUMO) and TiO_2 conduction band states is responsible for the ultrafast injection rates whereas the significantly slower recombination rates with the oxidized dye are presumably due to the weak electronic coupling between the oxidized state orbitals (assumed to be HOMO) and the TiO_2 conduction band states. In addition, the large apparent driving force (1.5 eV> λ) suggests inverted region kinetics. The driving force dependence is still debated and numerous studies have been reported on this issue.[45]

A complication arising when trying to correlate the kinetics to a single parameter is the difficulty of holding the rest of the parameters constant. A distribution of dye-binding sites and orientations in a porous system results in a complex system and will consequentially lead to a variation of experimental observations. The recombination kinetics has mostly been characterized for metal-based complexes, in particular

ruthenium complexes. The recombination rate has been studied as function of driving force,[103] distance[105,106] and electron concentration in the TiO.[86,107]

The kinetics of the electron-transfer reactions of organic dyes is not as well characterized, in particular for reactions such as recombination and regeneration.[87,101,108,109] Studies on coumarin dyes have shown reduced electron injection efficiencies in the absence of lithium cations, which was suggested to depend on a higher degree of geminate recombination as a result of injection into surface states.[61] Nanosecond spectroscopy on a series of coumarin-based dyes with varying linker conjugations showed different recombination kinetics under low light intensity conditions.[110] The different recombination rates showed non-trivial linker conjugation dependence and were not correlated to the photo-stability of the cation.[110]

For the use of novel dyes a central question to answer is whether the recombination with the oxidized dye limits the solar cell performance. The two competitive processes are the recombination and the regeneration of the oxidized dye, reactions *2a* and *3* in Figure 3.4.1.

The transient absorption spectrum of the oxidized dye can be followed in the absence and presence of redox electrolyte from PIA measurements (section 2.2.4). Any restrictions concerning the dye regeneration will appear as spectral evidence of the surviving oxidized dye in the presence of the redox electrolyte. A trace of non-regenerated oxidized dye, in the time regime of 10 ms to s, was only detected for the **TT** dye (*Paper II*) in this thesis as shown in Figure 3.6.2 (right). For the other series studied, the longer-lived oxidized dyes were all successfully regenerated in the presence of redox electrolyte. PIA measurements are restricted to timescales of 0.1 ms to s. Thus for identification of the nature of the faster recombination processes; other time-resolved studies are required.

Wiberg et al. performed femto-second laser studies on the **L2** and **L2A3** dyes, having different acceptor groups, when adsorbed onto TiO_2.[87] The anchoring groups yield different dye excited state potentials (see section 3.5.1) and also show different degree of conjugation on the anchoring groups. It was suggested that the electron injection from **L2** with a cyanoacetic acid acceptor group also acting as anchoring group results in electrons located further into the TiO_2 particle. On the other hand, the **L2A3** dye, with a rhodanine-3-acetic acid acceptor group having an anchoring group not being part of the conjugation (lack of electron density) results in electron injection into states closer to the surface allowing fast recombination.[87] The origin of the fast recombination must be further substantiated. Aspects to be further considered are the surface properties of the TiO_2, decouple the parameters electronic coupling and excited state potential as well as controlling the dye orientation on the surface.

For the majority of the dyes when employed in a complete DSC configuration showed varying interfacial electron recombination that was correlated to the degree of generated dark current, i.e. recombination with the electrolyte (section 2.1.2). It was therefore concluded that even though the recombination kinetics to the dye cation could play a role, there appeared to be a correlation between the dye structure and the degree of electron recombination with acceptor species in the electrolyte. This issue is discussed in the following section.

3.7.2. Recombination with the acceptor species in the electrolyte

For solar cells with efficient dye regeneration, the losses will be dominated by electron recombination with acceptor species in the redox electrolyte. The redox electrolyte often consists of about 10 times higher iodide concentration (typically ~0.5 M) than iodine (typical 50 mM) to restrain the degree of recombination with electrolyte acceptor species. To provide efficient mass transportation as well as having an efficient reduction of I_3^- at the counter electrode, allowing high photocurrents, a small amount of acceptor species (iodine/triiodide) is still required in the DSC.

The recombination with acceptor species in the electrolyte is often referred to as dark current, as it is partially independent on light. In contrast, the recombination pathway to the oxidized dye requires light and does not occur in the dark.

The dark current generation was observed to depend on the dye structure and was described in *Papers III, IV* and further investigated in *Paper V*.

3.7.2.1. The influence of dye structures on V_{oc} and electron recombination

Different strategies can be employed to reduce the electron recombination with the electrolyte. A dense dye layer increasing the distance between the TiO_2 surface and the redox species has been attained by larger dye structures and/or by the introduction of alkyl chains located on the linker or the donor unit.[39,40,42,111,112] The incorporation of hydrophobic chains and/or bulky units into the dye structure, although successful, still shows different degrees of electron recombination depending on, for example, the structure of the dye linker conjugation.[39,113,114]

O'Regan discussed the correlation between the dye nature and electron lifetimes, based on the observation that the major limitation of novel dyes is their reduced V_{oc} values, in particular in comparison to the champion dyes **N3**/**N719**. Recently, the shorter electron lifetimes observed for several dyes were addressed by Durrant, Palomares and Mori as enhanced electron recombination with acceptor species in the electrolyte.[115-118] The origin of enhanced electron recombination observed for some dyes was suggested to be correlated with a complex formation between the ruthenium-based dye and iodine.[116] Mori and co-workers studied series of coumarin, carbazole and indoline organic dyes suggesting that larger dye molecules keep triiodide further away from the TiO_2 surface and hence causing longer electron lifetimes and higher V_{oc}.[118] It was also suggested that negatively charged atoms in the dye molecule attract cations in the electrolyte, which in turn can due to electrostatics induce a high local I_3^- concentration at the interface.[118]

3.7.2.2. The influence of the TPA dye linker conjugation on the V_{oc}

In *Paper III*, the linker conjugation was extended to enhance the absorption properties of the dyes as discussed in section 3.1.

The generated photocurrent increased in agreement with the enhanced spectral response attained by the extension of the linker conjugation. The produced photovoltage, V_{oc}, on the other hand decreased with the extension of the linker conjugation, i.e. the size of the dye, interestingly this is the opposite behavior compared to the trend observed for coumarin dyes.[118] The photovoltaic parameters for DCSs

based on the linker dyes are presented in Table 3.7.1. The smallest dye **L0** shows the highest V_{oc} (but not the highest J_{sc}), and is the only dye reaching equally high V_{oc} (735 mV under examined conditions) as the champion ruthenium-based dye **N719.**

Table 3.7.1 Current and voltage characteristics of DSCs (3µm thick working electrode) based on the **L0-L4** and **N719** (*Paper III*).

Dye	V_{oc} [mV]	η[%]	FF	J_{sc}[mA/cm^2]
[a]**L0**	735	1.55	0.73	2.89
L1	735	2.75	0.69	5.42
L2	710	3.08	0.68	6.42
L3	635	2.73	0.66	6.55
L4	580	1.70	0.64	4.56
N719	735	1.99	0.75	3.63

Electrolyte used: 0.6 M TBAI, 0.1 M LiI, 0.05 M I_2, 0.5 M 4-TBP electrolyte in acetonitrile. J_{sc} is the short-circuit photocurrent density, V_{oc} is the open-circuit voltage, FF is the fill factor and η the power conversion efficiency. [a] The **L0** dye was previously studied by Kitamura et al.[37]

The dark current–voltage characteristics showed a clear correlation between linker length and degree of generated dark current, see *Paper III*. Extended linker conjugation appears to enhance the recombination with the redox electrolyte. The same trend was observed for the rhodanine dyes (*Paper IV*). In Figure 3.7.2 both electron lifetime and dark-current characteristics are presented for three rhodanine-3-acetic acid linker dyes, here referred to as **L0A3**, **L1A3** and **L2A3**.

The **L2A3** dye showed most pronounced recombination, and it was estimated that some of the charge was also lost at short circuit conditions and could partly explain the poor IPCE observed for this dye employed in DSCs (*Paper IV*).

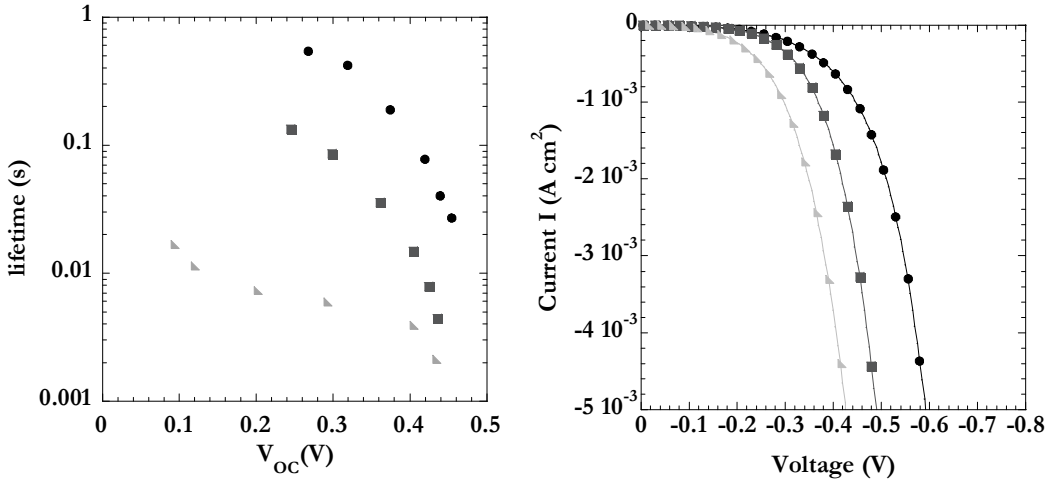

Figure 3.7.2 (left) Electron lifetime as function of open circuit voltage, (right) Dark Current- Voltage characteristics of DSCs consisting of **L0A3** (●), **L1A3** (■) and **L2A3** (►) based on the acceptor group rhodanineacetic-3-acid. Electrolyte: 0.5 M LiI and 0.05 mM I_2 in acetonitrile.

For the linker series based on cyanoacetic acid (*Paper III*) the amount of adsorbed dye, the dye load, decreased for the larger dyes, whereas for the rhodanine dyes (*Paper IV*) the higher dye loads were found for the larger dyes. The dye load could be correlated to the coverage of the surface and hence how efficient the dye layer blocks the approach of acceptor species, such as iodide and iodine.

The correlation between the dye conjugation and the photovoltaic performance was earlier observed by Hara et al. suggesting that the presence of aggregated/pi-stacked dyes restrained the photocurrent and hence the photovoltage.[119,120] In this thesis, it was observed that even though the photocurrent was enhanced due improved spectral properties, the photovoltage always appeared to decrease. The influence of the dye linker conjugation was further investigated in *Paper V*.

3.7.2.3. Investigating the origin of enhanced recombination with the electrolyte

In *Paper V* the origin of different V_{oc} was studied for the three different linker dyes **L0**, **L1** and **L3**. From Equations 1.5.1-1.5.2, differences in V_{oc} could be due to different conduction band positions and/or different electron concentrations in the TiO_2.

Performing charge extraction in the dark (applied bias) for sensitized and non-sensitized samples confirmed that the conduction band edge position mostly depended on the redox electrolyte and less on the presence of the dye. The different V_{oc} values could thus not be attributed to different TiO_2 conduction band edge positions. A significant difference in electron lifetimes was measured among solar cells based on the **L0**, **L2** and **L3** dyes. This confirms that the difference observed in V_{oc} for DSCs based on the different linker dyes was due to different electron recombination rates.

Furthermore, it was observed that the dyes showed different surface blocking properties. Current-voltage characteristics showed that increasing the dye loads of **L0** and **L2** resulted in longer electron lifetimes. On the other hand, increasing the dye load of **L3** gave limited increase in electron lifetimes. The enhanced dye loads resulted in enhanced photocurrents for all three dyes, but had very different effects on the electron recombination.

Figure 3.7.3 (left) depicts how the electron lifetime (measured at V_{oc}= 0.5 V) varies with the iodine concentration. **L3** based DSCs showed less dependence on the iodine concentration suggesting a different interaction between the dye and the acceptor species in the electrolyte. This was further supported by voltage decay measurements in the dark and dark current-voltage characteristics as depicted in Figure 3.7.3 (right). By estimating the conduction band edge position for the non-sensitized case it was confirmed that the presence of the **L3** dye enhances the electron recombination.

Polarizability and the position of partially negative atoms are dye structure properties discussed to influence the possible interaction between dye and surrounding acceptor species in the electrolyte.

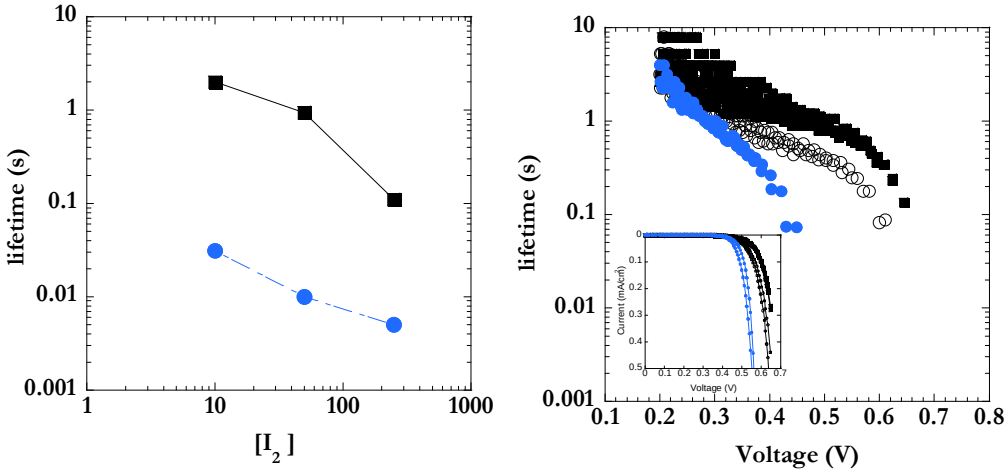

Figure 3.7.3 (left) The electron lifetimes for DSCs based on **L0** (squares) and **L3** (circles) at V_{oc}= 0.5 V as a function of I_2 concentration. (right) Electron lifetime as a function of voltage (dark voltage-decay experiments) bare TiO_2 versus (empty circles), **L0** (filled squares) and **L3** (filled circles) DSCs. Inset: dark current-voltage characteristics for the same set of cells.

Preliminary FT-Raman results (not published) on **L0** and **L3** dye solutions in combination with iodine showed fluorescence from the combination **L3**-iodine (I_2). The fluorescence shows up as a baseline offset as depicted in Figure 3.7.4. Experiments performed on **L0** and **L3** dye solutions in combination with triiodide ($TBAI_3$) did not show any fluorescence (data not shown). An apparent fluorescence from the excitation of a possible charge-transfer complex indicated that there may be a complex formation between the **L3** dye and I_2. It is possible that such dye- I_2 complex is responsible for the accelerated electron recombination observed for **L3** based DSCs.

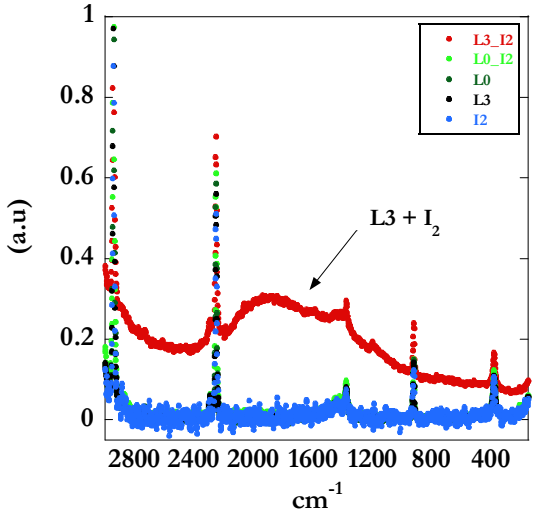

Figure 3.7.4 Raman spectra of **L0** and **L3** dye solution with and without I_2 in acetonitrile. The concentration used were [25mM I_2], [0.25 mM **L0**], [0.25 mM **L3**], [0.25mM I_2 : 0.25mM **L0**] and [0.25mM I_2 : 0.25mM **L0**], in acetonitrile. A YAG laser operating at 1024 nm was used.

3.7.2.4. TPA-rhodanine dyes and recombination with the electrolyte

An interesting comparison is the electron lifetimes as a function of V_{oc} between TPA-rhodanine dyes (*Paper IV*) and the indoline analogue, **D149**.[36,118] The latter has previously shown record efficiencies. Another interesting comparison is **L0A3** and **L0**, differing in their anchoring group. The dye structures are depicted in Figure 3.7.5. How the electron lifetimes vary between these dyes is illustrated in Figure 3.7.6. In both cases the TPA-rhodanine dyes showed significantly enhanced recombination.

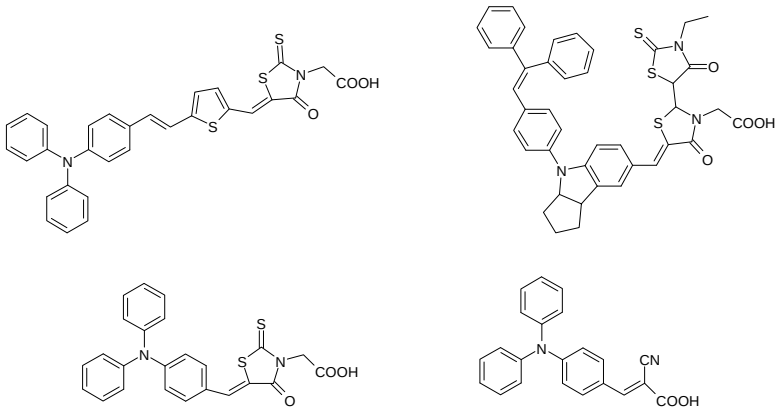

Figure 3.7.5 Molecular structure of dyes showing different lifetimes (top) **L2A3** (left) and **D149** (right), (bottom) **L0A3** (left) and **L0** (right).

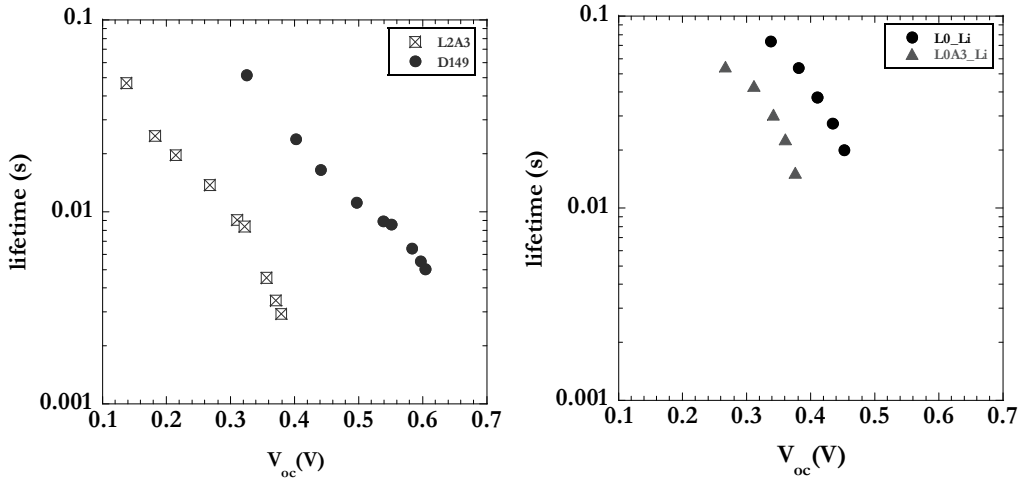

Figure 3.7.6 Electron lifetime as function of V_{oc}, in dye-sensitized solar cells based on (left) **D149** (circles) and **L2A3** (squares), based on 4 μm thick TiO_2 and an electrolyte consisting of 0.6 M DMPImI, 0.1 M LiI, and 0.05 M I_2 in acetonitrile and (right) **L0** (circles) and **L0A3** (triangles) based on ~3 μm thick TiO_2 and an electrolyte consisting of 0.6 M LiI, and 0.05 M I_2 in acetonitrile.

To understand the origin of specific dye/electrolyte species interactions is of importance to improve the general guidelines for future dye design. The main drawback for organic dyes up to date, even though showing excellent photocurrents, is the overall lower V_{oc}, in particular compared to ruthenium-based dyes.[40,118] With regards to the development and design of compatible new dyes and charge mediators, the ability to control desired and undesired intermolecular interactions would be of high interest.

3.8. The influence of the additive 4-TBP on the DSC performance

As mentioned in section 1.5.2 the TiO_2 energetics are affected by the nature of the surface charge. The additive 4-TBP (Figure 3.8.1) is commonly used in the redox electrolyte. Kay et al. noted that upon the inclusion of this additive an increased V_{oc} could be obtained with limited influence on the photocurrent.[121]

4-TBP acts as a weak base due to the lone electron pair located at the nitrogen, giving the molecule a dipole character. Alteration of the conduction band edge of TiO_2 towards negative potentials has been assigned to this additive, due to surface adsorption[70] and the origin is analogous to the conduction band edge shift observed for adsorptive cations such as Li^+, as discussed in section 1.5.2.[60,66]

Nakade et al. observed that using 4-TBP resulted in higher V_{oc} in the presence of Li^+ compared to TBA^+.[66] It was discussed that the surface adsorption of 4-TBP may depend on the nature of the coexisting cations. In addition, 4-TBP has been suggested to alter the recombination with the electrolyte.[60] It has been discussed whether the possibility of complex formation between 4-TBP and iodine may reduce the electron recombination due to less accessible electron acceptors.[60,122-124]

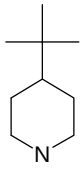

Figure 3.8.1 Molecular structure of 4-tert-butyl-pyridine, a potential-increasing additive widely used in liquid electrolyte based DSCs.

The use of 4-TBP in combination with organic dyes has given both excellent results[39,125] as well as significantly reduced IPCE.[70,126]

The influence of 4-TBP on the photovoltaic efficiency for DSCs based on **L1A3** and **L2** is shown in Table 3.8.1, where a 140 mV change in V_{oc} is obtained in the presence of 4-TBP. It may be noted that the order of voltage enhancement is similar to the one observed by Nakade et al.[66] (about 150 mV) but smaller than the one observed by Boschloo et al.[60](about 260 mV), observe that these studies were performed with the **N719** dye. This indicates that the experimental conditions, such as TiO_2 surface properties and electrolyte composition, are also decisive for the obtained interfacial surface charge.

Table 3.8.1 Photovoltaic performance of DSCs based on **L1A3** (*Paper IV*) and **L2** dyes in the presence and absence of 0.5 M 4-TBP in the redox electrolyte.

Dye	V_{oc} [mV]	η[%]	FF	J_{sc}[mA/cm²]
L1A3	0.44	2.3	0.55	10.5
L1A3/TBP	0.58	2.0	0.58	5.9
L2	0.54	3.64	0.55	12.44
L2/TBP	0.68	4.72	0.65	10.72

By plotting extracted charge as function of voltage (Figure 3.8.2) it may be observed that for a given amount of charge, different values of Voc are obtained with and without 4-TBP. This can be interpreted as a conduction band shift, a shift of the electronic states of TiO2 towards negative potential.

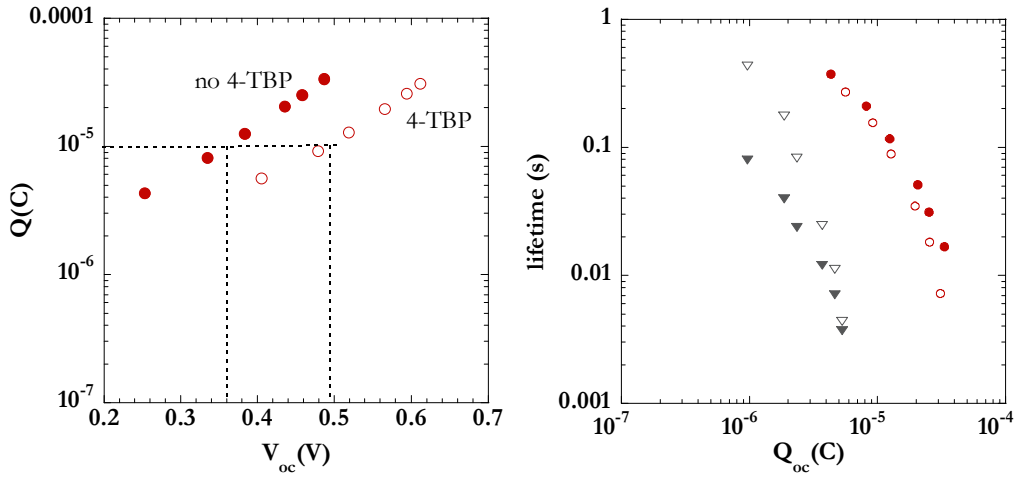

Figure 3.8.2 (left) Extracted charge as a function of V_{oc} for DSCs based on **L2.** (right) Electron lifetime as function of extracted charge, in dye-sensitized solar cells based on **L1A3** (triangles) and **L2** (circles) with 4-TBP (filled) and without 4-TBP (empty) in the redox electrolyte.

A conduction band shift of about 150 mV can be observed for the charge-voltage relation shown in Figure 3.8.2 (left). This is in agreement with previously observed conduction band edge shift for DSCs based on **N719**.[60,66]

On the other hand, no significant change in electron lifetime was observed upon the presence or absence of 4-TBP depicted for **L1A3** and **L2** in Figure 3.8.2 (right). This is in agreement with the V_{oc} enhancement of the same order as the conduction band edge shift in the presence of 4-TBP observed for **L2.** This suggests that for the dyes examined here, the 4-TBP had no significant blocking effect in terms of keeping electron acceptor species (triiodide-iodine) away from the TiO_2 surface. It is possible that the nature of the organic dye layer is different compared to the dye layer formed by **N719** and hence resulting in different interfacial blocking.[60]
Even though the blocking effect of 4-TBP appears to vary among the studied cases in the literature the electrostatic effect appears to be consistent, yielding about 150 mV negative conduction band edge shift in the presence of 4-TBP for several examined conditions. [60,66,127]

The IPCE are shown in Figure 3.8.3 (top) for **L2** and **L0A3** in the presence and absence of 4-TBP. As observed the IPCE of the rhodanine-3-acetic acid dye, **L0A3**, is significantly reduced in the presence of 4-TBP whereas the cyanoacrylic acid (**L2**) dye

shows less dependence. The IPCE based on the **N3** dye is also shown for comparison, showing a behavior similar to that of **L2** in the presence of 4-TBP, see Figure 3.8.3 (bottom). Considering the estimated excited state potentials, -1.1 V for **L0A3** (*Paper IV*) and – 0.75 V for **N3**,[8] versus NHE, it is rather surprising that a negative conduction band edge shift appears to only affect the IPCE of the former. These results supports that the ultra-fast processes concerning the rhodanine dyes might be more correlated to the combination of the non-conjugated anchoring group and the less favorable energetics. It is of high interest to decouple these two parameters to gain understanding in the how to approach a desired excited state potential for organic dyes.

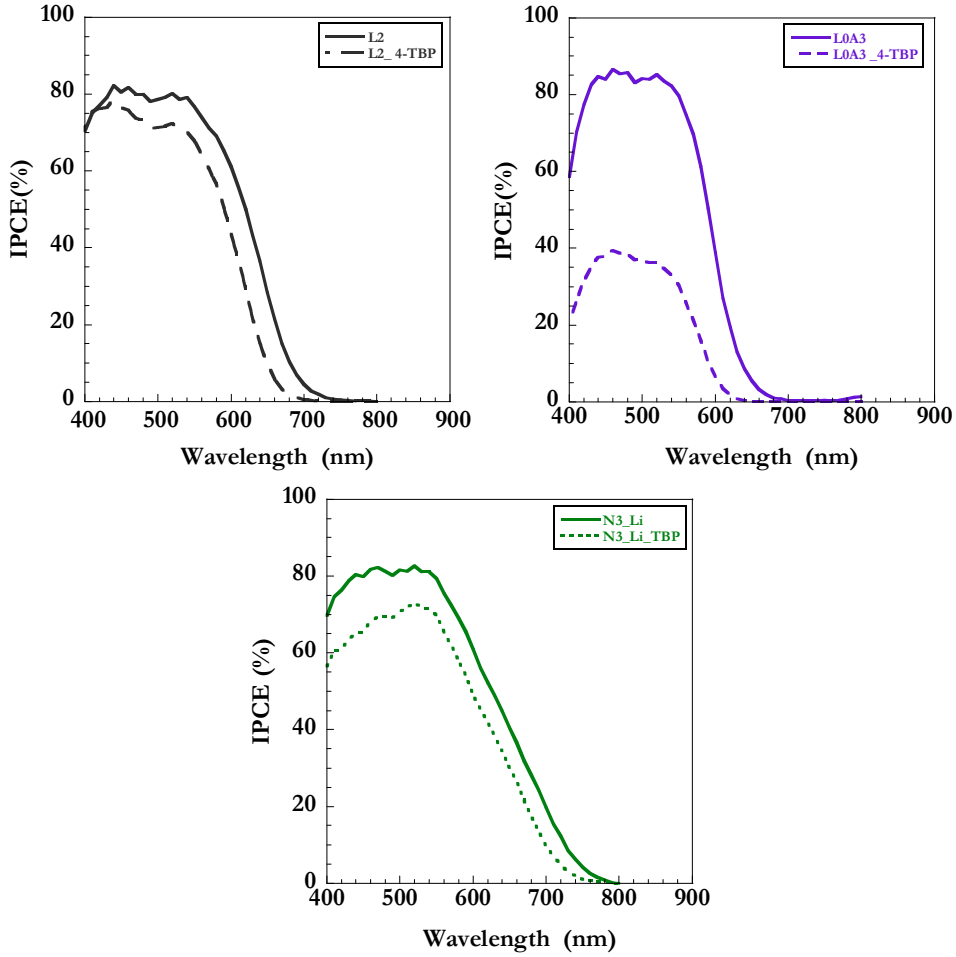

Figure 3.8.3 Spectra of monochromatic incident photon-to-current conversion efficiency (IPCE) for DSCs based on (top left) **L2A1**, (top right) **L0A3** (*Paper IV*) and (bottom) **N3**. Electrolyte: 0.5 M LiI, 0.05 M I_2 with (dotted line) and without (solid line) 0.5 M 4-TBP in acetonitrile.

A qualitative estimation of the apparent injection yield (at this time scale) in the presence and absence of 4-TBP can be done by comparing the amplitude of the differential absorption of the oxidized dye in a PIA experiment (see sections 2.2.4 and 3.6.1). The PIA differential spectrum of the **L1A3** oxidized dye is shown in Figure 3.8.4 (left) and shows a negative absorption, negative bleach, at 540 nm and a positive absorption at 690 nm.

By monitoring the differential absorption decay, larger amplitude of the oxidized dye was obtained for an electrolyte containing 0.5 M $LiClO_4$ and a significantly smaller

absorption amplitude for an electrolyte containing 0.5 M 4-TBP in acetonitrile. This was observed for all three dyes and is depicted for **L1A3** in Figure 3.8.4 (right). The long time scales of the PIA measurement, 10 µs-10 s, and yields limited information about the processes occurring at faster time scales. A low PIA signal may originate from poor injection and/or pronounced fast recombination with the oxidized dye. Faster time resolved techniques are needed to investigate the origin of the lower PIA amplitude observed in the presence of 4-TBP.

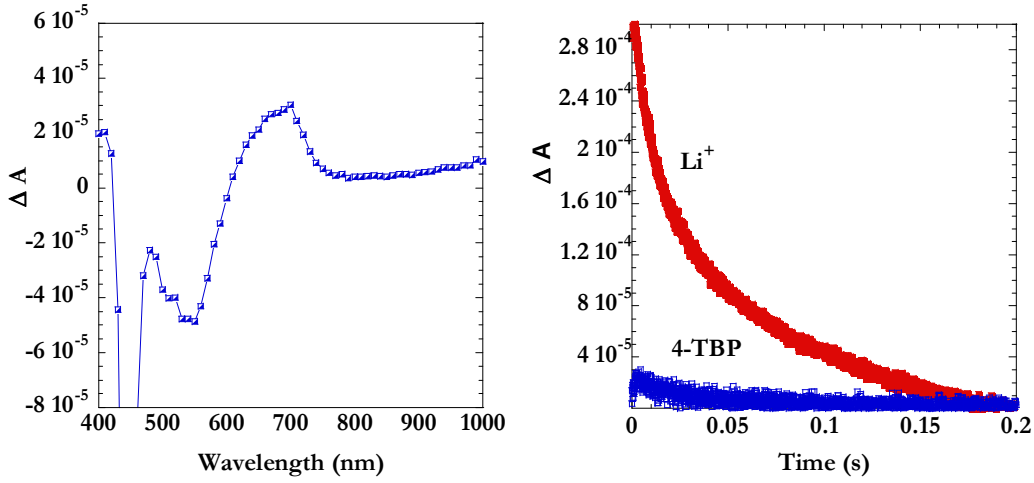

Figure 3.8.4 (left) Photoinduced transient absorption spectum of **L1A3** sensitized nanostructured TiO_2 film excitation wavelength 450 nm, modulation frequency 10 Hz. (right) Transient absorption decay at 690 nm of **L1A3** sensitized nanostructured TiO_2 film in the presence of 0.5 M lithium perchlorate and 0.5 M 4-TBP in acetonitrile,

3.9. The influence of "dye aggregates" on the DSC performance

3.9.1. When is dye aggregates discussed

The formation of dye aggregates refers to a specific dye-dye interaction that will influence the dye sensitization and the dye layer properties when adsorbed onto the TiO_2 surface.[70,72,80,96] The influence of dye-dye interaction or dye aggregation on the photovoltaic performance of DSCs has been reported to be either advantageous,[72,96,128] due to broader and/or additional absorption bands enhancing the spectral response or disadvantageous,[70,71] due to non-injecting dyes and/or dye excited-state quenching[129] leading to less efficient electron injection.[70,130]

In this thesis the discussion will be limited to the latter aspect. The discussion concerning disadvantageous dye aggregates arises when a dye with appropriate absorption spectrum, estimated energy levels and high dye load, yields unexpectedly low photocurrents.[33,81,121] Apart from reduced photocurrents, the presence of dye aggregates is often confirmed by spectral shift and/or additional absorption peaks observed in the absorption spectrum of the dye-sensitized TiO_2 films.[70,96] Additional spectral peaks are a quite strong evidence of aggregate formation and are usually observed for flat dyes such as merocyanines forming various types of aggregates due to several dye packing possibilities.[119,131] For many of the currently used organic dyes for DSC application there is actually no direct evidence for the presence of aggregates but rather indirect

indications of the presence of inactive/non-injecting dyes. As mentioned in section 2.1.2, the parameters determining IPCE can be expressed as;

$$IPCE(\%) = LHE \cdot \Phi_{inj} \cdot \eta_{reg} \cdot \eta_{cc}$$

The presence of non-injecting dyes/aggregated dyes at the surface can in principle affect all parameters even though the discussion about aggregates often refers to dyes not contributing to the electron injection. This effect is not included in any of the terms in the given equation. The presence of non-injecting dyes/dye aggregates may be eliminated by the addition of coadsorbents into the dye solution resulting (in many cases) a reduction in dye load but an increase in photocurrent.[70,121] In general, there is a trade-off between the dye-coadsorbent ratio that depends on the nature of the dye and the coadsorbent.

3.9.2. Dye structures and non-injecting dyes/dye aggregates

Dye structures leading to this problematic are often flat and/or largely conjugated. Other parameters such as solvent and semiconductor properties can also influence the dye aggregate formation.[131] To avoid "aggregate"-related problems the dye structure can be modified with side ring,[71] bulky donor units,[39,132] alkyl chains located on the linker or the donor unit.[40-42,111,112,133-136]

Hara and co-workers studied the effect of different positions of hexylthiophene substituents in carbazole dyes showing that complex molecular design is required for an optimal solar cell performance.[111] The use of alkyl chains positioned on the donor unit has shown excellent results for TPA-based dyes, where an alkyl chain length of six showed optimal efficiency.[41] However, for dye structures modified with alkyl chains and/or bulky units the use of coadsorbent in the dye bath is still reported and not all alkyl-chain modified dyes result in enhanced photovoltaic properties.[39,113,114,137]

3.9.3. Dyes structures and coadsorbents

From an earlier study it was apparent that the dye structural properties are more decisive than the dye spectral properties for three dyes, **D29**, **D35**, **D37** (Figure 3.9.1) with varying bulkiness and number of donor substituents.[69]

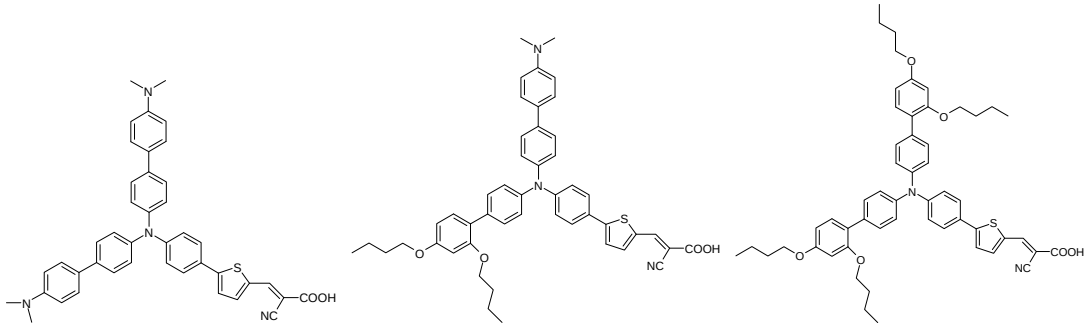

Figure 3.9.1 Molecular structures of sensitizers **D29**, **D37** and **D35**, *Paper VI*.

In *Paper VI*, it was investigated how dye modifications (alkoxy chains) perform in comparison to the external use of coadsorbent in the role of providing reduced amount of injecting dyes/aggregated dyes and providing effective surface blocking impeding interfacial recombination. A comparative study was performed on the dyes **D29**, **D35** and **D37** in the presence and absence of the coadsorbent chenodeoxycholic acid (**CDCA**) in the dye bath solution, see 3.9.4 (left).

The photovoltaic results are presented in Table 3.9.1. The trend was obvious and clear. In the presence of **CDCA**, the **D29** dye, with less bulky donating units, showed a reduction in dye load but a pronounced improvement in the photovoltaic performance whereas the **D35** dye, bearing four alkoxy chains on the donating units, was more or less insensitive to the presence of the **CDCA**. The study shows that coadsorbent-free DSCs can be attained by strategic dye design. By comparing DSCs based on **D29-CDCA** and solely **D35**, it was concluded that the internal dye structure properties were superior to the external use of **CDCA** for the examined conditions.

In Figure 3.9.2 the absorption spectra of dye and dye/**CDCA**-sensitized TiO_2 films show no spectral differences, even though the latter reduce the dye load and increase the IPCE. Due to the absence of direct evidence confirming dye aggregate formation, it is only possible to ascertain the presence of non-injecting dyes in the case of **D29** DSCs.

Table 3.9.1 Current and voltage characteristics of DSCs based on **D29** and **D35** dyes,[a] with and without **CDCA** during the sensitization (*Paper VI*).

Dye	J_{sc} (mA/cm^2)	V_{oc} (V)	FF	η (%)	η (%) ↑	Dye load (10^{-8} mol/cm^2)
D29[b]	7.98	0.66	0.47	2.22		7.51
D29/CDCA	11.15	0.71	0.52	4.09	84	4.10
D35[c]	12.02	0.78	0.54	5.07		5.24
D35/CDCA	11.84	0.77	0.56	5.10	0.6	4.57

[a] Photovoltaic performance under AM 1.5 irradiation of DSCs based on **D29** and **D35** dyes. Electrolyte: 0.6 M tetrabutylammonium iodide (TBAI), 0.1 M LiI, 0.05 M I_2, 0.5 M 4-*tert*-butylpyridine (4-TBP), 0.05 M guanidinium thiocyanate (GuSCN) in acetonitrile. Dye bath: [b] acetonitrile and [c] ethanol solution (2×10^{-4} M) with and without 6 mM **CDCA**.

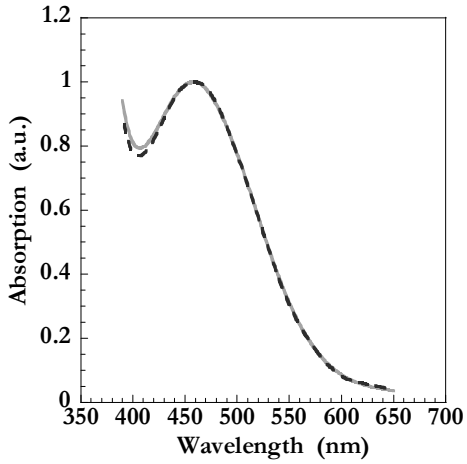

Figure 3.9.2 Normalized absorption spectra of **D29** on TiO_2 (1μm), sensitized in an acetonitrile dye solution (0.2 mM) with (solid line) and without (dotted line) the **CDCA** (6 mM) (*Paper VI*).

The improvement of V_{oc} when using coadsorbents has been ascribed to a negative conduction band shift,[138] enhanced injection yield and longer electron lifetimes due to the surface protection by the coadsorbent.[70,71,80,121] The influence of the dye on the recombination in the presence of coadsorbents is complex due to the unknown dye-coadsorbent surface concentrations.

In *Paper VI*, it is described how an increased number of active **D29** dye molecules provided by the presence of the **CDCA**, improved the solar cell efficiency due to improvements of both J_{sc} and V_{oc}.

The electron lifetime as function of extracted charge (Figure 3.9.3) shows that the electron recombination is impeded in the case of **D29**/**CDCA**-DCSs compared to **D29**-DSCs. It is possible that the coadsorbent provides an evenly distributed dye layer and/or that the adsorbed **CDCA** improves the surface blocking against electron recombination.

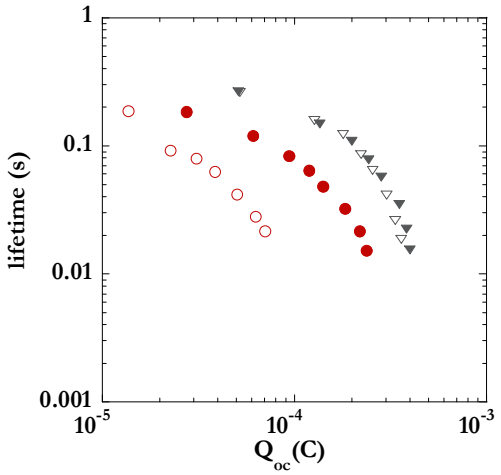

Figure 3.9.3 Electron lifetime as a function of extracted charge under open-circuit conditions for DSCs based on **D29** (circles) and **D35** (triangles), respectively, with (filled) and without (empty) **CDCA** during the sensitization.

3.9.4. The dye/coadsorbent/semiconductor interface

There is of course a trade-off between the synthetic work required for structural modifications and the use of a dye-coadsorbent mixture in the dye bath. Two examples of widely used coadsorbents are depicted in Figure 3.9.4 a-b and the latter (Figure 3.9.4c) was recently reported to successfully retard the interfacial electron recombination for DSCs based on a ruthenium sensitizer.[139]

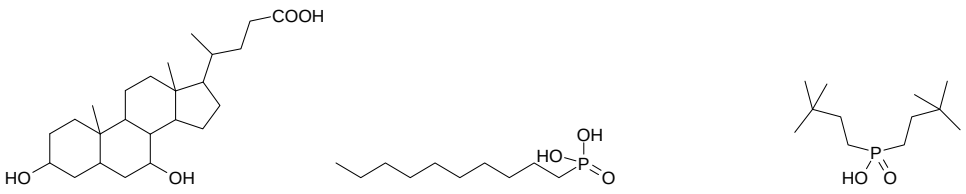

Figure 3.9.4 The molecular structure of the coadsorbents used in *Paper VII*. (left) chenodeoxycholic acid (**CDCA**), (middle) dodecylphosphonic acid (**DPA**) and (right) dineohexyl bis-(3, 3-dimethyl-butyl)-phosphinic acid (**DINHOP**).[139]

To get more insight of the properties of dye/coadsorbents/semiconductor interface a study was performed based on the **D29** (see Figure 3.9.1) dye in combination with three coadsorbents, **CDCA**,[70,121] **DPA**[140,141] and **DINHOP**[139] (*Paper VII*). By means of the surface-sensitive technique Photoelectron spectroscopy (PES) the dye/coadsorbent ratios can be determined and are presented in Table 3.9.2.[73] The surface concentrations can be evaluated by directly comparing the intensities of the sulphur and phosphor signals, respectively.

The surface concentration of **DPA** is about three times higher than that of **DINHOP**. In the **D29**/**DPA** and **D29**/**DINHOP** samples the sulphur to phosphor relationship is *1:3.5* and *3:1* respectively, showing that the **DPA** and **DINHOP** molecules to a large extent exchange with the **D29** dye molecules. On the contrary, the similar relative surface concentrations between carbon and sulphur, see Table 3.9.2, indicate that the **CDCA**, if present at the surface, must adsorbed in a rather different way compared to **DPA** or **DINHOP**.

Table 3.9.2 Relative amounts of elements present on the TiO_2 surface on the investigated dye-sensitized samples. To facilitate comparison the relative amounts are normalized versus the amount of sulphur (*Paper VII*).

Element	**D29**	**D29/DPA**	**D29/DINHOP**	**D29/CDCA**
Sulphur	1	1	1	1
Phosphor	0	3.5	0.34	0
Carbon	41	72	49	41
Nitrogen	3.6	3.4	3.7	3.6

Identical samples were also characterized in the context of DSCs. Enhanced photocurrents were obtained when employing **DPA** and **DINHOP** even though the dye load of **D29** was reduced, see Figure 3.9.5 (left). The different surface concentration of **DPA** and **DINHOP** yields the similar improvements in the photocurrents. The improvement in IPCE in the presence of these coadsorbents was larger when using thicker TiO_2 films, indicating that the sensitizing dye layer might be different in thin and thick films, respectively (Figure 3.9.5, inset).

For **CDCA** the dye load was less affected and the photocurrent was slightly decreased. It is noticeable that using equal ratios of **D29-CDCA** in two different solvents, acetonitrile (*Paper VI*) ethanol (*Paper VII*), yield enhanced performance in the case of acetronitrile and a decrease in performance in the case of ethanol. It is evidently that the examined conditions will influence the dye/solvent/coadsorbent interplay resulting in different dye layer properties.

The effect of the coadsorbents on the surface blocking and the electron recombination was modest for all cases, see Figure 3.9.5 (right). The role of **DPA** and **DINHOP** in the case of **D29** using ethanol as a solvent indicates that the coadsorbents exchange positions with the dyes and thus do not affect the surface coverage to a greater extent.

The role of coadsorbents in DSCs is a complicated matter and some general guidelines are required. Even though trial and error approaches may still be used, the number of choices may be reduced if gaining some understanding of the dye/coadsorbent/semiconductor interfacial properties.

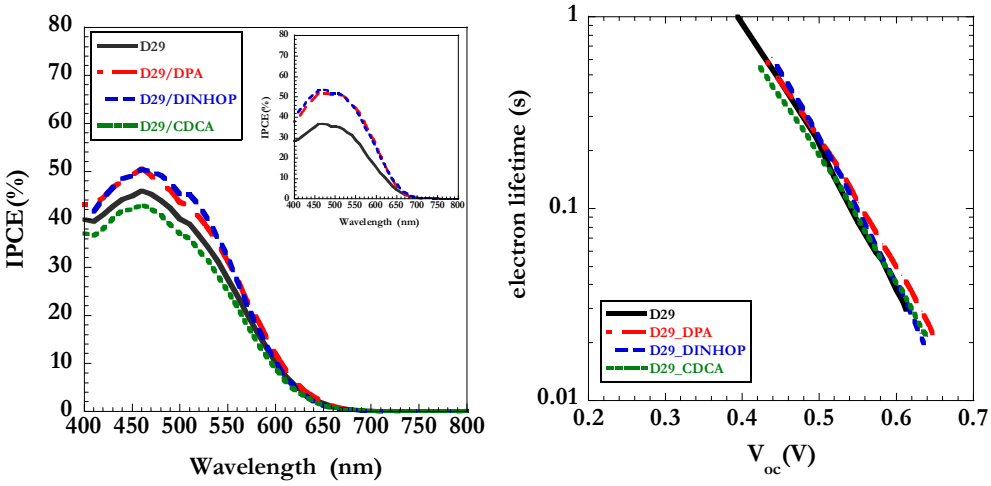

Figure 3.9.5 (left) Spectra of monochromatic incident photon to current conversion efficiency (IPCE) of 4 μm DSCs based on the organic dye **D29** sensitized in 200 μM ethanol dye solution (i) plain, (ii) 50 μM **DPA** and (iii) 50 μM **DINHOP** and (iv) 6mM **CDCA**, inset IPCE for 12 μm DSCs based on the organic dye **D29**, **D29**/**DPA** and **D29**/**DINHOP**. (right) Electron lifetime as function of V_{oc} for the 4 μm DSCs. Electrolyte: 0.6 M TBAI, 0.1 M LiI, 0.5 M 4-TBP and 0.05 M I_2 in acetonitrile.

Conclusions and future outlook

The series of dyes studied in this thesis are summarized in Chart 1 (Appendix C), where the concluding remarks in each project is specified. The challenge consisted in finding the limiting position of the dye energetics without sacrificing the function of the vital electron-transfer processes related to the dye. The core of this thesis is the identification of the processes and properties limiting the performance of the DSC sensitized with novel organic dyes.

Dye structure design. Improved light-harvesting properties and systematic energy level tuning of the dyes were accomplished by the dye structure modifications used in this thesis. However, dye induced electron recombination limited the virtue of the spectral properties. Therefore, considering future dye design, it is of interest to introduce bulky units to dyes with beneficial spectral properties to prove the concept of combining the better of the two worlds. The TPA-rhodanine dyes, obviously showing enhanced recombination compared to its indoline counterpart should be modified with a bulky donor unit. Considering that the absorption onset for the TPA-rhodanine dyes extends out to 700-800 nm, an attempt should be made to improve their surface blocking properties.

Among the series of dyes studied herein, three electron-transfer processes were identified to be altered consequently limiting the DSC performance.

Fast electron-transfer processes. The rhodanine dyes in *Paper IV* showed excellent spectral properties, but the photocurrent generation showed great sensitivity to the alteration of the conduction band position of the TiO_2. The combination of slightly lower excited state potential (LUMO) in combination with the non-conjugated anchoring group appears to be decisive for ultra-fast electron transfer processes such as electron injection and fast recombination to the cation. It is of high interest to decouple these properties and to verify the limiting position of the excited state of organic dyes. The origin of the fast recombination should also be addressed. Other closely related dye families should be investigated, as well as how the modification of the semiconductor surface (overlayer, coadsorbents) influences the recombination kinetics.

The effect of practical parameters such as dye sensitization, aggregate formation, presence of coadsorbents and redox electrolyte on the dye kinetics remain to be addressed. In addition, series of organic dyes designed to act as model systems should be studied in DSC configuration to explore the behavior of perturbed ideal systems.

Dye regeneration. As described in *Paper II* two pyrrolidine dyes, differing in only one conjugated unit (phenyl and thiophenes) showed different ground state potentials at 0.8 V and 0.5 V vs. NHE, respectively. By means of photoinduced absorption (PIA) measurements, limited dye regeneration was identified for the latter case whereas the former did not show any apparent limitation. The dye ground state redox potential of the dye can still be improved to an intermediate value as suggested by this study.

The regeneration kinetics of different organic dyes, also in combination with new charge mediators, is of general interest and deserves more attention.

Dye induced interfacial recombination to the electrolyte. Despite the narrow absorption band often observed for many organic dyes, respectable photocurrents are continuously reported. In contrast, significantly lower photovoltages are generally observed for DSCs based on organic dyes. The main drawback has been identified, by us (*Papers III-V*) and by others, to be an enhanced interfacial recombination with the electrolyte, induced by the presence of certain dyes. How efficiently the different dyes protect the surface and the possible interaction with redox species were further investigated in *Paper V*. DSCs based on the more conjugated dyes showed enhanced recombination in comparison to bare TiO_2. They also showed less iodine concentration dependent recombination kinetics. These results are in agreement with the hypothesis of a specific dye-redox species interaction being responsible for the enhanced interfacial recombination.

The iodide/triiodide redox couple is still the redox couple used in the champion solar cells and is therefore always of high interest. It should be verified if there is a fundamental interaction between certain dyes and iodine or triiodide molecules in the absence of the DSC configuration. By means of techniques such as IR, Raman, UV-vis, PES and CV it should be possible to gain information of how and where the interaction occurs. Theoretical calculations should also be able to support such data. Moreover, gaining fundamental understanding of the interaction between dye and redox species is of high importance for the future design of new charge mediators. Thus it would be possible to design molecules showing desired interactions to, for example, facilitate the dye regeneration. Another aspect to be undertaken when considering the compatibility between dyes and novel charge mediators is to protect the surface of TiO_2 from the charge accepting units.

Part of the problem with interfacial recombination has been reported to be solved by structural dye modifications. The introduction of bulky alkyl chains provides dye layer properties having surface-insulating effects often resulting in enhanced electron lifetimes and improved photovoltages. The properties of the formed dye layer can be improved both by structural modifications of the dye and/or the introduction of coadsorbents. Both have common purposes, to suppress negative dye-dye interaction as well as providing surface protection to suppress recombination. For the set of dyes studied in *Paper VI* it was shown that dyes with intrinsic dye sterical properties are superior to the external use of a coadsorbent when employed in DSCs.

However, considering the advantages of short simple synthetic routes, the use of coadsorbents is still of importance. There is limited information about properties of the adsorbed dye layer in the presence of different coadsorbents. One of the reasons is the difficulty to quantify the dye/coadsorbent ratio on the TiO_2 surface. An attempt to understand the interfacial properties of such a system was made in *Paper VII*. The study revealed to what extent various coadsorbents exchange with dye molecules on the TiO_2 surface. Quantitative information about the dye-coadsorbent surface concentrations will facilitate further understanding of the interfacial properties of DSCs.

To gain further understanding of the interfacial complexity of the semiconductor/dye/electrolyte components fundamental studies *closely* related to the working solar cell device should be performed.

Acknowledgement

I would like to express my sincere gratitude to:

Anders Hagfeldt, my supervisor, for accepting me as PhD student and for being so positive and encouraging during all these years. You are great and one of a kind!

Swedish Research Council, Swedish Energy Agency and **KTH** for funding.

Gerrit Boschloo for help and support during the years. **Tomas Edvinsson** for sharing your knowledge, collaborations and support especially during the beginning of my PhD. **Håkan Rensmo** for being an exceptional teacher and for rewarding collaborations. **Shogo Mori** for two excellent weeks in Japan, collaboration, feedback, guidance and support.

Maria Quintana, **Daniel Hagberg**, **Joanna Wiberg**, **Lars Kloo**, **Gerrit Boschloo** and **Anders Hagfeldt** for proof-reading my thesis.

Daniel Hagberg, my excellent colleague and friend, for great dyes, nice afterworks and the HOMO-LUMO library. **Maria Quintana**, mi amiga, my friend, for intriguing ZnO collaborations, pisco, salsa and support when finishing my thesis. **Maria Hahlin** and **Erik M. J. Johansson** at Uppsala University for interesting collaborations about the interfacial complexity of solar cells. **Joanna Wiberg** at Chalmers Technological Institute, for ultra-fantastic laser spectroscopy collaborations. **Jarl Nissfolk** for impedance, ZnO and the red fox. **Kazuteru Nonomura** for collaborations and many nice non-scientific conversations. **Licheng Sun** and all members of his group for being so friendly and helpful, in particular **Martin. K. Karlsson** and **Peng Qin** for nice collaborations. **Tore Brinck** and **Mats Linder** at Physical Chemistry KTH for calculations, discussions and collaborations. **Lars Kloo** for valuable discussions. **Lena Skowron** for all the help with administrative things. All current and past group members of the **Hagfeldt group**, in particular my excellent collaborators **Eva Unger** and **Xiao Jiang**. **Cecilia Lalander**, **Kristofer Fredin**, **Leif Häggman**, **Teresa Lana-Villareal** and **Fernando Bogzolian** for providing positive and enjoyable working environment.

Håkan Rensmo, **Jarl Nissfolk**, **Tomas Edvinsson** and **Shogo Mori** for inspiring, motivating and encouraging discussions. I learned a lot from you!!

My **family** and **friends** for being there through the years.

My beloved **Martin Lindhe** for your endless love and support.

Appendix A

My contribution

Paper I.
Performed initial dye characterization and photovoltaic work, helped with the manuscript.

Paper II.
Responsible for the photovoltaic work of the project, wrote main parts of the related conclusion and discussions in the manuscript.

Paper III.
Major contribution to the initiation of the project.
Responsible for the dye characterization and parts of the photovoltaic work of the project, wrote the related conclusion and discussions in the manuscript.

Paper IV.
Major contribution to the initiation of the project.
Responsible for the photovoltaic work of the project, wrote the related conclusion and discussions in the manuscript.

Paper V.
Major contribution to the initiation of the project, responsible for the photovoltaic work and wrote main parts of the manuscript.

Paper VI.
Major contribution to the initiation of the project, contributed to discussion and wrote minor parts of the manuscript.

Paper VII.
Major contribution to the initiation of the project.
Responsible for the photovoltaic work of the project, wrote the related conclusion and discussions in the manuscript.

Did not perform any organic synthesis, NMR, calculations or photon electron spectroscopy work.

Appendix B

Table 1. The ground state redox potential measured for two different dyes in solution (0.1 M $TBAPF_6$) versus adsorbed onto TiO_2.

Dye	**L0**	**L3**
$E_{pot}(D/D^+)$ vs NHE on TiO_2	1.30	1.13
$E_{pot}(D/D^+)$ vs NHE in solution	1.37	1.07

Table 2. The estimated $E_{0\text{-}0}$ values from the intercept of the absorption and emission spectra of **L2** in different solvents and on TiO_2. For the latter, the estimation obtained from 10 % of the absorption onset is also given.

L2 in/on	MeCN	DCM	Tol	TiO_2	TiO_2 (10 % onset)
$E_{0\text{-}0}$ (eV)	2.48(deprot) 2.26(plain)	2.1	2.23	2.31	2.25

Table 3. [a]The estimated $E_{0\text{-}0}$ values from the intercept of the absorption and emission spectra for deprotonated linker dyes in MeCN and from 10 % absorption onset of the dyes adsorbed on TiO_2. [b]The redox potential of the linker dyes in solution. [c]The corresponding estimated excited state potentials.[d] The absorption maximum on TiO_2 given in eV and [e]the corresponding estimated excited state potential (non-relaxed).

Dye	[a]$E_{0\text{-}0}$(eV) 10% onset TiO_2/sol	*[d]E(eV)/ λ(nm) Abs max on TiO_2*	[b]$E_{pot}(D/D^+)$ vs NHE in sol	[c]$E(D^*/D^+)$ vs NHE in TiO_2/sol	*[e]E(D*) vs NHE in sol if calc with Abs max on TiO_2*
L0	2.58/ 2.90	*3.19*	1.37	-1.21/-1.53	*-1.82*
L1	2.32/ 2.64	*3.068*	1.21	-1.11/-1.43	*-1.86*
L2	2.25/ 2.48	*3.035*	1.13	-1.12/-1.35	*-1.905*
L0A3	2.23/ 2.38	*2.82*	1.27	-0.96/-1.11	*-1.55*
L1A3	2.06/ 2.19	*2.69*	1.15	-0.91/-1.04	*-1.54*
L2A3	1.97/2.08	*2.62*	0.98	-0.99/-1.10	*-1.64*

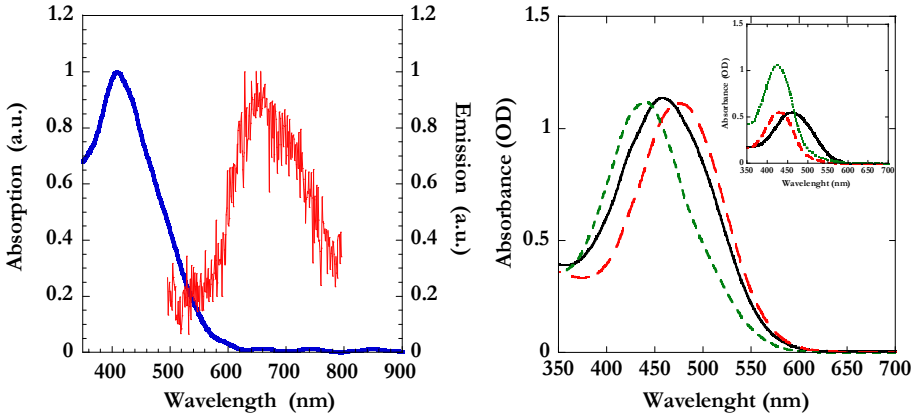

Figure 1. (right) Nomalized absorption and emission spectra of **L2** adsorbed on TiO_2. (left) Absorption spectra of the **L2** dye in MeCN solution before ultra sonication (solid line), after 1 h (lines) and after ultra sonication (dotted line). Inset: Ultra sonicated dye solutions, different **L2** dye batches.

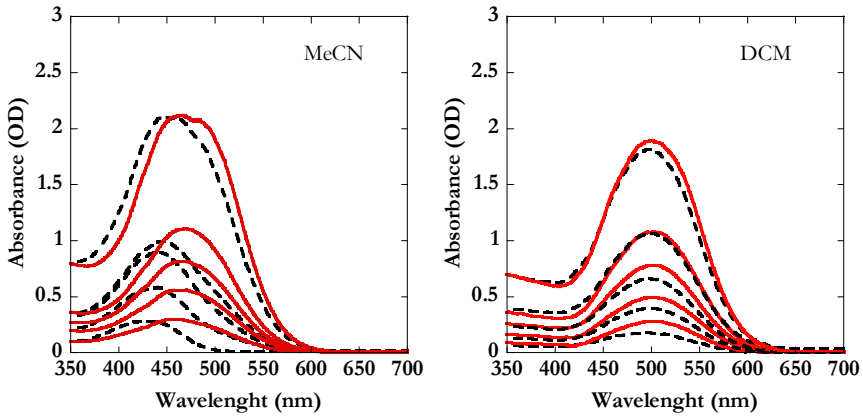

Figure 2. Absorption spectra of different concentrations of the **L2** dye solutions (left) in MeCN (dotted line) and ten days after (solid line), (right) in DCM (dotted line) and ten days after (solid line).

Appendix C

Chart 1.

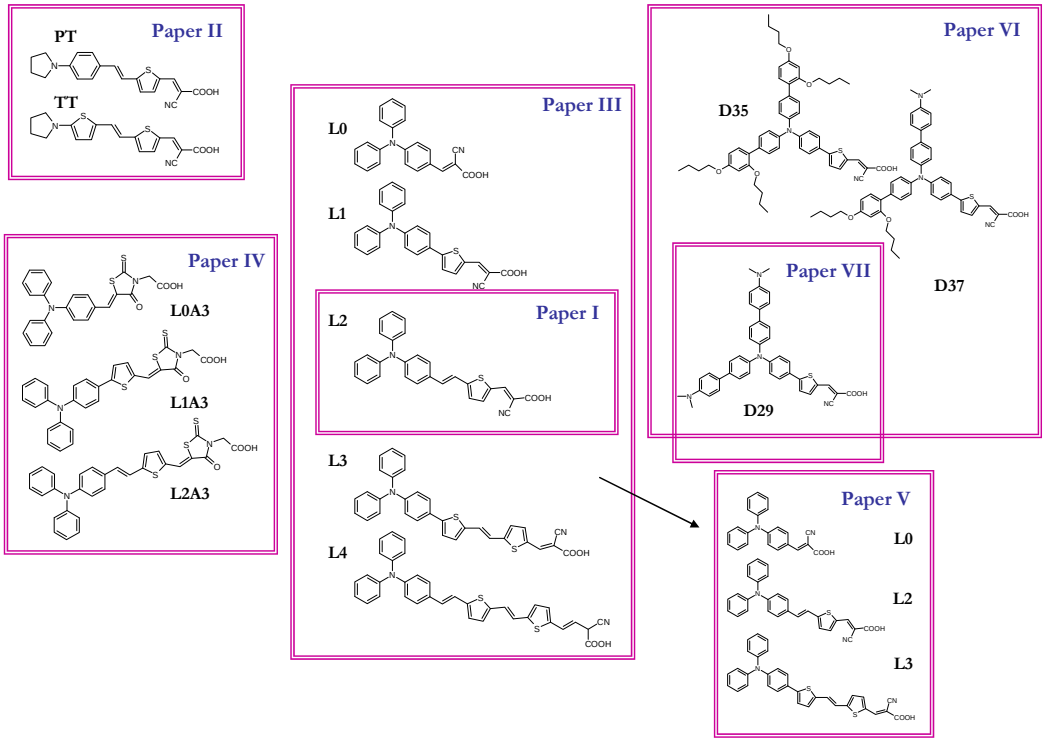

Paper I. The triphenylamine (TPA) based **L2** dye showed promising solar cell efficiencies, and was used for further dye modifications.

Paper II. Photoinduced absorption results imply limited dye regeneration of the **TT** dye, with a ground state redox potential at 0.5 V vs. NHE compared to ~ 0.3-0.4 for the iodide/triiodide redox couple. The dye regeneration appears to be limited by the insufficient driving force.

Paper III. Tuning of the dye (**L0-L4**) energy levels was accomplished; however parallel undesired interfacial recombination as function of dye conjugation was observed for the larger, more conjugated dyes. Dye surface orientation and surface coverage were discussed.

Paper IV. Additional broadening of the dye absorption spectra was attained by introducing a new anchoring group, the rhodanine-3-acetic acid. The photocurrent generation was very sensitive to the energetics of the TiO_2. A lower excited state potential and a non-conjugated anchoring group were discussed to limit the injection yield. The dyes also show enhanced interfacial recombination as function of increased dye size and conjugation.

Paper V. The more conjugated dyes showed enhanced electron recombination with the electrolyte compared to the smallest dye **L0** and bare TiO_2. **L3** shows less sensitivity to the concentration of iodine in the electrolyte. The dye appears to attract redox acceptor species resulting in enhanced interfacial recombination.

Paper VI. Intrinsic dye sterical properties of the dye are superior to the external use of coadsorbent (**CDCA**) for the examined conditions.

Paper VII. Adsorption of **D29** onto TiO_2 from ethanol solution was studied in the presence of three different coadsorbents. **DPA** and **DINHOP** exchange to a large extent with the **D29** dye molecules and increase the photocurrents. For **CDCA** the dye load was less affected and the photocurrent was slightly decreased.

References

(1) Lewis, N. S. *Science* **2007**, *315*, 798-801.
(2) Fujishima, A.; Honda, K. *Nature* **1972**, *238*, 37-38.
(3) Gerischer, H.; Willig, F. *Top. Curr. Chem* **1976**, *61*, 31.
(4) Memming, R. *Semiconductor Electrochemistry, Wiley-VCH Verlag GmbH, Weinheim* **2001**.
(5) Tsubomura, H.; Matsumura, M.; Nomura, Y.; Amamiya, T. *Nature* **1976**, *261*, 402-403.
(6) Desilvestro, J.; Gratzel, M.; Kavan, L.; Moser, J.; Augustynski, J. *J. Am. Chem. Soc.* **1985**, *107*, 2988-2990.
(7) Oregan, B.; Gratzel, M. *Nature* **1991**, *353*, 737-740.
(8) Nazeeruddin, M. K.; Kay, A.; Rodicio, I.; Humphry-Baker, R.; Muller, E.; Liska, P.; Vlachopoulos, N.; Gratzel, M. *J. Am. Chem. Soc.* **1993**, *115*, 6382-6390.
(9) Chiba, Y.; Islam, A.; Watanabe, Y.; Komiya, R.; Koide, N.; Han, L. *Jpn. J. Appl. Phys.* **2006**, L638.
(10) *3rd International Conference on the Industrialisation of Dye Solar Cells DSC-IC 09* http://www.dsc-ic.com/index.php **2009**.
(11) Green, M. A.; Emery, K.; Hishikawa, Y.; Warta, W. *Prog. Photovolt.* **2008**, *16*, 435-440.
(12) Green, M. A.; Emery, K.; Hishikawa, Y.; Warta, W. *Prog. Photovolt.* **2009**, *17*, 320-326.
(13) Keis, K.; Magnusson, E.; Lindstrom, H.; Lindquist, S. E.; Hagfeldt, A. *Sol. Energy Mater. Sol. Cells* **2002**, *73*, 51-58.
(14) Quintana, M.; Edvinsson, T.; Hagfeldt, A.; Boschloo, G. *J. Phys. Chem. C* **2007**, *111*, 1035-1041.
(15) Quintana, M.; Marinado, T.; Nonomura, K.; Boschloo, G.; Hagfeldt, A. *J. Photochem. Photobiol. A* **2009**, *202*, 159-163.
(16) Green, A. N. M.; Palomares, E.; Haque, S. A.; Kroon, J. M.; Durrant, J. R. *J. Phys. Chem. B* **2005**, *109*, 12525-12533.
(17) Qin, P.; Zhu, H. J.; Edvinsson, T.; Boschloo, G.; Hagfeldt, A.; Sun, L. C. *J. Am. Chem. Soc.* **2008**, *130*, 8570-8571.
(18) Qin, P.; Linder, M.; Brinck, T.; Boschloo, G.; Hagfeldt, A.; Sun, L. C. *Adv. Mater* **2009**, *21*, 2993-2994.
(19) Wang, P.; Zakeeruddin, S. M.; Comte, P.; Charvet, R.; Humphry-Baker, R.; Gratzel, M. *J. Phys. Chem. B* **2003**, *107*, 14336-14341.
(20) Green, A. N. M.; Chandler, R. E.; Haque, S. A.; Nelson, J.; Durrant, J. R. *J. Phys. Chem. B* **2005**, *109*, 142-150.
(21) Boschloo, G.; Hagfeldt, A. *Manuscript in preparation*.
(22) Gorlov, M.; Kloo, L. *Dalton Trans.* **2008**, 2655-2666.
(23) Bach, U.; Lupo, D.; Comte, P.; Moser, J. E.; Weissortel, F.; Salbeck, J.; Spreitzer, H.; Gratzel, M. *Nature* **1998**, *395*, 583-585.
(24) Snaith, H. J.; Moule, A. J.; Klein, C.; Meerholz, K.; Friend, R. H.; Gratzel, M. *Nano Letters* **2007**, *7*, 3372-3376.
(25) Mozer, A. J.; Wada, Y.; Jiang, K. J.; Masaki, N.; Yanagida, S.; Mori, S. N. *Appl. Phys. Lett.* **2006**, *89*.

(26) Boschloo, G.; Marinado, T.; Nonomura, K.; Edvinsson, T.; Agrios, A. G.; Hagberg, D. P.; Sun, L.; Quintana, M.; Karthikeyan, C. S.; Thelakkat, M.; Hagfeldt, A. *Thin Solid Films* **2008**, *516*, 7214-7217.
(27) Nazeeruddin, M. K.; Zakeeruddin, S. M.; Humphry-Baker, R.; Jirousek, M.; Liska, P.; Vlachopoulos, N.; Shklover, V.; Fischer, C. H.; Gratzel, M. *Inorg. Chem.* **1999**, *38*, 6298-6305.
(28) Nazeeruddin, M. K.; Pechy, P.; Gratzel, M. *Chem. Comm.* **1997**, 1705-1706.
(29) Nazeeruddin, M. K.; Pechy, P.; Renouard, T.; Zakeeruddin, S. M.; Humphry-Baker, R.; Comte, P.; Liska, P.; Cevey, L.; Costa, E.; Shklover, V.; Spiccia, L.; Deacon, G. B.; Bignozzi, C. A.; Gratzel, M. *J. Am. Chem. Soc.* **2001**, *123*, 1613-1624.
(30) Wang, P.; Klein, C.; Humphry-Baker, R.; Zakeeruddin, S. M.; Gratzel, M. *J. Am. Chem. Soc.* **2005**, *127*, 808-809.
(31) Kuang, D. B.; Klein, C.; Ito, S.; Moser, J. E.; Humphry-Baker, R.; Evans, N.; Duriaux, F.; Graetzel, C.; Zakeeruddin, S. M.; Graetzel, M. *Adv. Mater.* **2007**, *19*, 1133-1137.
(32) Sayama, K.; Hara, K.; Mori, N.; Satsuki, M.; Suga, S.; Tsukagoshi, S.; Abe, Y.; Sugihara, H.; Arakawa, H. *Chem. Commun.* **2000**, 1173-1174.
(33) Hara, K.; Sato, T.; Katoh, R.; Furube, A.; Ohga, Y.; Shinpo, A.; Suga, S.; Sayama, K.; Sugihara, H.; Arakawa, H. *J. Phys. Chem. B* **2003**, *107*, 597-606.
(34) Wang, Z. S.; Cui, Y.; Hara, K.; Dan-Oh, Y.; Kasada, C.; Shinpo, A. *Adv. Mater.* **2007**, *19*, 1138-1141.
(35) Horiuchi, T.; Miura, H.; Uchida, S. *Chem. Comm.* **2003**, 3036-3037.
(36) Horiuchi, T.; Miura, H.; Sumioka, K.; Uchida, S. *J. Am. Chem. Soc* **2004**, *126*, 12218-12219.
(37) Kitamura, T.; Ikeda, M.; Shigaki, K.; Inoue, T.; Anderson, N. A.; Ai, X.; Lian, T. Q.; Yanagida, S. *Chem. Mater.* **2004**, *16*, 1806-1812.
(38) Thomas, K. R. J.; Hsu, Y. C.; Lin, J. T.; Lee, K. M.; Ho, K. C.; Lai, C. H.; Cheng, Y. M.; Chou, P. T. *Chem. Mater.* **2008**, *20*, 1830-1840.
(39) Hagberg, D. P.; Yum, J. H.; Lee, H.; De Angelis, F.; Marinado, T.; Karlsson, K. M.; Humphry-Baker, R.; Sun, L. C.; Hagfeldt, A.; Gratzel, M.; Nazeeruddin, M. K. *J. Am. Chem. Soc* **2008**, *130*, 6259-6266.
(40) Koumura, N.; Wang, Z. S.; Mori, S.; Miyashita, M.; Suzuki, E.; Hara, K. *J. Am. Chem. Soc* **2006**, *128*, 14256-14257.
(41) Yum, J. H.; Hagberg, D. P.; Moon, S. J.; Karlsson, K. M.; Marinado, T.; Sun, L. C.; Hagfeldt, A.; Nazeeruddin, M. K.; Gratzel, M. *Angew. Chem. Int. Ed.* **2009**, *48*, 1576-1580.
(42) Zhang, G. L.; Bala, H.; Cheng, Y. M.; Shi, D.; Lv, X. J.; Yu, Q. J.; Wang, P. *Chem. Commun.* **2009**, 2198-2200.
(43) Mishra, A.; Fischer, M. K. R.; Bauerle, P. *Angew. Chem. Int. Ed.* **2009**, *48*, 2474-2499.
(44) Marcus, R., A. *J. Phys. Chem.* **1956**, 966.
(45) Ardo, S.; Meyer, G. J. *Chem. Soc. Rev.* **2009**, *38*, 115-164.
(46) Haque, S. A.; Palomares, E.; Cho, B. M.; Green, A. N. M.; Hirata, N.; Klug, D. R.; Durrant, J. R. *J. Am. Chem. Soc* **2005**, *127*, 3456-3462.
(47) Koops, S. E.; O'Regan, B. C.; Barnes, P. R. F.; Durrant, J. R. *J. Am. Chem. Soc.* **2009**, *131*, 4808-4818.
(48) Pelet, S.; Moser, J. E.; Gratzel, M. *J. Phys. Chem. B* **2000**, *104*, 1791-1795.
(49) Clifford, J. N.; Palomares, E.; Nazeeruddin, M. K.; Gratzel, M.; Durrant, J. R. *J. Phys. Chem. C* **2007**, *111*, 6561-6567.

(50) Mori, S. N.; Kubo, W.; Kanzaki, T.; Masaki, N.; Wada, Y.; Yanagida, S. *J. Phys. Chem. C* **2007**, *111*, 3522-3527.
(51) Hagfeldt, A.; Gratzel, M. *Chem. Rev.* **1995**, *95*, 49-68.
(52) Sodergren, S.; Hagfeldt, A.; Olsson, J.; Lindquist, S. E. *J. Phys. Chem.* **1994**, *98*, 5552-5556.
(53) Dloczik, L.; Ileperuma, O.; Lauermann, I.; Peter, L. M.; Ponomarev, E. A.; Redmond, G.; Shaw, N. J.; Uhlendorf, I. *J. Phys. Chem. B* **1997**, *101*, 10281-10289.
(54) Peter, L. *J. Electroanal. Chem.* **2007**, *599*, 233-240.
(55) Peter, L. *Phys. Chem. Chem. Phys.* **2007**, *9*, 2630–2642.
(56) van de Lagemaat, J.; Frank, A. J. *J. Phys. Chem. B* **2000**, *104*, 4292-4294.
(57) Redmond, G.; Fitzmaurice, D. *J. Phys. Chem.* **1993**, *97*, 1426-1430.
(58) Watson, D. F.; Meyer, G. J. *Coord. Chem. Rev.* **2004**, *248*, 1391-1406.
(59) Nakade, S.; Kubo, W.; Kitamura, T.; Wada, Y.; Yanagida, S. *Organic Photovoltaics Iv* **2004**, *5215*, 24-31.
(60) Boschloo, G.; Haggman, L.; Hagfeldt, A. *J. Phys. Chem. B* **2006**, *110*, 13144-13150.
(61) Furube, A.; Katoh, R.; Hara, K.; Sato, T.; Murata, S.; Arakawa, H.; Tachiya, M. *J. Phys. Chem. B* **2005**, *109*, 16406-16414.
(62) Green, M. A. *Solar cells. Operating principle, technology and system application, Prentice-Hall, Inc.Englewood Cliffs* **1998**.
(63) Green, M. A. **2004**.
(64) Hagberg, D. P. *PhD Thesis, Synthesis of organic chromophores for dye-sensitized solar cells, Universitetsservice AB, Stockholm* **2009**.
(65) Duffy, N. W.; Peter, L. M.; Rajapakse, R. M. G.; Wijayantha, K. G. U. *Electrochem. Comm.* **2000**, *2*, 658-662.
(66) Nakade, S.; Kanzaki, T.; Kubo, W.; Kitamura, T.; Wada, Y.; Yanagida, S. *J. Phys. Chem. B* **2005**, *109*, 3480-3487.
(67) Boschloo, G.; Hagfeldt, A. *Chem. Phys. Lett.* **2003**, *370*, 381-386.
(68) Ehret, A.; Stuhl, L.; Spitler, M. T. *J. Phys. Chem. B* **2001**, *105*, 9960-9965.
(69) Hagberg, D., P.; Jiang, X.; Gabrielsson, E.; Linder, M.; Marinado, T.; Brinck, T.; Hagfeldt, A.; Sun, L. *J. Mater. Chem.* **2009**, DOI: 10.1039/b911397p.
(70) Hara, K.; Dan-Oh, Y.; Kasada, C.; Ohga, Y.; Shinpo, A.; Suga, S.; Sayama, K.; Arakawa, H. *Langmuir* **2004**, *20*, 4205-4210.
(71) Wang, Z. S.; Hara, K.; Dan-Oh, Y.; Kasada, C.; Shinpo, A.; Suga, S.; Arakawa, H.; Sugihara, H. *J. Phys. Chem. B* **2005**, *109*, 3907-3914.
(72) Hara, K.; Wang, Z. S.; Sato, T.; Furube, A.; Katoh, R.; Sugihara, H.; Dan-Oh, Y.; Kasada, C.; Shinpo, A.; Suga, S. *J. Phys. Chem. B* **2005**, *109*, 15476-15482.
(73) Johansson, E. M. J.; Edvinsson, T.; Odelius, M.; Hagberg, D. P.; Sun, L. H.; Hagfeldt, A.; Siegbahn, H.; Rensmo, H. *J. Phys. Chem. C* **2007**, *111*, 8580-8586.
(74) Gillaizeau-Gauthier, I.; Odobel, F.; Alebbi, M.; Argazzi, R.; Costa, E.; Bignozzi, C. A.; Qu, P.; Meyer, G. J. *Inorg. Chem.* **2001**, *40*, 6073-6079.
(75) Zakeeruddin, S. M.; Nazeeruddin, M. K.; Pechy, P.; Rotzinger, F. P.; HumphryBaker, R.; Kalyanasundaram, K.; Gratzel, M.; Shklover, V.; Haibach, T. *Inorg. Chem.* **1997**, *36*, 5937-5946.
(76) Galoppini, E. *Coord. Chem. Rev.* **2004**, *248*, 1283-1297.
(77) Leon, C. P.; Kador, L.; Peng, B.; Thelakkat, M. *J. Phys. Chem. B* **2006**, *110*, 8723-8730.

(78) Nazeeruddin, M. K.; Humphry-Baker, R.; Liska, P.; Gratzel, M. *J. Phys. Chem. B* **2003**, *107*, 8981-8987.
(79) Finnie, K. S.; Bartlett, J. R.; Woolfrey, J. L. *Langmuir* **1998**, *14*, 2744-2749.
(80) Wang, Z. S.; Cui, Y.; Dan-Oh, Y.; Kasada, C.; Shinpo, A.; Hara, K. *J. Phys. Chem. C* **2007**, *111*, 7224-7230.
(81) Benko, G.; Kallioinen, J.; Korppi-Tommola, J. E. I.; Yartsev, A. P.; Sundstrom, V. *J. Am. Chem. Soc.* **2002**, *124*, 489-493.
(82) Kuang, D. B.; Ito, S.; Wenger, B.; Klein, C.; Moser, J. E.; Humphry-Baker, R.; Zakeeruddin, S. M.; Gratzel, M. *J. Am. Chem. Soc.* **2006**, *128*, 4146-4154.
(83) Katoh, R.; Furube, A.; Barzykin, A. V.; Arakawa, H.; Tachiya, M. *Coord. Chem. Rev.* **2004**, *248*, 1195-1213.
(84) Durrant, J. R.; Haque, S. A.; Palomares, E. *Coord. Chem. Rev.* **2004**, *248*, 1247-1257.
(85) Durrant, J. R.; Haque, S. A.; Palomares, E. *Chem. Comm.* **2006**, 3279-3289.
(86) Haque, S. A.; Tachibana, Y.; Willis, R. L.; Moser, J. E.; Gratzel, M.; Klug, D. R.; Durrant, J. R. *J. Phys. Chem. B* **2000**, *104*, 538-547.
(87) Wiberg, J.; Marinado, T.; Hagberg, D. P.; Sun, L. C.; Hagfeldt, A.; Albinsson, B. *J. Phys. Chem. C* **2009**, *113*, 3881-3886.
(88) Hara, K.; Horiuchi, H.; Katoh, R.; Singh, L. P.; Sugihara, H.; Sayama, K.; Murata, S.; Tachiya, M.; Arakawa, H. *J. Phys. Chem. B* **2002**, *106*, 374-379.
(89) Moser, J. E.; Wolf, M.; Lenzmann, F.; Gratzel, M. *Phys. Chem.* **1999**, *212*, 85-92.
(90) Katoh, R.; Kasuya, M.; Furube, A.; Fuke, N.; Koide, N.; Han, L. Y. *Sol. Energy Mater. Sol. Cells.* **2009**, *93*, 698-703.
(91) Katoh, R.; Furube, A.; Kasuya, M.; Fuke, N.; Koide, N.; Han, L. *J. Mater. Chem.* **2007**, *17*, 3190-3196.
(92) Heimer, T. A.; Darcangelis, S. T.; Farzad, F.; Stipkala, J. M.; Meyer, G. J. *Inorg. Chem.* **1996**, *35*, 5319-5324.
(93) Hao, Y.; Yang, X. C.; Cong, J. Y.; Tian, H. N.; Hagfeldt, A.; Sun, L. C. *Chem. Comm.* **2009**, 4031-4033.
(94) Asbury, J. B.; Hao, E. C.; Wang, Y. Q.; Lian, T. Q. *J. Phys. Chem. B* **2000**, *104*, 11957-11964.
(95) Hara, K.; Tachibana, Y.; Ohga, Y.; Shinpo, A.; Suga, S.; Sayama, K.; Sugihara, H.; Arakawa, H. *Sol. Energy Mater. Sol. Cells.* **2003**, *77*, 89-103.
(96) Sayama, K.; Tsukagoshi, S.; Hara, K.; Ohga, Y.; Shinpou, A.; Abe, Y.; Suga, S.; Arakawa, H. *J. Phys. Chem. B* **2002**, *106*, 1363-1371.
(97) Anderson, N. A.; Ai, X.; Chen, D. T.; Mohler, D. L.; Lian, T. Q. *J. Phys. Chem. B* **2003**, *107*, 14231-14239.
(98) Bauer, C.; Boschloo, G.; Mukhtar, E.; Hagfeldt, A. *J. Phys. Chem. B* **2002**, *106*, 12693-12704.
(99) Oskam, G.; Bergeron, B. V.; Meyer, G. J.; Searson, P. C. *J. Phys. Chem. B* **2001**, *105*, 6867-6873.
(100) Alebbi, M.; Bignozzi, C. A.; Heimer, T. A.; Hasselmann, G. M.; Meyer, G. J. *J. Phys. Chem. B* **1998**, *102*, 7577-7581.
(101) Moser, J. E.; Gratzel, M. *Chem. Phys.* **1993**, *176*, 493-500.
(102) Hasselmann, G. M.; Meyer, G. J. *J. Phys. Chem. B* **1999**, *103*, 7671-7675.
(103) Kuciauskas, D.; Freund, M. S.; Gray, H. B.; Winkler, J. R.; Lewis, N. S. *J. Phys. Chem. B* **2001**, *105*, 392-403.
(104) Qu, P.; Meyer, G. J. *Langmuir* **2001**, *17*, 6720-6728.

(105) Clifford, J. N.; Palomares, E.; Nazeeruddin, M. K.; Gratzel, M.; Nelson, J.; Li, X.; Long, N. J.; Durrant, J. R. *J. Am. Chem. Soc.* **2004**, *126*, 5225-5233.
(106) Haque, S. A.; Handa, S.; Peter, K.; Palomares, E.; Thelakkat, M.; Durrant, J. R. *Angew. Chem. Int. Ed.* **2005**, *44*, 5740-5744.
(107) Clifford, J. N.; Yahioglu, G.; Milgrom, L. R.; Durrant, J. R. *Chem. Comm.* **2002**, 1260-1261.
(108) Tatay, S.; Haque, S. A.; O'Regan, B.; Durrant, J. R.; Verhees, W. J. H.; Kroon, J. M.; Vidal-Ferran, A.; Gavina, P.; Palomares, E. *J. Mater. Chem.* **2007**, *17*, 3037-3044.
(109) Forneli, A.; Planells, M.; Sarmentero, M. A.; Martinez-Ferrero, E.; O'Regan, B. C.; Ballester, P.; Palomares, E. *J. Mater. Chem.* **2008**, *18*, 1652-1658.
(110) Katoh, R.; Furube, A.; Mori, S.; Miyashita, M.; Sunahara, K.; Koumura, N.; Hara, K. *Energy. Environ. Sci.* **2009**, *2*, 542-546.
(111) Wang, Z. S.; Koumura, N.; Cui, Y.; Takahashi, M.; Sekiguchi, H.; Mori, A.; Kubo, T.; Furube, A.; Hara, K. *Chem. Mater.* **2008**, *20*, 3993-4003.
(112) Zhang, G.; Bai, Y.; Li, R.; Shi, D.; Wenger, S.; Zakeeruddin, S., M.; Grätzel, M.; Wang, P. *Energy. Environ. Sci.* **2009**, *2*, 92–95.
(113) Ito, S.; Miura, H.; Uchida, S.; Takata, M.; Sumioka, K.; Liska, P.; Comte, P.; Pechy, P.; Graetzel, M. *Chem. Comm.* **2008**, 5194-5196.
(114) Li, R. Z.; Lv, X. J.; Shi, D.; Zhou, D. F.; Cheng, Y. M.; Zhang, G. L.; Wang, P. *J. Phys. Chem. C* **2009**, *113*, 7469-7479.
(115) O'Regan, B. C.; Lopez-Duarte, I.; Martinez-Diaz, M. V.; Forneli, A.; Albero, J.; Morandeira, A.; Palomares, E.; Torres, T.; Durrant, J. R. *J. Am. Chem. Soc.* **2008**, *130*, 2906-2907.
(116) O'Regan, B. C.; Walley, K.; Juozapavicius, M.; Anderson, A.; Matar, F.; Ghaddar, T.; Zakeeruddin, S. M.; Klein, C.; Durrant, J. R. *J. Am. Chem. Soc.* **2009**, *131*, 3541-3548.
(117) Reynal, A.; Forneli, A.; Martinez-Ferrero, E.; Sanchez-Diaz, A.; Vidal-Ferran, A.; O'Regan, B. C.; Palomares, E. *J. Am. Chem. Soc.* **2008**, *130*, 13558-13567.
(118) Miyashita, M.; Sunahara, K.; Nishikawa, T.; Uemura, Y.; Koumura, N.; Hara, K.; Mori, A.; Abe, T.; Suzuki, E.; Mori, S. *J. Am. Chem. Soc.* **2008**, *130*, 17874-17881.
(119) Sayama, K.; Tsukagoshi, S.; Mori, T.; Hara, K.; Ohga, Y.; Shinpou, A.; Abe, Y.; Suga, S.; Arakawa, H. *Sol. Energy Mater. Sol. Cells* **2003**, *80*, 47-71.
(120) Hara, K.; Miyamoto, K.; Abe, Y.; Yanagida, M. *J. Phys. Chem. B* **2005**, *109*, 23776-23778.
(121) Kay, A.; Gratzel, M. *J. Phys. Chem.* **1993**, *97*, 6272-6277.
(122) Kusama, H.; Sugihara, H. *J. Comput. Chem.* **2005**, *26*, 1372-1382.
(123) Huang, S. Y.; Schlichthorl, G.; Nozik, A. J.; Gratzel, M.; Frank, A. J. *J. Phys. Chem. B* **1997**, *101*, 2576-2582.
(124) Schlichthorl, G.; Huang, S. Y.; Sprague, J.; Frank, A. J. *J. Phys. Chem. B* **1997**, *101*, 8141-8155.
(125) Hagberg, D. P.; Edvinsson, T.; Marinado, T.; Boschloo, G.; Hagfeldt, A.; Sun, L. C. *Chem. Comm.* **2006**, 2245-2247.
(126) Hara, K.; Nishikawa, T.; Kurashige, M.; Kawauchi, H.; Kashima, T.; Sayama, K.; Alka, K.; Arakawa, H. *Sol. Energy Mater. Sol. Cells.* **2005**, *85*, 21-30.

(127) Marinado, T.; Hagberg, D. P.; Hedlund, M.; Edvinsson, T.; Johansson, E. M. J.; Boschloo, G.; Rensmo, H.; Brinck, T.; Sun, L. C.; Hagfeldt, A. *Phys. Chem. Chem. Phys.* **2009**, *11*, 133-141.

(128) Mann, J. R.; Gannon, M. K.; Fitzgibbons, T. C.; Detty, M. R.; Watson, D. F. *J. Phys. Chem. C* **2008**, *112*, 13057-13061.

(129) Ghosh, P. K.; Bard, A. J. *J. Phys. Chem.* **1984**, *88*, 5519-5526.

(130) He, J. J.; Benko, G.; Korodi, F.; Polivka, T.; Lomoth, R.; Akermark, B.; Sun, L. C.; Hagfeldt, A.; Sundstrom, V. *J. Am. Chem. Soc.* **2002**, *124*, 4922-4932.

(131) Nuesch, F.; Moser, J. E.; Shklover, V.; Gratzel, M. *J. Am. Chem. Soc.* **1996**, *118*, 5420-5431.

(132) Ning, Z. J.; Zhang, Q.; Wu, W. J.; Pei, H. C.; Liu, B.; Tian, H. *J. Org. Chem.* **2008**, *73*, 3791-3797.

(133) Kim, S.; Choi, H.; Baik, C.; Song, K.; Kang, S. O.; Ko, J. *Tetrahedron* **2007**, *63*, 11436-11443.

(134) Choi, H.; Baik, C.; Kim, S.; Kang, M. S.; Xu, X.; Kang, H. S.; Kang, S. O.; Ko, J.; Nazeeruddin, M. K.; Gratzel, M. *New J. Chem.* **2008**, *32*, 2233-2237.

(135) Zhang, X. H.; Wang, Z. S.; Cui, Y.; Koumura, N.; Furube, A.; Hara, K. *J. Phys. Chem. C* **2009**, *113*, 13409-13415.

(136) Koumura, N.; Wang, Z. S.; Miyashita, M.; Uemura, Y.; Sekiguchi, H.; Cui, Y.; Mori, A.; Mori, S.; Hara, K. *J. Mater. Chem.* **2009**, *19*, 4829-4836.

(137) Kim, C.; Choi, H.; Kim, S.; Baik, C.; Song, K.; Kang, M. S.; Kang, S. O.; Ko, J. *J. Org. Chem.* **2008**, *73*, 7072-7079.

(138) Neale, N. R.; Kopidakis, N.; van de Lagemaat, J.; Gratzel, M.; Frank, A. J. *J. Phys. Chem. B* **2005**, *109*, 23183-23189.

(139) Wang, M.; Li., X.; Lin, H.; Pechy, P.; Zakeeruddin, S. M.; Grätzel, M. *Dalton Trans.* **2009**, DOI: 10.1039/b908673k.

(140) Wang, P.; Zakeeruddin, S. M.; Humphry-Baker, R.; Moser, J. E.; Gratzel, M. *Adv. Mater.* **2003**, *15*, 2101-2102.

(141) Wang, P.; Klein, C.; Humphry-Baker, R.; Zakeeruddin, S. M.; Gratzel, M. *Appl. Phys. Lett.* **2005**, *86*.